NASA
CR
2079
pt.1
c.1

NASA CONTRACTOR REPORT

NASA CR-
LOAN COPY: RE
AFWL (DOL
KIRTLAND AFB
0061199
TECH LIBRARY KAFB, NM

NASA CR-2078

PROJECT FOG DROPS

Part I: Investigations of Warm Fog Properties

by R. Pilie, W. Eadie, E. Mack,
C. Rogers, and W. Kocmond

Prepared by
CORNELL AERONAUTICAL LABORATORY, INC.
Buffalo, N.Y. 14221
for George C. Marshall Space Flight Center

NATIONAL AERONAUTICS AND SPACE ADMINISTRATION • WASHINGTON, D. C. • AUGUST 1972

TECH LIBRARY KAFB, NM

0061199

M197

TECHNICAL REPORT STANDARD TITLE PAGE

1. REPORT NO. CR 2078	2. GOVERNMENT ACCESSION NO.	3. RECIPIENT'S CATALOG NO.
4. TITLE AND SUBTITLE PROJECT FOG DROPS PART I: * INVESTIGATIONS OF WARM FOG PROPERTIES		5. REPORT DATE August 1972
		6. PERFORMING ORGANIZATION CODE 126-61-13-01-10
7. AUTHOR(S) R. Pilie, W. Eadie, E. Mack, C. Rogers, and W. Kocmond		8. PERFORMING ORGANIZATION REPORT # RM-3005-M-5
9. PERFORMING ORGANIZATION NAME AND ADDRESS Cornell Aeronautical Laboratory, Inc. Buffalo, New York 14221		10. WORK UNIT NO.
		11. CONTRACT OR GRANT NO. NASW-2126
12. SPONSORING AGENCY NAME AND ADDRESS NASA Washington, D. C.		13. TYPE OF REPORT & PERIOD COVERED CONTRACTOR REPORT
		14. SPONSORING AGENCY CODE

15. SUPPLEMENTARY NOTES

* Part II is CR-2079, PROJECT FOG DROPS, Laboratory Investigations

16. ABSTRACT

A detailed study was made of the micrometeorological and microphysical characteristics of eleven valley fogs occurring near Elmira, New York. Observations were made of temperature, dew point, wind speed and direction, dew deposition, vertical wind velocity, and net radiative flux. In fog, visibility was continuously recorded and periodic measurements were made of liquid water content and drop-size distribution. The observations were initiated in late evening and continued until the time of fog dissipation. The vertical distribution of temperature in the lowest 300 meters and cloud nucleus concentrations at several heights were measured from an aircraft before fog formation. The behavior of these parameters before and during fog are discussed.

A numerical model was developed to investigate the life cycle of radiation fogs. In the atmosphere, the model predicts the temporal evolution of the vertical distributions of temperature, water vapor, and liquid water as determined by the turbulent transfer of heat and moisture. The model includes the nocturnal cooling of the earth's surface, dew formation, fog drop sedimentation, and the absorption of infrared radiation by fog. The capabilities and limitations of the model are examined.

17. KEY WORDS	18. DISTRIBUTION STATEMENT

19. SECURITY CLASSIF. (of this report)	20. SECURITY CLASSIF. (of this page)	21. NO. OF PAGES	22. PRICE
Unclassified	Unclassified	150	$3.00

* For sale by the National Technical Information Service, Springfield, Virginia 22151

TABLE OF CONTENTS

Section		Page
	LIST OF TABLES	iii
	LIST OF FIGURES	iv
	ABSTRACT	vii
	SUMMARY	viii
	ACKNOWLEDGEMENTS	xi
I.	INTRODUCTION	1
II.	FIELD INVESTIGATIONS	3
	Visual Observations and Visibility Data	7
	• Surface Observations	7
	• Fog Top Altitude	15
	Micrometeorological Data	16
	• Low Level Temperature Data	16
	• Temperature Aloft	29
	• Summary of Temperature Data	35
	• Low Level Dew Point Data	40
	• Dew Deposition and Evaporation Rates	49
	• Wind Speed and Direction	50
	• Vertical Wind Speed and Direction	55
	• Radiation	59
	Fog Microphysics Data	60
	• Drop-Size Distributions	60
	• Liquid Water Content	65
	• Summary of Surface Microphysical Properties of the Fog	70
	• Drop-Size Distributions Aloft	76
	• Cloud Nucleus Observations	80
III.	DISCUSSION OF EXPERIMENTAL RESULTS	84
	• Fog Formation Processes at Elmira	84
	• The Role of Dew in the Fog Life Cycle	91
	• Evolution of Drop-Size Distributions and Associated Implications	94
IV.	NUMERICAL MODELING OF RADIATION FOG	99
	Introduction	99
	• Brief Description of Model	99
	• Previous Work	100

Section	Page
Numerical Model	102
• Major Assumptions	102
• Equations	102
List of Symbols	102
Major Equations	103
Saturation Adjustment	104
Radiation	104
Exchange Coefficients	106
Terminal Velocity of Fog Drops	109
• Boundary Conditions	110
Upper and Lower Boundaries	110
The Surface	110
• Computational Procedure	111
Grid System	111
Implicit Integration	112
Summary of Computational Sequence	113
Timing	114
• Initial Conditions and Constants	115
Results	116
• General Characteristics of Model Fogs	116
• Example of Model Fog Formation	118
Temperature Structure Prior to Fog Formation	118
Temperature Structure After Fog Formation	126
• Exchange Coefficient as a Function of Thermal Stratification	128
• Model Behavior as a Function of Input Parameters	130
• Dew Formation	131
• Summary	132
REFERENCES	135

LIST OF TABLES

Table No.		Page
I	Instrumentation	4
II	Extremes of Deviation of Observed Temperature Relative to Average Temperature	24
III	Growth of Droplets at 0.3%S on Nuclei of Different Activation Supersaturations	97
IV	Description of Temperature Profiles Observed During Nocturnal Cooling	123
V	Model Behavior as a Function of u^*	125
VI	Stratification of Numerical Experiments by K -Value at the 10 m Level	130

LIST OF FIGURES

Figure No.		Page
1	Topography Near the Elmira Field Site	5
2	Schematic of Chemung County Airport Showing Instrumentation Sites	6
3	Visibility vs Time 8/22/70	9
4	Visibility vs Time 9/12/70	10
5	Visibility vs Time 9/2/70	11
6	Visibility vs Time 8/13/70	12
7	Visibility vs Time 8/26/70	13
8	Fog Top Altitude as a Function of Time	17
9	Average Fog Top Altitude as a Function of Time After Formation	18
10	Temperatures and Dew as Functions of Time 8/22/70	20
11	Temperatures and Dew as Functions of Time 9/12/70	21
12	Temperatures and Dew as Functions of Time 9/2/70	22
13	Model Fog Temperatures - Surface to 17 m	25
14	Temperature as a Function of Time 8/14/70	28
15	Temperature Aloft 8/22/70 and 9/2/70	31
16	Temperature Aloft 8/13/70	32
17	Summary of Temperatures at 30 and 60 m as a Function of Time (8 fogs) (Corrected for Sunrise Effect)	33
18	Summary of Temperatures at 90 and 120 m as a Function of Time (8 fogs) (Corrected for Sunrise Effect)	34
19	Vertical Distribution of Temperature Relative to Temperature of Fog Top	36

Figure No.		Page
20	Model Temperature Profiles - Pre-Fog and Fog Formation Periods	37
21	Model Temperature Profiles in Fog	38
22	Tracings of Typical Dew Point Data at Different Times in Fog Life Cycle (8/21-8/22/70)	41
23	Dew Points as Functions of Time 8/22/70	43
24	Dew Points as Functions of Time 9/12/70	44
25	Dew Points as Functions of Time 9/2/70	45
26	Dew Point Model	47
27	Dew Point as Function of Time 8/14/70	48
28	Dew Formation-Evaporation Model--Spread in Data Points is Shown	51
29	Wind Data 8/22/70	53
30	Wind Data 9/2/70	54
31	Vertical Wind Speed as Function of Time (9/11-12/70)	56-57
32	General Envelope of Peaks in Vertical Wind Speed (Isolated Peaks Neglected) 9/12/70	58
33	Drop-Size Distributions Obtained on 2 Sept 1970	64
34	Drop-Size Distributions Obtained on 8/25/70	66
35	Drop-Size Distributions Obtained on 8/22/70	67
36	Drop-Size Distributions Obtained on 9/12/70	68
37	Comparison of Liquid Water Content Measurements Made with a Gelman High Volume Sampler and Simultaneous Values Obtained by Integrating the Absolute Drop-Size Distribution	69
38	Visibility and Microphysics Data Obtained on 8/22/70	71
39	Visibility and Microphysics Data Obtained on 9/12/70	72
40	Visibility and Microphysics Data Obtained on 9/2/70	73

Figure No.		Page
41	Visibility and Microphysics Data for Seven Fogs	74
42	Mean Drop Sizes as Functions of Time for Seven Fogs	75
43	Normalized Drop-Size Distributions Obtained Aloft on 8/22/70	77
44	Normalized Drop-Size Distributions Obtained Aloft on 9/12/70	78
45	Variations of Mean Drop Radius with Time and Height	79
46	Vertical Profiles of Cloud Nucleus Concentration at Three Times - Average Data from 12 Flights at S = 0.3%	81
47	Haze Nuclei Data	82
48	Nocturnal Cross Valley Circulation (After Wagner)	86
49	The Nocturnal Mountain Wind	87
50	Calculated Dew Point Change between t = -6 Hours and t = -0.5 Hour Required to Produce Measured Dew Deposition in Same Time Interval	92
51	Model Fog Top Heights vs Time. Numbering Labels Particular Numerical Experiment for Which Data are also Shown in Figure 52	117
52	Model Fog Liquid Water Content vs Time	119
53	Example of Model Time-Height Variation of Liquid Water Content (in mg/m^3)- Case (1) in Figures 51 and 52	120
54	Pre-Fog Temperature Profile in Model and Observations	121
55	Comparison of Model Temperature Profiles to Observed Profiles for Pre-Fog Conditions	124
56	Model Low-Level Temperature Profile Evolution in Fog After Surface Net Radiation Becomes Negligible	127
57	Evolution of Turbulent Exchange Coefficient Profile for Model Simulation in Which Low-Level Temperature Profile Becomes Lapsed	129

SUMMARY

Extensive measurements were made of micrometeorological and microphysical characteristics of eleven fogs in the Chemung River Valley near Elmira, New York. Temperature was measured at five levels between 0 and 17 m, dew point at three levels, and wind speed and direction at two levels. Net radiative flux and vertical wind velocity were measured at 17 m. Visibility was observed at three locations at a height of four feet, and dew deposition was measured at the surface. Observations began in late evening and continued until the time of fog dissipation. After fog formed, drop samples were collected for size distribution analysis and liquid water content was measured at 15-minute intervals or less. The vertical distribution of temperature from 0 to 300 m and cloud nucleus concentrations were measured from an aircraft at three-hour intervals before fog formation. Temperature measurements and drop sample collections were made in fog at altitudes above 60 m.

Remarkably consistent patterns of temperature, dew point, and dew deposition behavior with time relative to fog formation were observed from six hours before fog formed to fog dissipation. Radiative cooling of the surface stimulated dew deposition and formation of temperature and dew point inversions. After midnight, maximum cooling occurred at a level equal to about two-thirds the eventual fog depth, apparently as a result of nocturnal valley circulations. When the low level atmosphere became about isothermal, fog formed aloft and grew downward under the influence of an instability caused by radiation from the fog top. Surface warming began when net radiation from the surface was reduced by fog aloft. When fog was fully developed, the temperature profile was approximately wet adiabatic in the lowest two-thirds of the fog and inverted at higher levels. After sunrise, fog temperature increased uniformly.

Dew deposition rate was uniform before fog formation and decreased to near zero between fog formation and sunrise. Evaporation of dew began at sunrise and continued until fog dissipation. The evaporation rate was sufficient to maintain saturation for approximately 2.5 hours within the fog as post sunrise temperatures increased. As the heating rate increased, evaporation was insufficient and the fog lifted.

As long as ambient wind speeds were low, the mountain wind controlled flow in the valley. Directional shear of 45-90° occurred frequently and 150 to 180° shear was occasionally observed between valley and hilltop winds. Bursts of vertical air motions, both up and down, occurred throughout the pre-fog period. Occasionally, persistent up- or downdrafts occurred for intervals of several minutes. Up and down motions of short duration occurred continuously after fog formation with typical velocities of 0.5 to 1 m sec^{-1} and occasionally as large as 2 m sec^{-1}.

The microphysical properties of fog change in a manner that is almost as consistent as the micrometeorological properties. Shallow ground fog usually occurs prior to the formation of deep valley fog. The ground fog consists of 100 to 200 droplets cm^{-3} distributed between 1 and 8 μm radius, with a mode at 3 to 4 μm. As deep fog begins to form, the drop concentration decreases to less than 5 cm^{-3} and the mode increases to 6 to 10 μm radius. Droplets smaller than 3 to 4 μm radius disappear completely. Total droplet concentration then increases slowly to a maximum at the first visibility minimum at which time small droplets reappear. Thereafter, the distribution contains droplets between 1 and 30 μm radius with a mode between 6 and 12 μm. In about half of the fogs, a second mode at 3 or 4 μm also exists. It appears that the initial visibility degradation at the surface occurs as a result of droplets being physically transported downward from the fog aloft and that new droplets are not generated in the very low levels until the first visibility minimum.

A numerical model was developed to investigate the life cycle of fogs which result both from the nocturnal cooling of the earth's surface by infrared radiation and from various vertical transfer processes. In the model, the atmospheric exchange coefficients are functions of friction velocity, height, and the predicted local thermal stability. After the earth's surface is cooled to the dew point, dew is allowed to form and water vapor is brought down to the surface by turbulent transfer. Upon fog formation, the influences of infrared absorption and radiation by fog, and fog drop sedimentation are included. The model has a one-dimensional vertical grid system which extends from one meter below the earth's surface to approximately one kilometer above the

surface. In the atmosphere, the model predicts the temporal evolution of the vertical distributions of temperature, water vapor, and liquid water as determined by radiative and turbulent transfer of heat, and turbulent transfer of moisture.

Because the temperature and dew point profiles decreased simultaneously during a simulation, the model behavior was quite sensitive to the overall level of turbulent transfer as controlled by the friction velocity. The model formed radiation fog with tops in the 10-40 m range but could not duplicate all the observed characteristics of the Elmira valley fog in a single simulation. This result suggests that two- or three-dimensional processes, e.g., valley circulations, may significantly influence the formation and properties of the Elmira valley fogs. The liquid water content of the deeper fogs generated was in the 300-500 mg/m^3 range, which is larger than the 150 mg/m^3 frequently observed in natural fogs. This discrepancy between observations and model results appears to lie in the inability of the model to predict deep fogs with realistic initial dew point spreads. The present model was able to reproduce a characteristic feature which occurs after fog forms, i.e., a rise of surface temperature and conversion of the low level temperature profile from inversion to lapse conditions. In the model, this behavior occurred when downward radiation emanating from the fog significantly reduced the net radiation from the earth's surface.

ACKNOWLEDGEMENTS

The authors wish to express their gratitude to members of the Atmospheric Sciences Section and Environmental Systems Department who participated in this program and who contributed many extra hours of their time during the performance of this project. In particular, special thanks are due Mr. George A. Zigrossi for his assistance in data taking and for his skillful maintenance of instrumentation and to Miss Christine R. Schurkus for typing this manuscript and for participating in the tedious reduction of drop-size data.

Thanks are due Mr. Ed Wronkowski, Airport Manager of the Chemung County Airport, Elmira, New York for allowing us to use the many airport facilities and services. We also wish to thank members of the Elmira ground control, headed by Mr. Jim Mengus, Chief Air Traffic Controller. Mr. William Garrecht, Chief of the Airways Facilities Section of the FAA was particularly helpful in arranging needed clearances for operating equipment in restricted areas of the airport.

We are indebted to Dr. Peter Kuhn, of the National Oceanic and Atmospheric Administration, for providing us with net radiometers and for assisting in the interpretation of the results.

Finally, our sincere appreciation is given to Mr. William A. McGowan, Chief, Aircraft and Airport Operating Problems Branch at NASA Headquarters, who has served as our project monitor for the past eight years and who has given us his continued encouragement and support throughout the performance of this project.

CHAPTER I

INTRODUCTION

During the summers of 1968 and 1969, Cornell Aeronautical Laboratory, Inc. (CAL), under the sponsorship of the Aeronautical Vehicle Division of NASA, performed extensive valley fog seeding tests near Elmira, New York. The seeding concept developed at CAL is one in which visibility is improved by introducing sized hygroscopic materials into the fog. The nuclei, upon entering the fog, cause a favorable redistribution of droplet size which often results in substantial visibility improvements. In approximately half of the airborne seeding experiments that were performed some visibility improvement was measured. These successful experiments were concentrated in the second half of the fog life cycle. Experiments performed shortly after fog formation were not successful. Similar relationships were observed in experiments performed by the Air Force Cambridge Research Laboratory and Meteorology Research, Inc., in Lakeport and the Noyo River Valley, California.

A review of the literature provided no explanation for the changes in the character of fog that might be responsible for the observed differences in seeding effectiveness. It was apparent that our lack of understanding of the temporal variations of the physical and dynamic characteristics of fog was beginning to limit progress in the development of fog dissipation procedures. To provide some of the needed information, therefore, the 1970 field program was designed to gather information on the entire fog life cycle. The field program was to be followed by an effort to formulate a dynamic model of valley fog. The goal was to set initial boundary conditions and input parameters in the computer model according to measurements obtained in the field and let the computer reproduce the variations in fog characteristics that were observed through the natural life cycle.

In addition to these investigations of the properties of natural fog, a series of laboratory experiments were performed to complete the investigation of the possibility of inhibiting fog formation through the use of evaporation inhibitors and to begin to study the effects of some common air pollutants on the characteristics of fog and on the seedability of fog. Tests were also initiated to examine the photochemical production of condensation nuclei. These experiments were conducted in anticipation of

our current study of coastal fogs at Vandenberg, California and in the Los Angeles Basin. Results of the laboratory tests are presented under separate cover.

Chapters II and III in this report cover the results of the field program. Results obtained from the numerical modeling effort are presented in Chapter IV.

CHAPTER II

FIELD INVESTIGATIONS

Field investigations were performed at the Chemung County Airport near Elmira, New York from 5 August through 15 September 1970. The general characteristics of the valley are illustrated in Figure 1, and locations of our instrumentation on the airport are shown in Figure 2. Transmissometers were located at the localizer, the tower site, and the glide slope. All other instrumentation listed in Table I was located at the tower site or on the Piper Aztec used for airborne observations.

Automatic instrumentation was usually turned on between 2100 and 0100 on the nights preceding the predicted fog formation. Manual observations were usually made at half-hour intervals from that time until fog dissipation and occasionally at much shorter intervals (as small as 30 seconds) when a particular characteristic of the atmosphere was being investigated in detail. Normally, aircraft observations were made at three-hour intervals from midnight until fog formation. After fog formation, regular aircraft observations were suspended for safety reasons until after daybreak. Shortly after sunrise, aircraft data were acquired from the surface to several thousand feet on takeoff through the fog and at approximately 45-minute intervals thereafter on ILS approaches to 60 m.

Measurements were made on 19 occasions when the probability of fog formation was estimated to be 50% or greater. Fog formed on 12 of these occasions and on two days for which the probability had been estimated at less than 50%. On five of the seven nights for which fog was forecast (probability >50%) but did not form, thin clouds drifted over the valley and inhibited surface cooling. On the other two nights, fog formed in other parts of the valley but not at the airport.

The data presented in this report are based on eleven of the twelve fogs sampled. Calibration of all equipment was not completed until 12 August 1970 so that only portions of the data pertaining to the fogs of 8 and 11 August are included in the summaries.

Table I

INSTRUMENTATION

		RECORDING INTERVAL	DATA QUALITY		
			GOOD	FAIR	POOR
SURFACE					
THREE TRANSMISSOMETERS (CAL)		CONTINOUS	X		
DROP SAMPLER (CAL-GELATIN)		15 MIN	X		
LIQUID WATER CONTENT (GELMAN)		30 MIN	X		
DROP CONCENTRATION (CAL) *		15 MIN	X ◄	———	► X
TEMPERATURE (SURFACE AND 10 cm)		30 MIN	X		
DEW WEIGHT (CAL)		30 MIN		X	
HAZE NUCLEI (CAL)		3 HR		X	
TOWER					
TEMPERATURE – 1 m, 3 m, 17 m	(FOXBORO)	CONTINUOUS	X		
DEW POINT – 1 m, 3 m, 17 m	(FOXBORO)	CONTINUOUS	X		
WIND SPEED & DIRECTION, 3 m, 17 m	(BEC & WHIT)	CONTINUOUS	X		
VERTICAL WIND SPEED, 17 m	(GILL)	CONTINUOUS		X	
NET RADIATION, 17 m	(APCL)	30 MIN			X
AZTEC					
CLOUD CONDENSATION NUCLEI (CAL)		3 HR	X		
TEMPERATURE	(REVERSE FLOW)	CONTINUOUS		X	
DEW POINT	(CAMB. INST.)	CONTINUOUS			X
DROP SAMPLER	(CAL)	100 FT VERT.	X		

*TWO METHODS WERE USED.

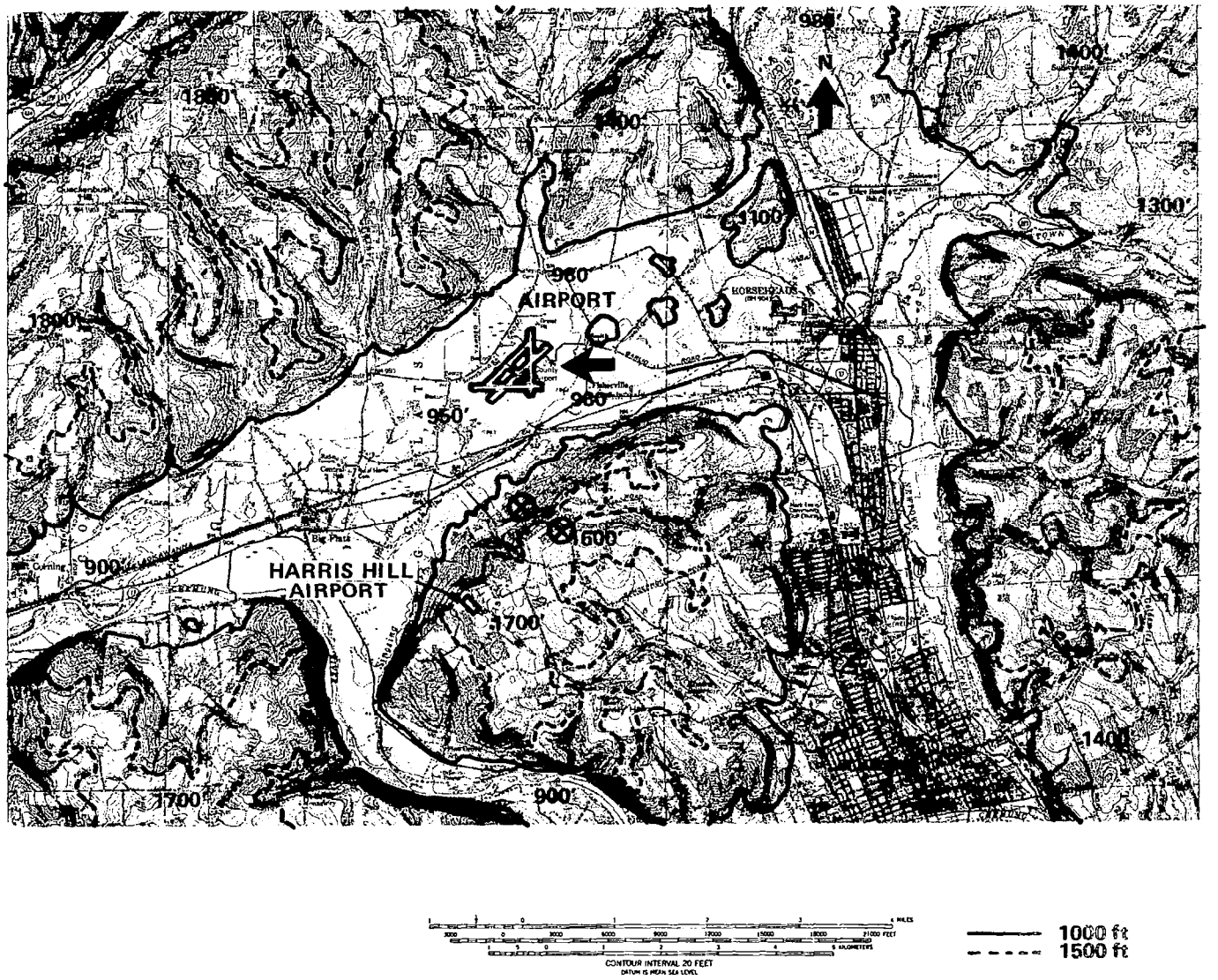

Figure 1 TOPOGRAPHY NEAR THE ELMIRA FIELD SITE

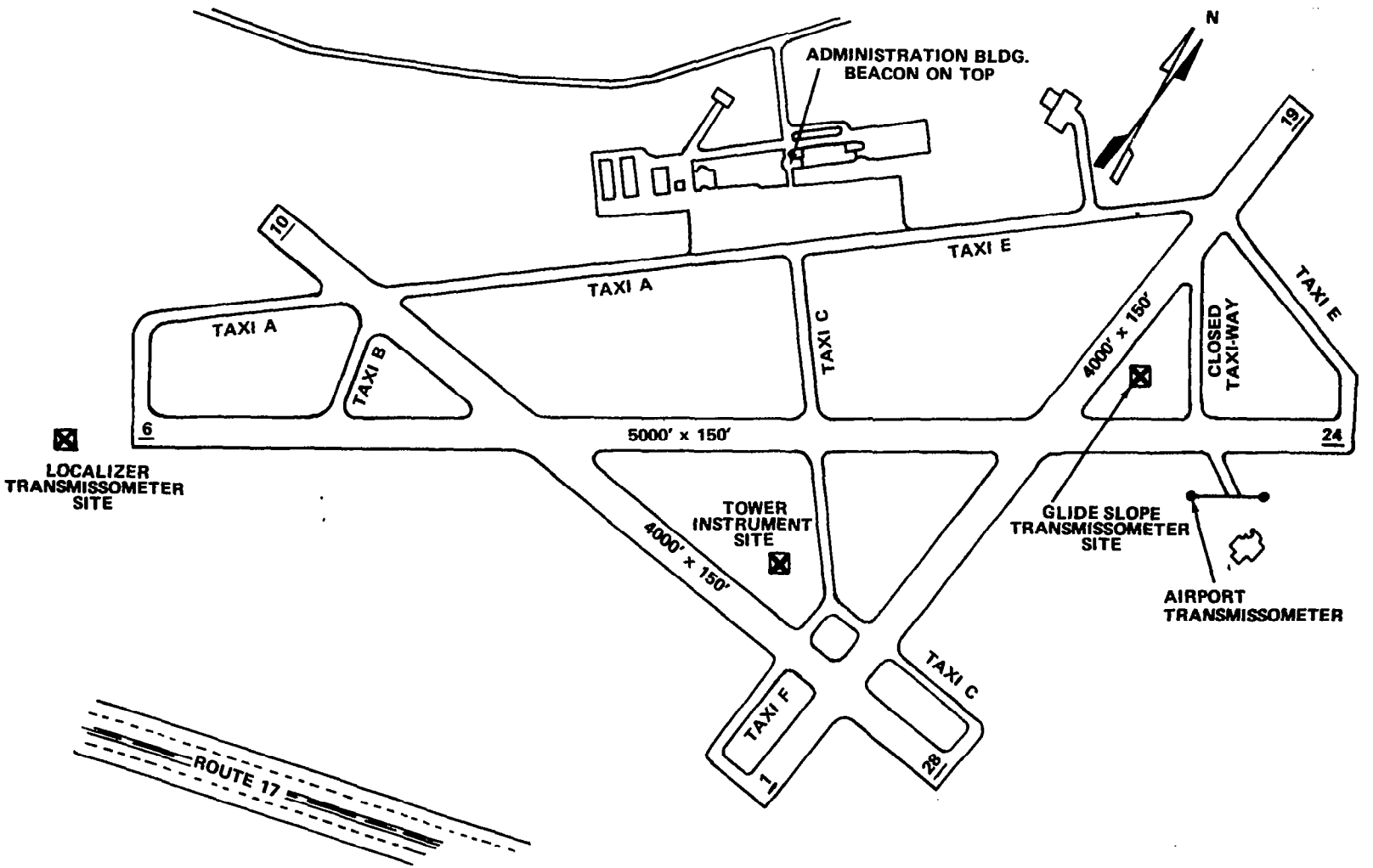

Figure 2 SCHEMATIC OF CHEMUNG COUNTY AIRPORT SHOWING INSTRUMENTATION SITES

Of the twelve fogs for which data were acquired, eight formed within the two hours preceding sunrise, three formed within the half hour after sunrise and one (14 August 1970) formed at 0015 EDT, an anomaly caused by the saturation of the valley air after an early evening thunderstorm. In the presentation of the data throughout this report, the two fogs of 22 August and 12 September are used as examples of typical persistent, dense fogs that form prior to sunrise. Data from 2 September 1970 are used to illustrate characteristics of fogs that form after sunrise. Other examples are sometimes presented to illustrate specific features of a given fog that do not fit the general patterns.

It should be recognized that all data were acquired in one valley and that attempts should be made to verify the findings at other locations.

VISUAL OBSERVATIONS AND VISIBILITY DATA

• Surface Observations

Visibility data were acquired from CAL-designed transmissometers located at three sites on the airport as indicated in Figure 2. The transmissometers were operated over 100 ft path lengths at a height of 4 ft above the surface. Each instrument was adjusted in situ to provide a measured transmitter beam width of less than 1°. Receiver beam width was adjusted in the laboratory to be less than 1°. Maximum overall error in the measurement of received light intensity was estimated to be ±5%, with the greatest limitation being imposed by the accuracy of the recorder (±1% full scale) at the lowest visibilities. This error is negligible in the low visibility region; e.g., at 1000 ft visibility, an error of ±5% in the measurement of received light produces an error of only ±100 ft in visibility. To minimize error due to drift in the transmissometers, a calibrate-signal was generated with a prism inserted into the transmitted beam to reflect a fixed fraction of the transmitted light into a second phototube mounted in the transmitter. The calibrate-phototube was operated from the same power supply as the receiver and its output was passed through the receiver electronics. Calibrate-signals were recorded for 20-second intervals every three minutes.

Continuously recorded transmissometer data were converted to meteorological visibility V in the standard manner. That is,

$$I = I_0 e^{-\beta x} \tag{1}$$

$$V = \frac{3.912}{\beta} \tag{2}$$

where I and I_0 are observed light intensities at the receiver after transmission through the turbid and clear media respectively, x is the transmission path length (100 ft in this case) and β is the extinction coefficient. Conversions were made at discrete times determined by changes in transmission characteristics or to coincide with the acquisition of drop samples.

Visibility data acquired during the three fogs used for illustrative purposes throughout this report (22 August, and 2 and 12 September 1970) are shown in Figures 3, 4, and 5. The data in Figures 3 and 4 are characteristic of persistent, dense fogs in Elmira and the data in Figure 5 are typical of fogs that formed shortly after sunrise. Figure 6, which shows data acquired on 13 August 1970, illustrates typical visibility fluctuations associated with patchy fog. Figure 7 illustrates the one case (26 August 1970) in which fog was persistent at two of the instrumented sites and patchy at the third.

Several features of the illustrative curves require explanation. The continuous curves show meteorological visibility obtained from transmissometer data. The x's show visual range as determined by an observer either by pacing off the appropriate distance or measuring it with an automobile odometer. The disagreement after daybreak is due to airlight and illustrates why daytime and nighttime scales are different on RVR equipment.

With the 100 ft baseline, the least count of the transmissometers was such that visibility in excess of about 13,000 ft was not distinguishable from infinity. The dashed portions of the curves simply indicate that visibility exceeded that value. Visual observations made during this period indicate that haze usually formed in late evening and limited visibility to about three

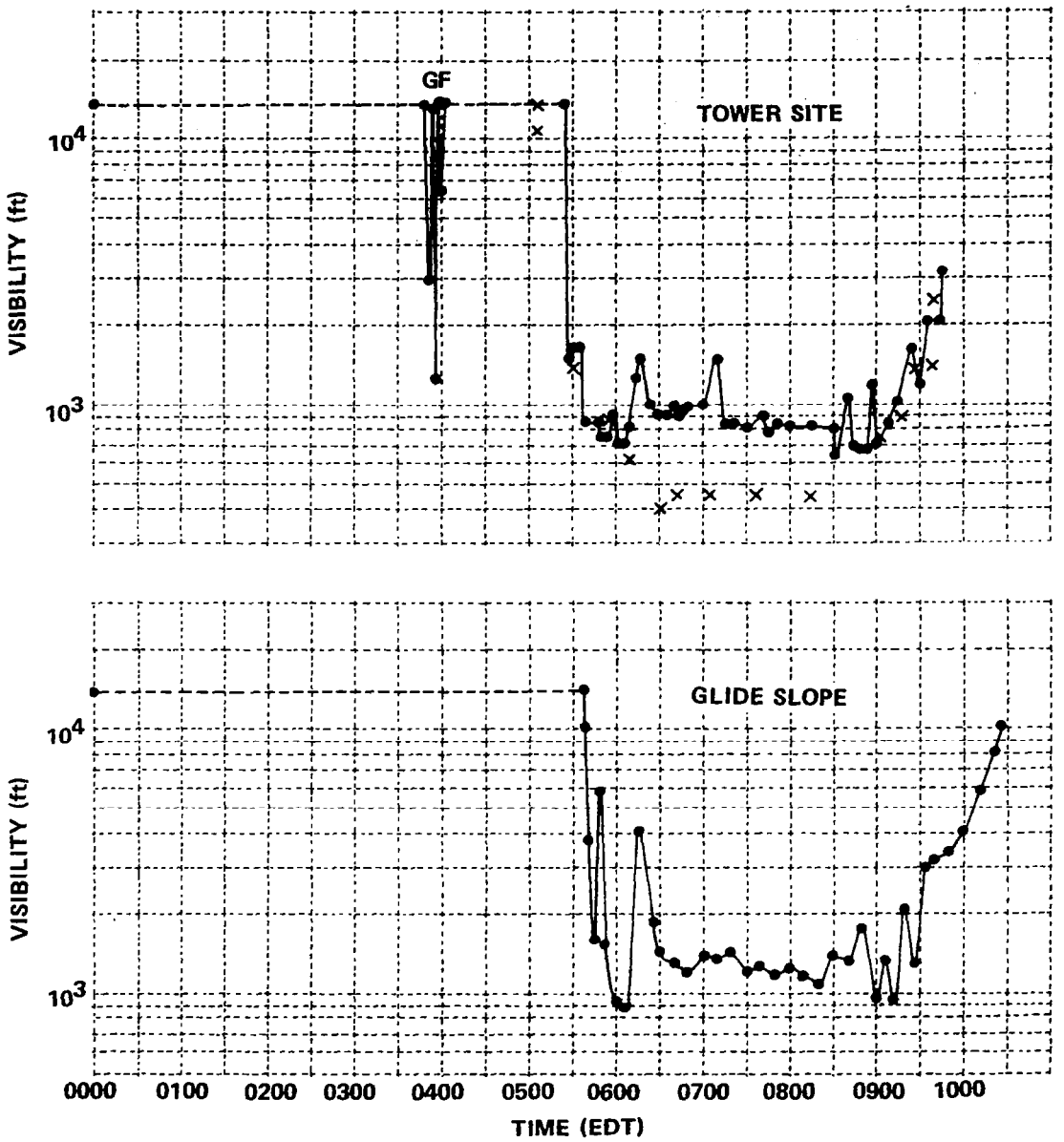

Figure 3 VISIBILITY VS TIME 8/22/70

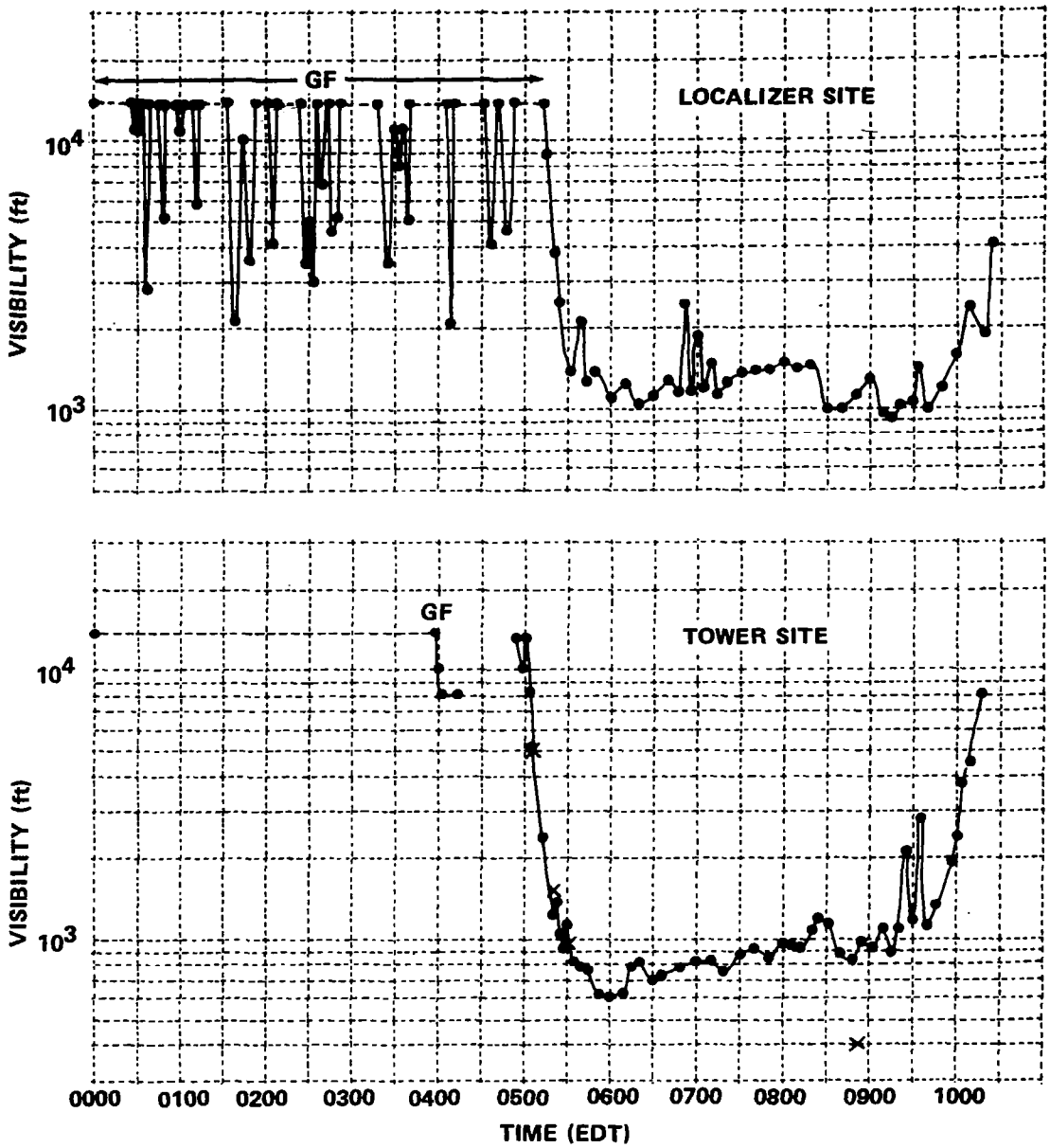

Figure 4 VISIBILITY VS TIME 9/12/70

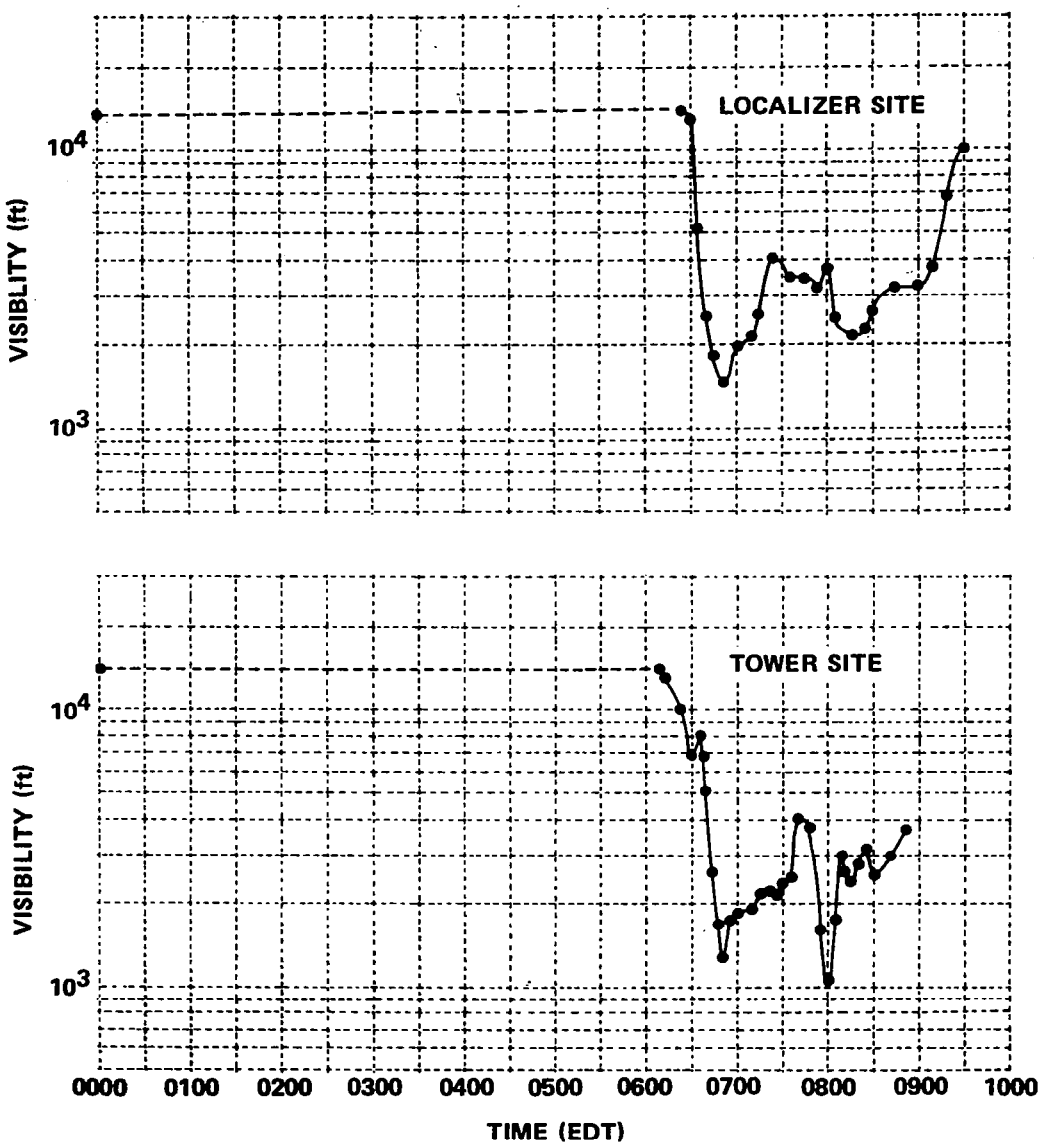

Figure 5 VISIBILITY VS TIME 9/2/70

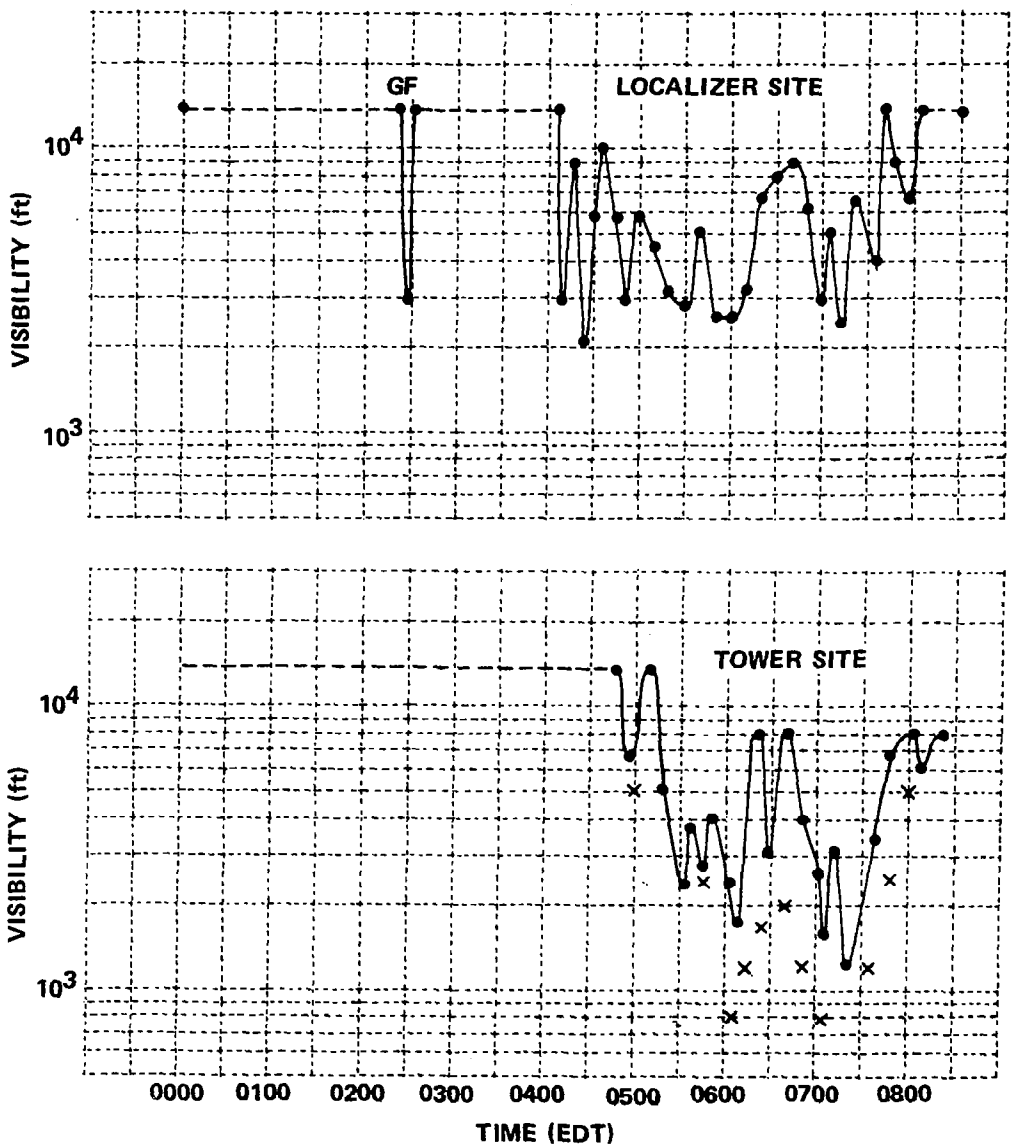

Figure 6 VISIBILITY VS TIME 8/13/70

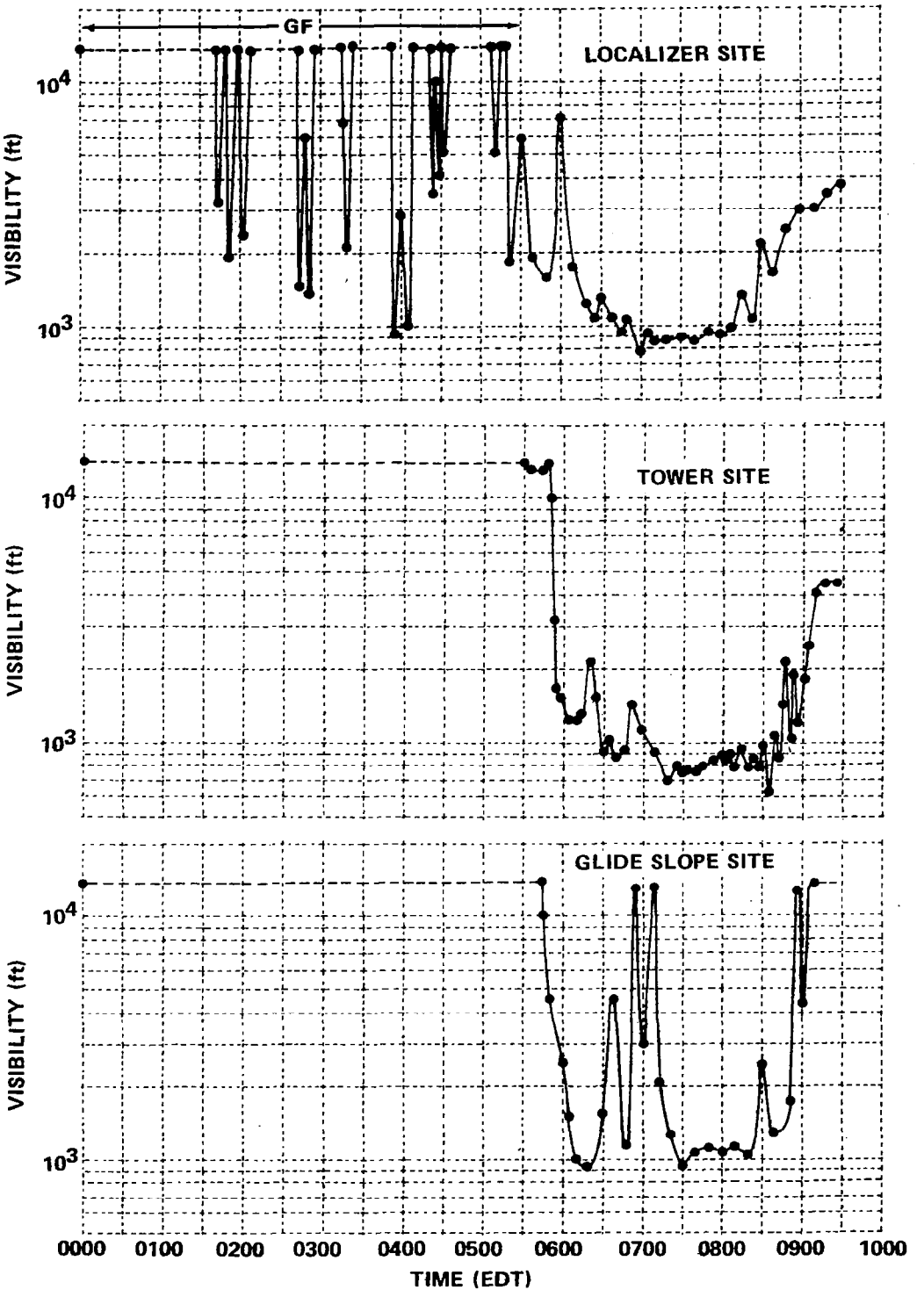

Figure 7 VISIBILITY VS TIME 8/26/70

miles around midnight. From that time until fog formation, haze density increased very slowly. Frequently during this period, patches of shallow ground fog (GF), ranging in depth from about 1 cm to 3 m, formed over the airport. Occasionally, as many as three layers, each about 1 m thick, which were separated by 1 to 2 m of clear air, were observed to extend as high as 10 m.

Shallow ground fog frequently formed in the vicinity of the tower site. Deeper ground fog, i.e., 1 m, was frequently observed to drift very slowly to the warm, dry runways surrounding the tower site and dissipate. Only infrequently, such as at 0400 EDT on 22 August 1970, was the ground fog deep enough to affect the transmissometer near the tower. The tranmissometer operated at the localizer site was in a slight depression and affected by ground fog approximately one-third of the time after midnight on many nights. The glide slope transmissometer, located on a slight mound, was never affected by the ground fog even though thin layers were frequently noted at that site.

Between an hour and a few minutes before fog formation, appearance of the haze, as observed in the beam of the airport tower beacon, changed from a continuous haze to streamers of dense haze or perhaps fog separated by clear regions. Shortly thereafter, the moon and stars became obscured as fog formed aloft.

On seven of the nine occasions for which written notes are available, fog was first observed aloft. On six of these occasions, the beacon on top of the tower (2000 ft away) was obscured while the base of the terminal building was clearly visible. On one occasion, when fog formed after daybreak (2 September 1970), fog was clearly observed to form aloft in a thin layer over most of the valley and "grow" downward. On one occasion (14 August 1970), a "wall" of fog advected in from the west and on one occasion when fog formed after daybreak, the visibility degradation appeared to occur at all levels simultaneously.

Throughout the period when fog was forming aloft, surface visibility remained greater than two miles. As indicated in the five illustrations, the decrease in surface visibility from 13,000 ft to less than half mile usually required less than five minutes. From that time visibility degraded more slowly with an average of 27 minutes (11 fogs) required between the initial observable decrease and the first minimum.

In general, the visibility behavior between the first minimum and fog dissipation followed one of two patterns and was essentially the same at the three transmissometers. Dense fogs, minimum visibility from 600 to 1200 ft, were quite persistent, with an average duration of four hours, and only minor fluctuations in visibility. Moderate fogs, including all fogs that formed after sunrise were characterized by minimum visibility exceeding 1200 ft and large visibility changes that occurred at intervals of one half to one hour. Average duration of the moderate fogs was approximately 2.5 hours.

Several attempts were made to discern more specific behavioral patterns of visibility but in most cases without success. There appears to be a fairly consistent, usually slight increase in visibility that occurs between one half and one hour after the first minimum. The only effect associated with sunrise is due to the change in illumination and not in the extinction coefficient. After the first minimum, there is no consistent variation of surface visibility with real time. Efforts to construct a model of visibility based on the physical properties of the fog therefore proved futile.

- Fog Top Altitude

The height of the fog top was determined visually using the altimeter on the Aztec during IFR approaches and wave-offs that were made after daybreak. From agreement of recorded altitude at times of takeoff and landing and from discussions with our pilots, we believe that measured altitudes are accurate to ± 10 m. In many cases, however, small-scale variations in fog top height with distance exceeded this value. The recorded data represent what the observer judged to be average in the vicinity of the penetration.

Data for the three illustrative fogs plus the fog of 11 August 1970 are presented in Figure 8. The latter case is presented because it includes the one measurement made before fog formation at the surface. It also contains one of the two measurements of fog top altitude that were made very nearly at the time of surface fog formation.

It is immediately apparent from Figure 8 that the fog top heights measured on the descent penetrations one to two miles east of the airport are consistently higher than those measured on the ascent penetrations one to two miles west of the airport. This altitude difference has been confirmed by flying at fog top height over the region. As shown in the average of all data, presented in Figure 9, the altitude difference averages slightly over 30 meters (100 ft) throughout the fog life cycle. The change in altitude is well correlated with the average increase of surface elevation of the base of the valley shown in Figure 1. It also appears that fog "piles up" at the east end of the valley before turning south with the drainage wind.

It is apparent in Figures 8c and 8d that the fog occasionally increases in height during the early portion of its life cycle. While this effect appears in the averages, the number of cases available for the first and fourth hour of the life cycle is not sufficient for drawing firm conclusions. (The limitation of in-fog flight to daylight hours limited early sampling and the paucity of long fogs limited sampling in the fourth hour.) In general, the fog top altitude remained approximately constant for the last hour or two before dissipation regardless of fog duration.

For the first hour or two after sunrise, the fog top had a smooth, gently rolling appearance similar to "mother of pearl". This texture changed to that characteristic of the tops of stratocumulus clouds as the fog aged.

MICROMETEOROLOGICAL DATA

- Low Level Temperature Data

Low level (0.0 to 17 m) temperature data were acquired on 11 fog days during the 1970 field operation in Elmira. The data consisted of:

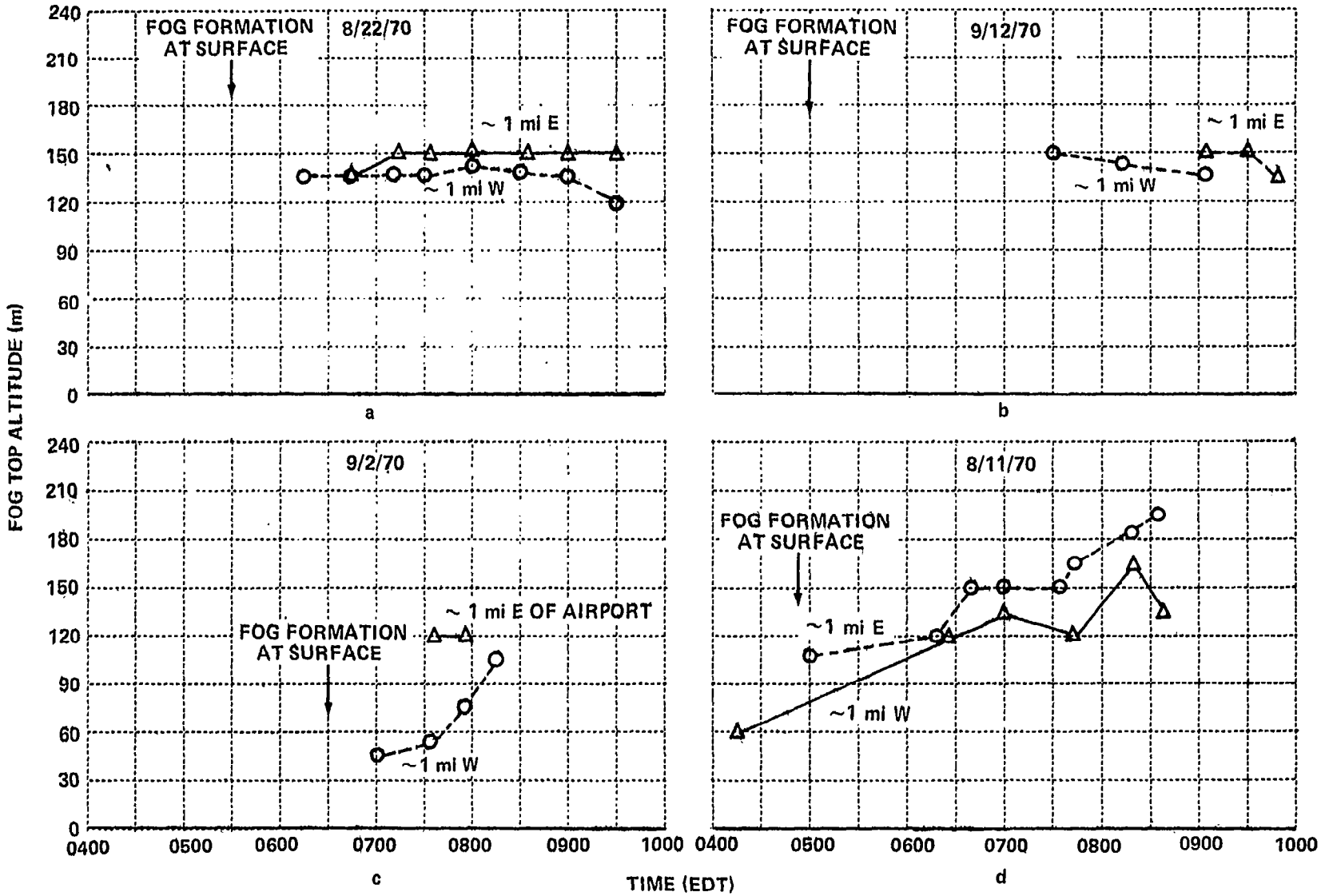

Figure 8 FOG TOP ALTITUDE AS A FUNCTION OF TIME

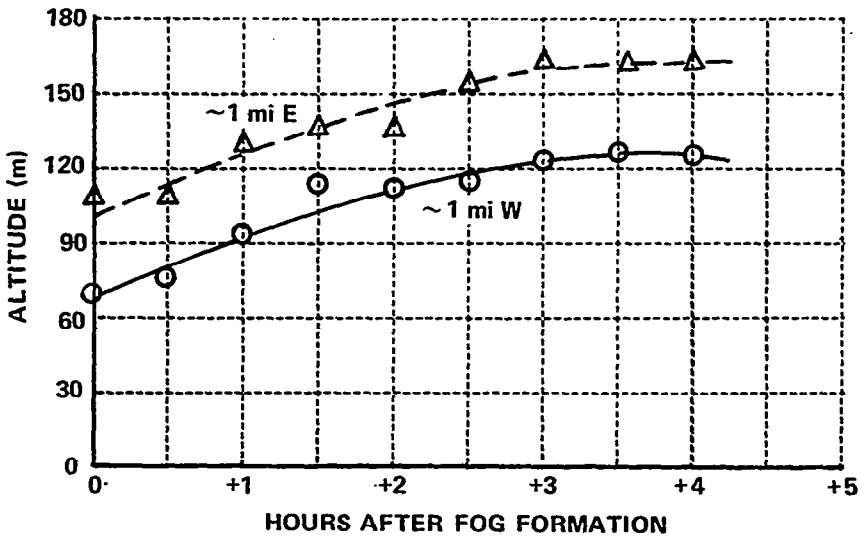

Figure 9 AVERAGE FOG TOP ALTITUDE AS A FUNCTION OF TIME AFTER FORMATION

1. Continuous recordings of temperature at the 1 m, 3 m, and 17 m levels using the Foxboro system.*

2. Manual observations at half-hour intervals using secondary standard mercury thermometers at the ground level (thermometer pressed onto matted grass) and at the 0.1 m level.

On several occasions during the six-week field program, the Foxboro system was calibrated against the secondary standard thermometers. The calibrations were performed in fog and on cloudy days by temporarily mounting the secondary standards at each resistance probe level and comparing manually observed temperature with the strip chart recordings. After appropriate fixed corrections were applied to the records, agreement was within 0.2°C absolute and within 0.1°C (relative) for a single resistance probe over periods of hours. Although intercomparisons of the secondary standards were always consistent to within 0.1°C, the proximity of the observer caused indicated temperature at the 0.1 m level to increase at a rate of a few tenths of a degree per minute whenever near calm winds existed. With the care taken in the field, we believe that errors due to this effect were limited to 0.2°C. In general, therefore, we estimate that all relative temperatures are good to ±0.2°C on a given day.

Temperatures were taken from the strip charts at half-hour intervals from the time observations began (usually between 2000 and 2300 EDT on night preceding the fog) and plotted with the surface and 0.1 m data against time. Typical data are presented in Figures 10 and 11 (22 August 1970 and 12 September 1970) for persistent fog and Figure 12 (2 September 1970) for fog that formed after sunrise. Several pertinent and consistent features may be noted from these curves.

In general, the low level inversion formed shortly after sunset and persisted with minor fluctuations in intensity (associated mainly with wind fluctuations) until the fog formed. With the exception of 2 September 1970, 12 September 1970, and very briefly on 26 August 1970, the inversion was

*Dyatherm Resistance Bulb Model DB-21B-226W and Recorder Model ERB.

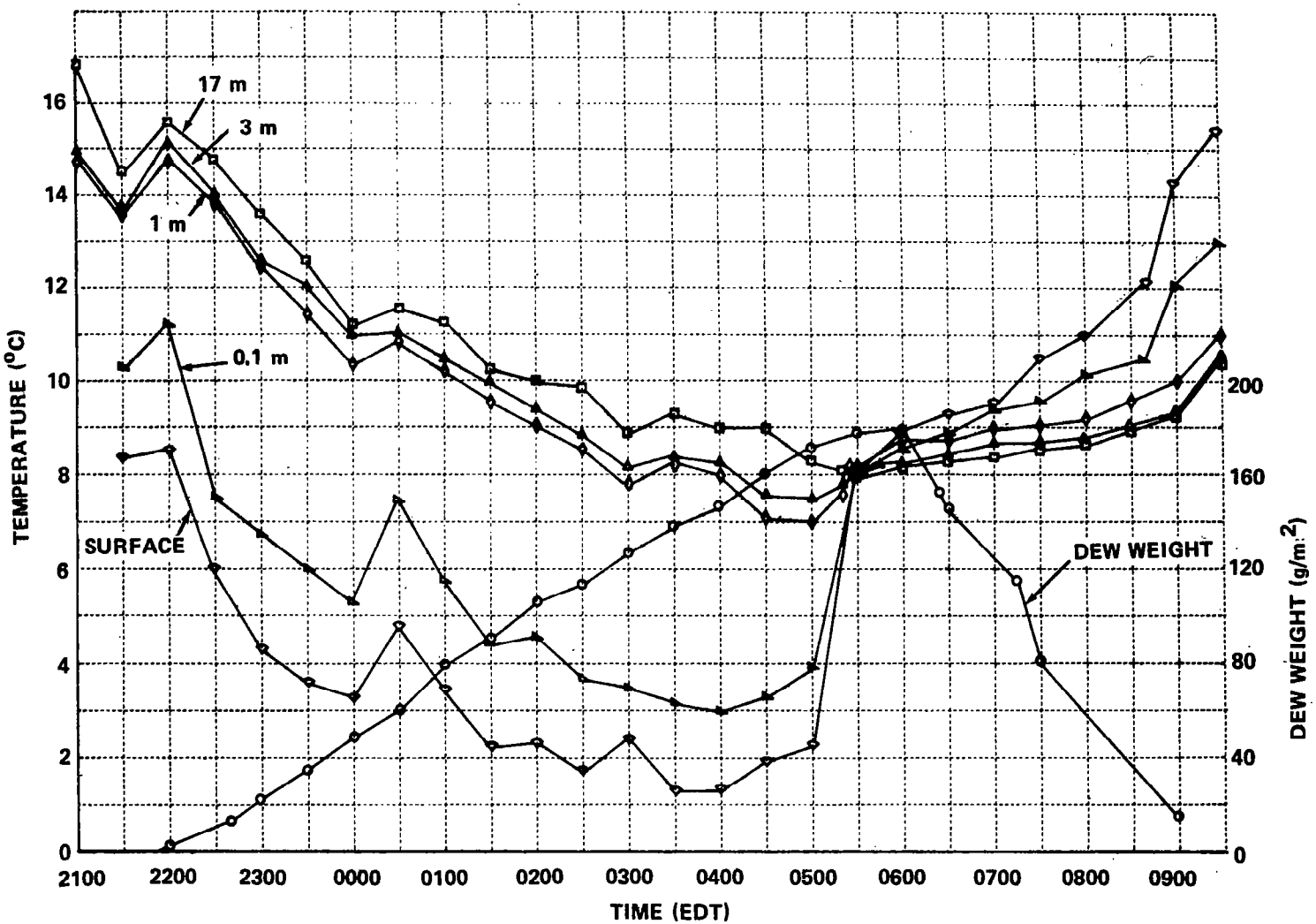

Figure 10 TEMPERATURES AND DEW AS FUNCTIONS OF TIME 8/22/70

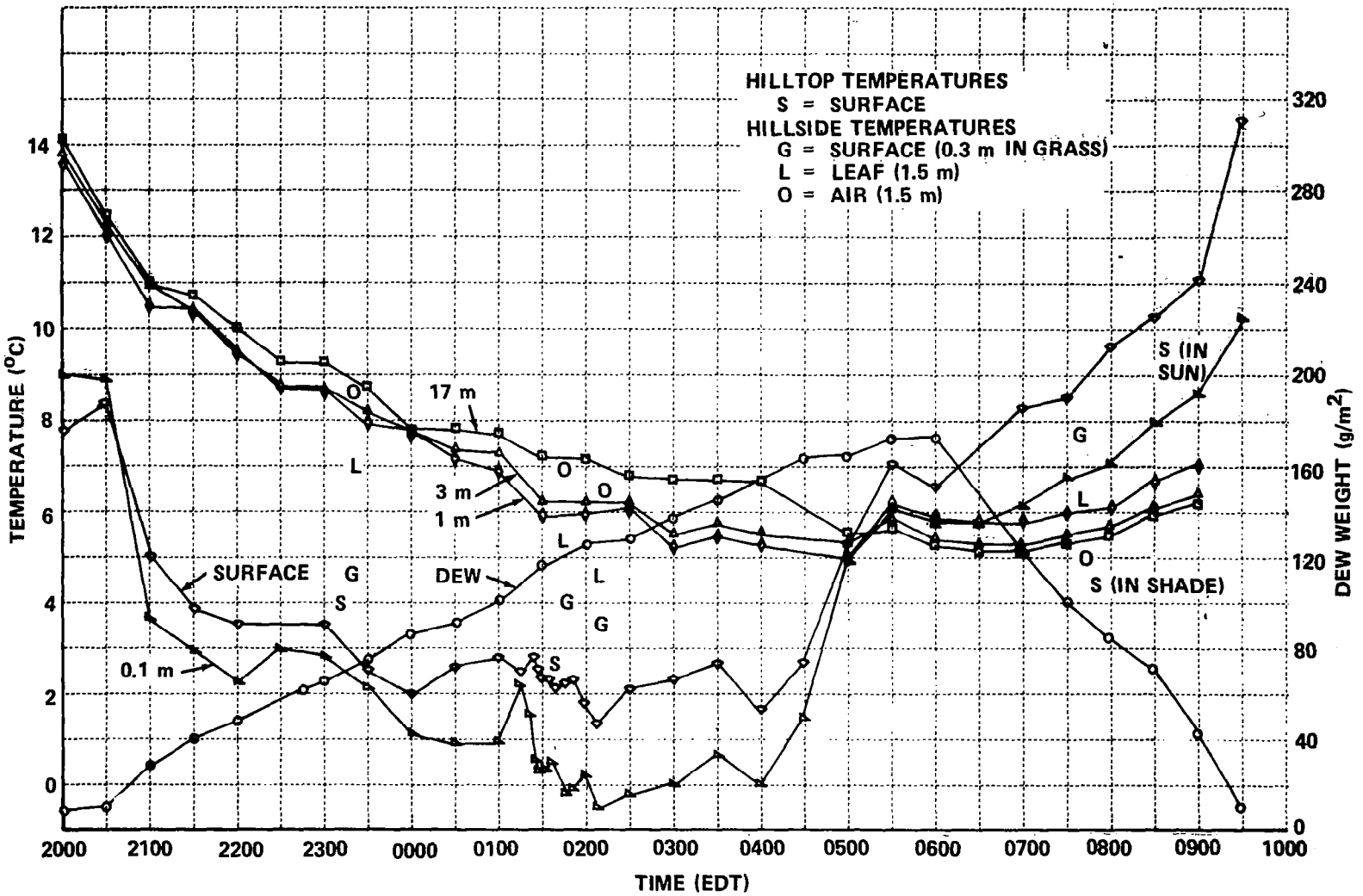

Figure 11 TEMPERATURES AND DEW AS FUNCTIONS OF TIME 9/12/70

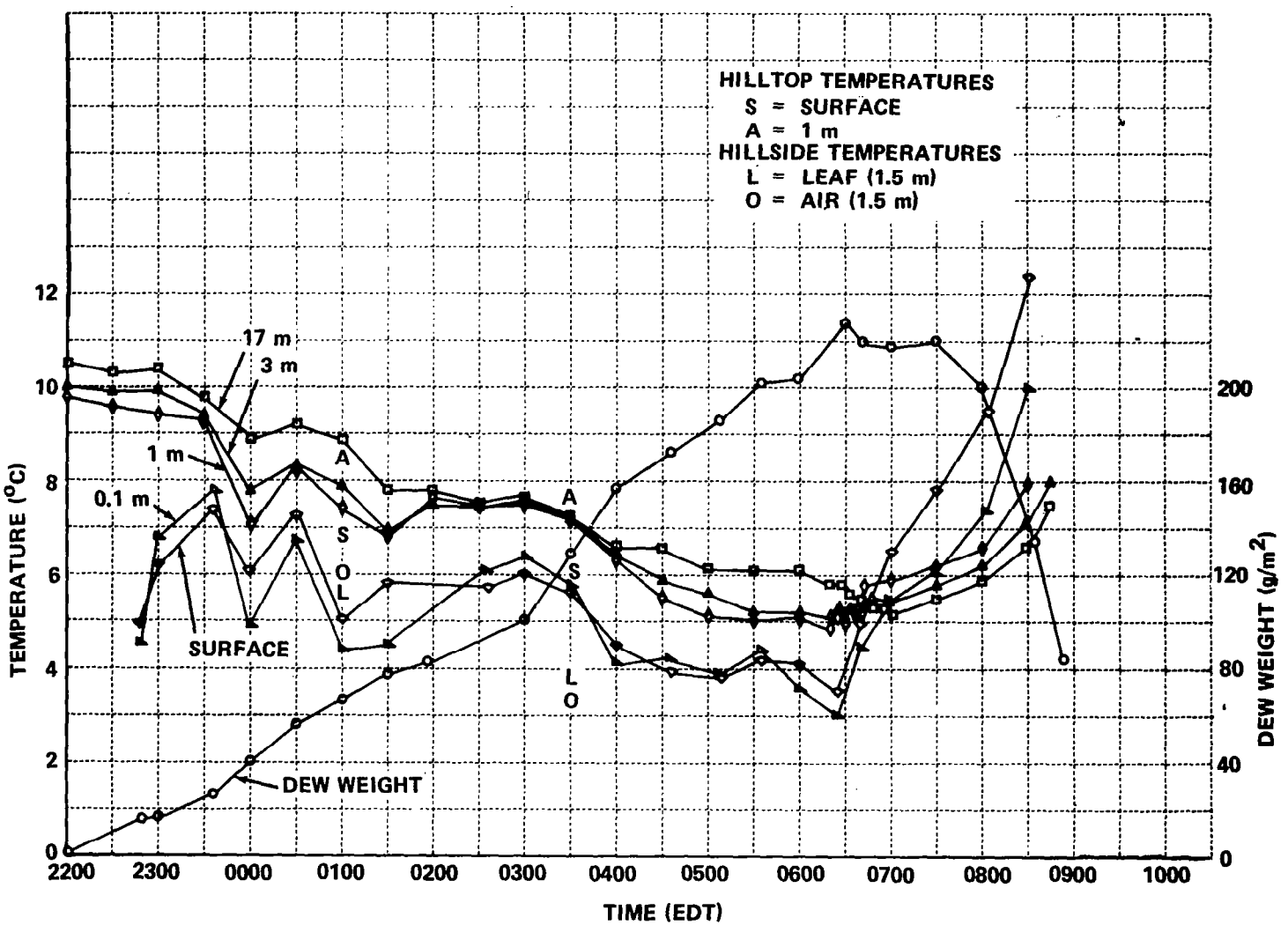

Figure 12 TEMPERATURES AND DEW AS FUNCTIONS OF TIME 9/2/70

most intense in the lowest 0.1 m and decreased in intensity to the 17 m level. The exceptions are illustrations of the "raised minimum" (Geiger, 1965, Chapter II) in temperature which often occurs on calm evenings.

Typically, between one hour and one-half hour before fog formation, the surface and 0.1 m temperatures began increasing rapidly. About one-half hour before fog formation, the 1 and 3 m temperatures began increasing and, on occasion, the 17 m temperature began decreasing slightly. At the time of fog formation, the low level inversion broke and a superadiabatic temperature lapse rate formed below 17 m. Between the time of fog formation and sunrise, low level temperatures remained approximately constant. Within a half hour after sunrise, the surface temperature began increasing rapidly and, with time lags that increased with height, all low level temperatures followed the same pattern. The post-sunrise surface heating occurred even with fog depths exceeding 150 m.

In the pre-fog period, temperature fluctuations of two to four degrees within a half-hour interval often occurred at the surface and 0.1 m levels. At times, these fluctuations were also noted at tower levels as illustrated in Figure 10 at 2200 EDTand 0030 EDT. These fluctuations were occasionally associated with wind speed fluctuations but most often were not explained.

Because of the consistency of the low-level temperature behavior on fog nights, a meaningful description of this behavior can be made in terms of averages and departures from the averages. Since the major change in vertical temperature distribution occurred at the time of fog formation, the initial averages were computed for times relative to the time of fog formation. Because a secondary change in behavior also occurred at sunrise and actual fog formation time ranged from ten minutes after to more than five hours before sunrise, this procedure masked the sunrise effect. We decided, therefore, to include average time of fog formation, 0530 EDT, in the model fog. Averages were computed from six hours before actual fog formation to one hour after fog formation, and these half-hour averages were arbitrarily assigned times relative to a 0530 EDT fog formation. To account for the post-sunrise effect, differences between the respective

0630 EDT observed temperatures on each day and observed temperatures at subsequent times were averaged. These data were used to shape the temperature vs time curves after sunrise (sunrise occurred at 0630 EDT ±8 minutes throughout the field program). The curves obtained for the first seven-hour interval were then extrapolated according to these shapes to 0930 EDT. Results of this analysis are displayed in Figure 13.

These curves were obtained from data on eight of the eleven fogs sampled. The fog of 14 August 1970 was eliminated because it was atypical in other respects, and complete temperature data were not available for 24 August 1970. Data from the fog of 12 September 1970 were not included initially because the averaging was completed before that fog occurred. Rather than make minor changes in the average values, it was decided to use that case as an illustration of how accurately the averages describe temperature variations associated with early morning fog at Elmira.

The accuracy with which the model fog temperatures portray actual fog temperatures relative to the time of fog formation is illustrated quantitatively in Table II, which shows the extremes of deviation of observed temperatures from model temperatures as a function of time during the eight fogs.

Table II

Extremes of Deviation of Observed
Temperature Relative to Average Temperature

Time (hours)	-6	-4	-2	-1	0	+1	+2	+3
Height								
Zero	2.5°C	2.7°C	1.8°C	2.5	1.2°C	1.5°C	0.6°C	1.2°C
0.1 m	2.4	2.5	2.3	2.2	1.2	0.5	0.2	0.5
1 m	1.6	0.8	0.4	0.7	0	0.3	0.2	0.5
3 m	1.4	0.8	0.4	0.7	0.3	0.3	0.2	0.6
17 m	1.2	0.7	0.4	0.6	0	0.5	0.2	0.4

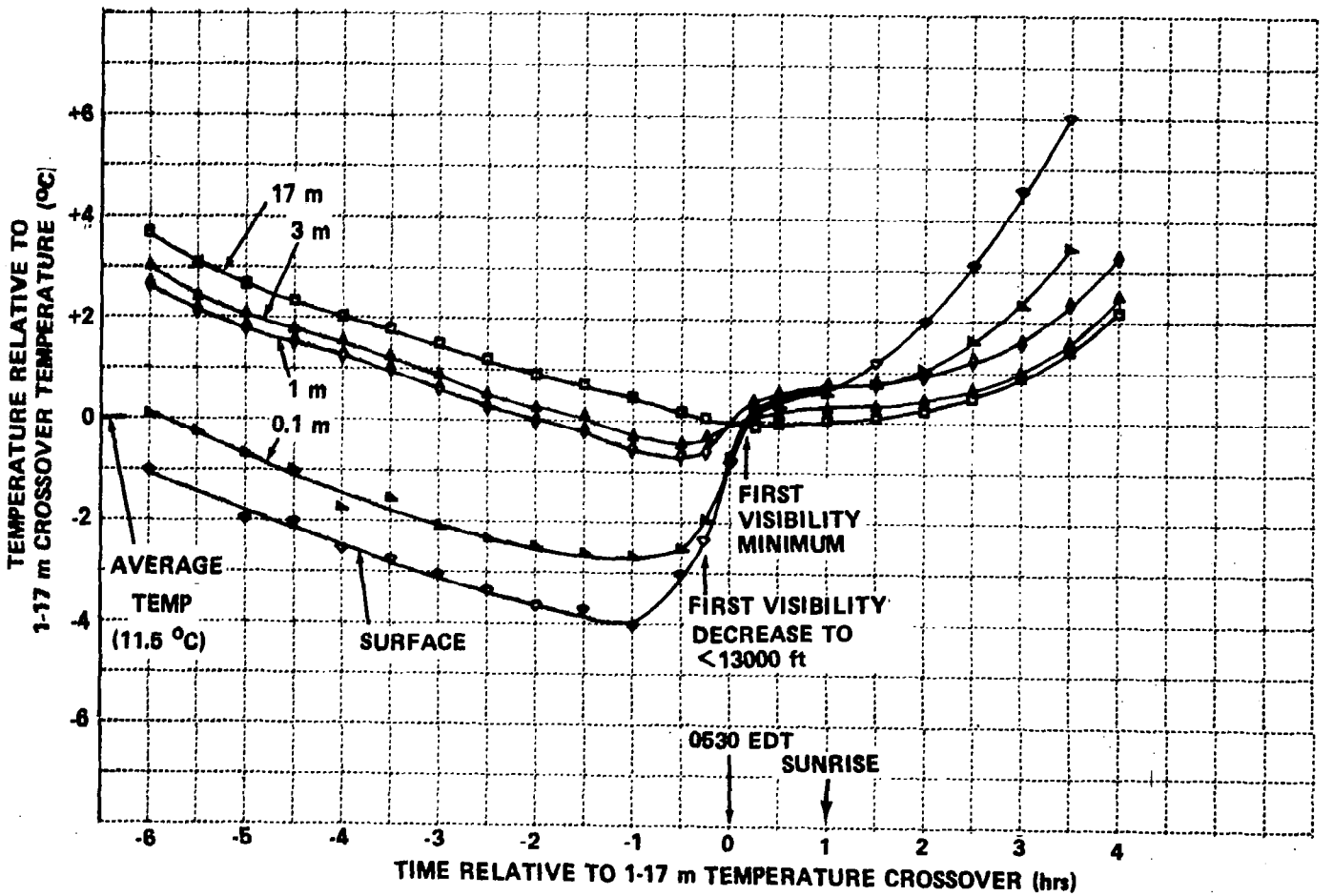

Figure 13 MODEL FOG TEMPERATURES – SURFACE TO 17m

To complete the discussion of the consistency of the model temperatures with actual temperatures, it is important to note that the 1 m-17 m temperature crossover occurred, on the average for these eight fogs, eight minutes after the first measurable visibility decrease and 9.3 minutes before the first visibility minimum. If all fogs are included, these averages increase to 12 and 13.5 minutes, respectively.

So far, the discussion of low-level temperature data has been confined to data obtained at the tower site in the valley. Late in the field program, when we began to suspect that horizontal heat transfer from the center valley region to the hills may be responsible for the initial fog formation aloft, a few measurements were made of low-level temperature on the hillsides and hilltops adjacent to the valley. These measurements were made with laboratory grade mercury thermometers that were semi-permanently installed in convenient locations at the two sites indicated by the symbol ⊗ on Figure 1. The hillside site was a cleared meadow with one-third meter high grass and occasional 1.5 m high brush. Since the hillsides are, in general, covered with a closed forest canopy roughly 10 m above the surface, we are not certain that the hillside data are representative. The hilltop site, a cleared field covered with 10 cm high winter wheat, was representative of most of the hills in the vicinity. Measurements were made with the thermometers taped to the grass at the surface and suspended between 1 and 1.5 m in the air. In addition, the temperature of the highest vegetation was measured on the hillside by wrapping the thermometer in living leaves at the 1.5 m level. The thermometers were calibrated to the nearest half degree.

The data obtained at these sites on 12 September 1970 and 2 September 1970 are presented in Figures 11 and 12, respectively. These are the only data obtained on fog nights; and because of infrequency of measurements, no detailed conclusions can be drawn. In general, it appears that the low-level temperatures at both sites on the hill behave in a manner similar to that noted in the center valley region. Perhaps most important is the fact that in all cases, surface and vegetation temperatures on the hill were significantly lower than air temperatures obtained at low levels at the valley floor. Air temperatures at both hillsites were either equal to or colder than low-level temperatures in the valley.

A number of pertinent characteristics of the model temperatures should be noted, and some conclusions may be drawn.

1. The average rate of temperature decrease, 0.6°C/hr, is constant from zero to 17 m from -6 hours to -1 hour (relative to the time of fog formation).

2. At some time, varying from one-half to one hour before fog formation, the temperatures at the surface and 0.1 m begin to increase. This temperature increase is associated with the decrease of net radiative heat transfer from the surface due to the formation of fog aloft. Similar measurements of low-level warming that accompanies the advent of clouds or fogs were made as early as 1838 (Wells, 1838).

3. The average temperatures of the 1 and 3 m levels begin to increase approximately one-half hour before the 1 m-17 m crossover and continue for one-half hour thereafter. The average temperature at the 17 m level decreases during the half hour prior to the crossover and is essentially constant from that time until after sunrise. The source of heat for the 1 m and 3 m temperature increases must be the air at higher levels during the initial half-hour period. During the last eight minutes of this period, the heat of condensation may contribute to this warming, but calculations based on observed liquid water content at the end of the period indicate that these contributions account for only 0.1°C or approximately 20% of the total change.

There appears to be no logical explanation for the observed temperature variations at the 1 m level after the 1 m-17 m temperature crossover. In particular, we do not understand what can cause the 1 m temperature to remain warmer than the air above and below that level. It is probable that this observed temperature difference is simply a manifestation of the 0.2°C accuracy of the measurements.

4. The temperature distribution in the lowest 17 m between fog formation and sunrise is superadiabatic and almost constant. In some cases, such as on 14 August 1970 (Figure 14) when fog formed long before sunrise, a slight temperature decrease of 0.1 to 0.2°C per hour was observable throughout the entire layer. This, we believe, is due to radiation from the fog top with heat being transferred upward from the surface.

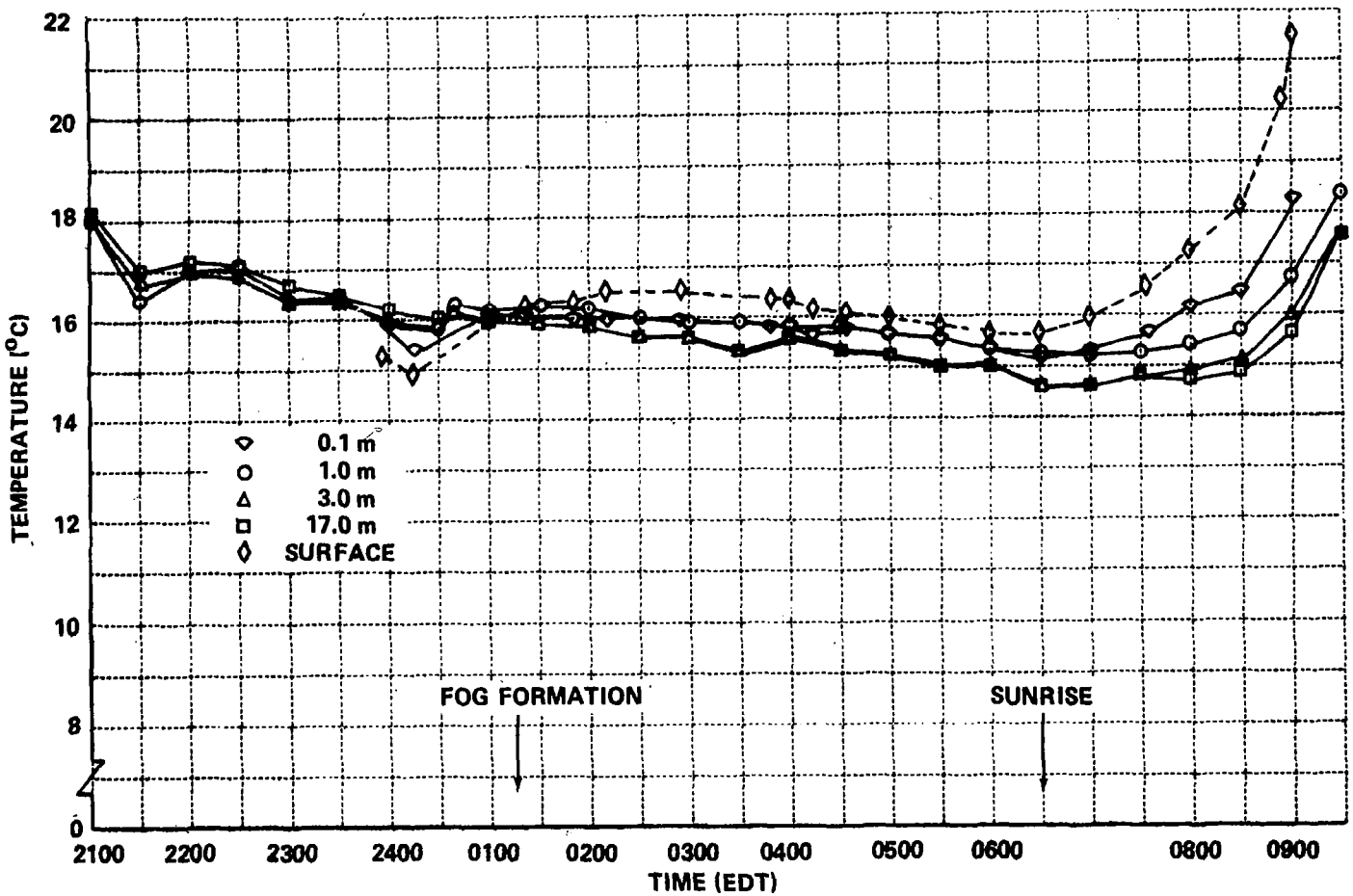

Figure 14 TEMPERATURE AS A FUNCTION OF TIME 8/14/70

5. The surface temperature rises at an increasing rate after sunrise and, as mentioned earlier, all low-level temperatures follow with time lags that increase with height. During this time, heat is being transferred from the ground to the air.

6. Low-level temperatures on the hillsides and at the hilltops behave in a manner similar to that observed in the center valley region. Surface temperatures at the hillsides and hilltops are colder than low-level air temperatures in the center valley region.

- Temperature Aloft

Temperature measurements at levels above 17 m were made from the CAL Aztec using a thermocouple mounted in a reverse-flow housing. These data and simultaneous data on pressure-altitude and indicated air speed were recorded digitally* at 0.4 second intervals. The raw data were processed in the IBM 360/65 computer to correct for dynamic heating and provide readouts of five-second averages at each altitude. The least count of the altimeter was approximately 10 m. Depending on rate of climb, one to three five-second averages were obtained over each altitude increment.

The reverse-flow housing was constructed according to the Pennsylvania State University design (Hosler et al., 1966). Dynamic heating corrections were applied in accordance with the wind tunnel calibration of this design described by Kelley and Breon (1967).

Subsequent to the completion of these experiments, the reverse-flow housing installation on the Aztec was calibrated in clear air against a Rosemont total temperature probe** in an attempt to resolve a hysteresis effect noted when comparing data acquired on sequential ascent and descent soundings at Elmira. This calibration indicated that the reverse-flow probe provides correct temperature measurements to within ±0.5°C during descent and level flight but revealed an angle of attack problem that produced

*Metro Data Systems Model DL620

**Model 102

absolute errors up to 2°C during ascent operations. Consequently, only data obtained during descent were used in the following analysis.

The data obtained on 22 August 1970 and 2 September 1970, presented in Figure 15, are typical of those obtained throughout the program. Note that all post-fog profiles extend to approximately the 60 m level where the aircraft took a waveoff because of limited ceiling. Extrapolation of the aircraft data to the surface invariably agreed with tower data to within ±0.5°C. On one occasion, 13 August 1970, visibility within the fog was sufficiently good to permit touch-and-go landings and provided an opportunity for direct comparison of aircraft and tower temperatures at the same altitude in fog. These data (separated for clarity) are presented in Figure 16 in lieu of data from 12 September 1970. (The aircraft configuration was altered prior to the 12 September experiment and temperature data were not recorded.)

Several pertinent features of these profiles are worth comment. Note that in each case, the maximum cooling rate in the last six hours before fog formation occurred at an altitude of approximately 100 m. Note also that, with the exception of the 0809 profile on 2 September 1970, all post-fog profiles show unstable temperature distributions at low levels changing to neutral and then stable distributions in the upper levels of the fog. In the exception noted, the fog top was at 50 m, the height of the lowest data point in the aircraft profile. In each of the cases shown, the steepest part of the inversion is slightly above the level of the fog top.

Because of the relatively few profiles obtained on most fog nights, we did not attempt to plot time histories of temperature with height on a nightly basis. Instead, in view of the excellent reproducibility of temperature vs time data obtained at low levels, we combined data from all fogs to extend the temperature model upward. The results are presented in Figures 17 and 18, with the dates of observation used as the symbols for each data point. As with the low-level temperature data, the pre-sunrise data are normalized to the time and temperature of the 1 and 17 m temperature crossover. Post-sunrise data are plotted in real time.

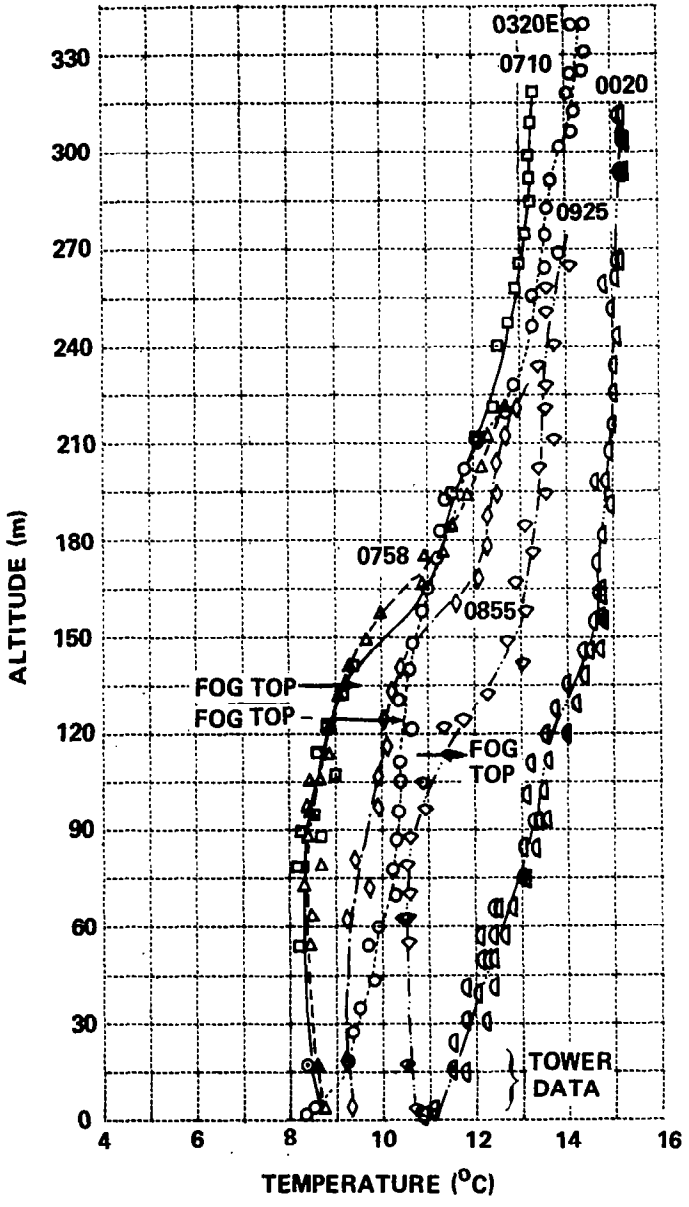

Figure 15a TEMPERATURE ALOFT 8/22/70

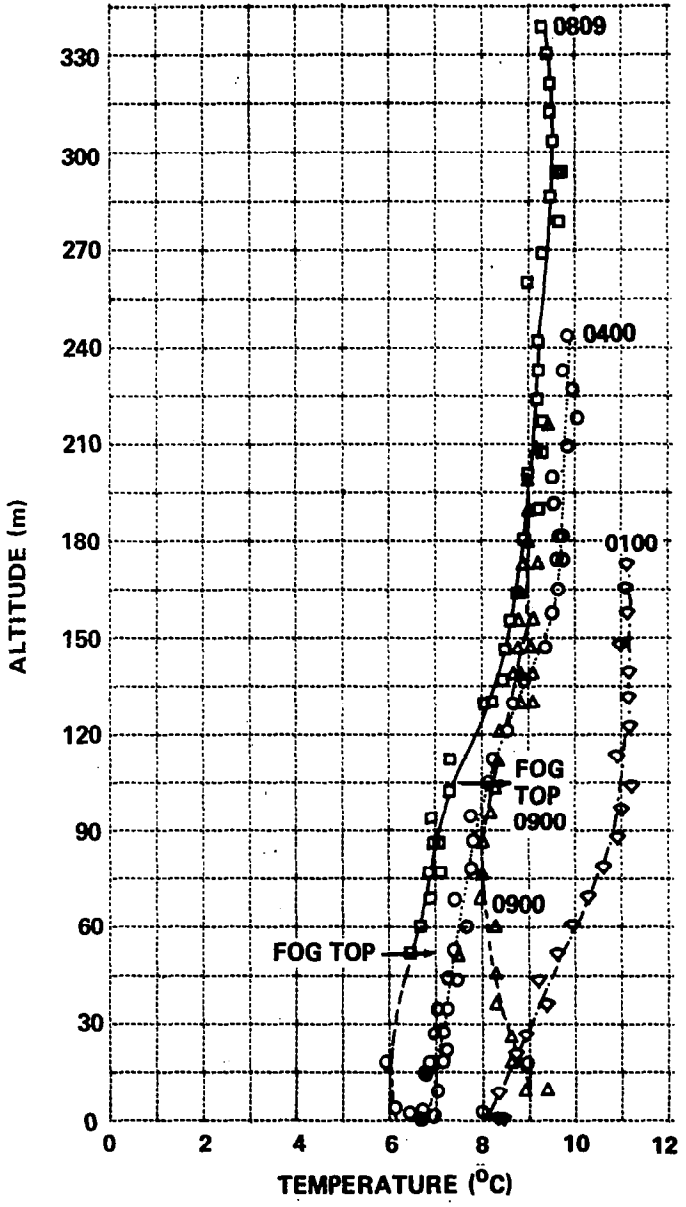

Figure 15b TEMPERATURE ALOFT 9/2/70

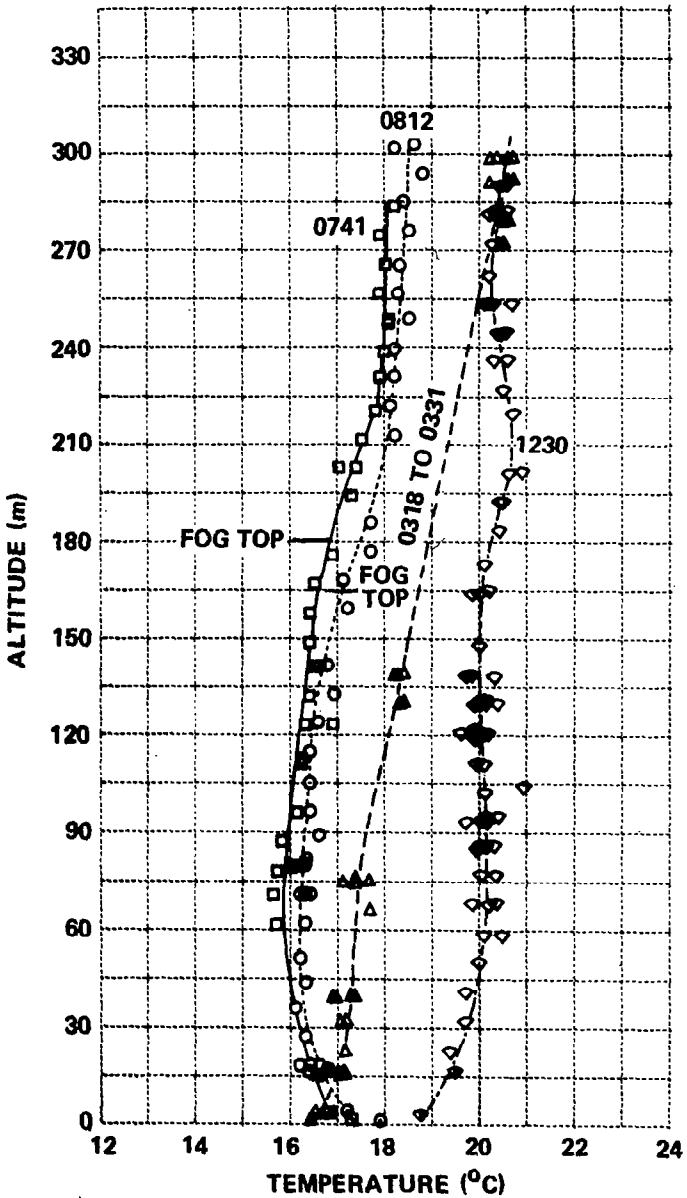

Figure 16a TEMPERATURE ALOFT 8/13/70

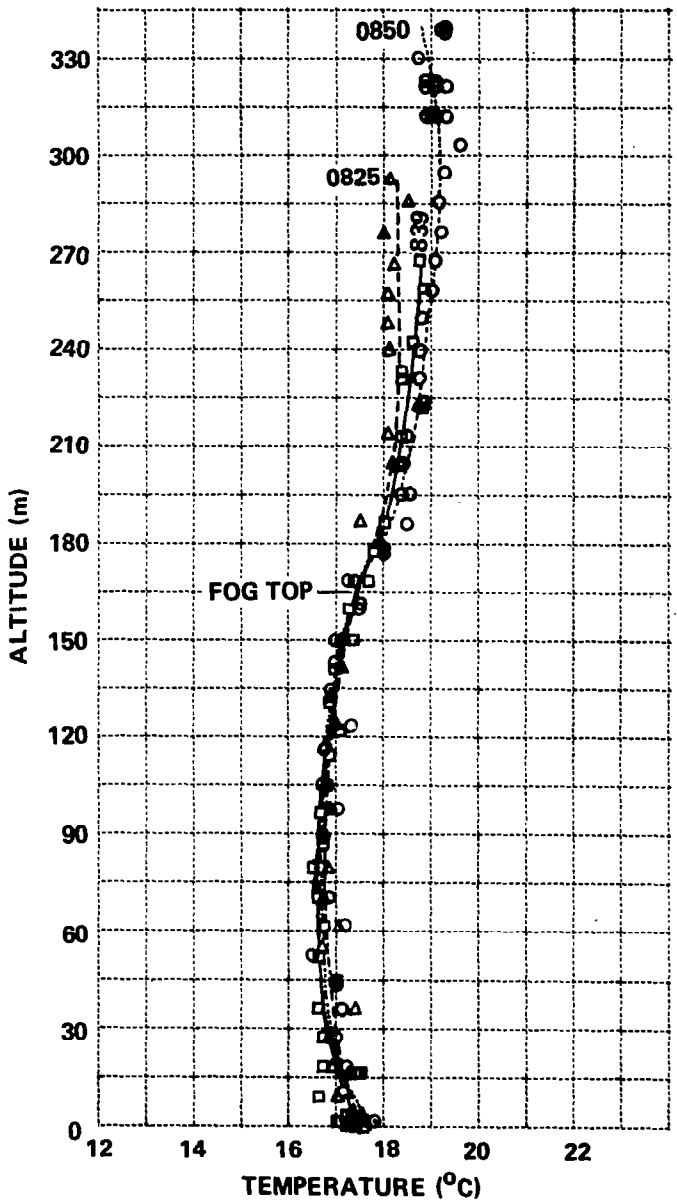

Figure 16b TEMPERATURE ALOFT 8/13/70

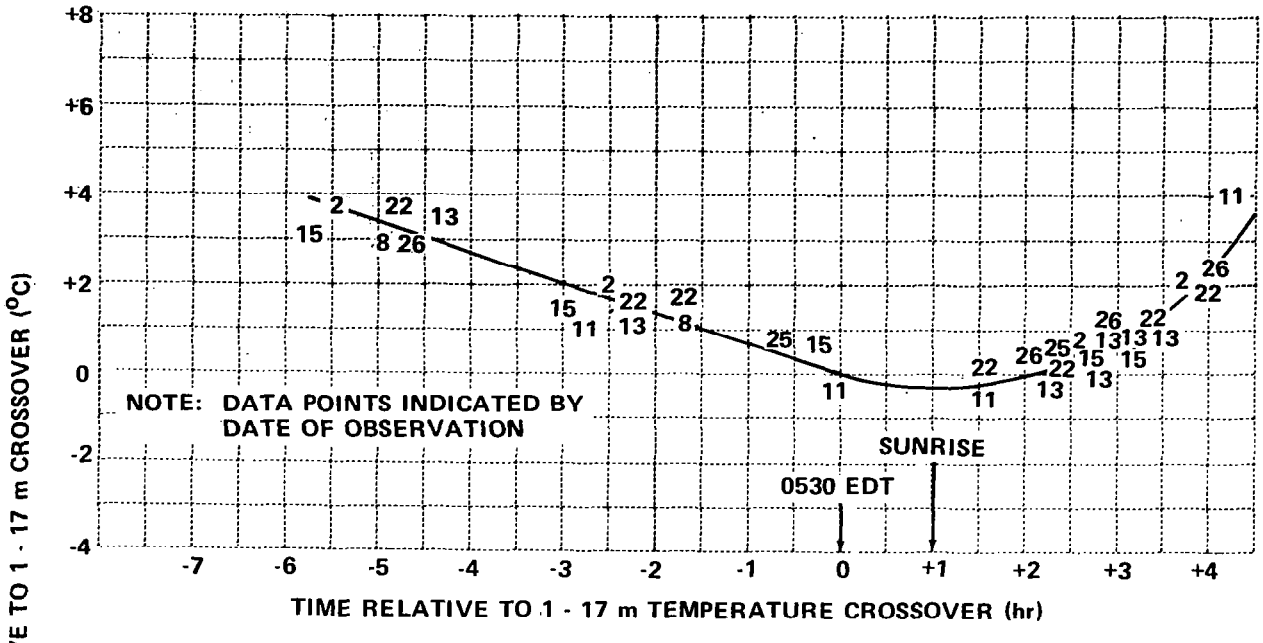

(a) MODEL FOG TEMPERATURE – 30 m LEVEL

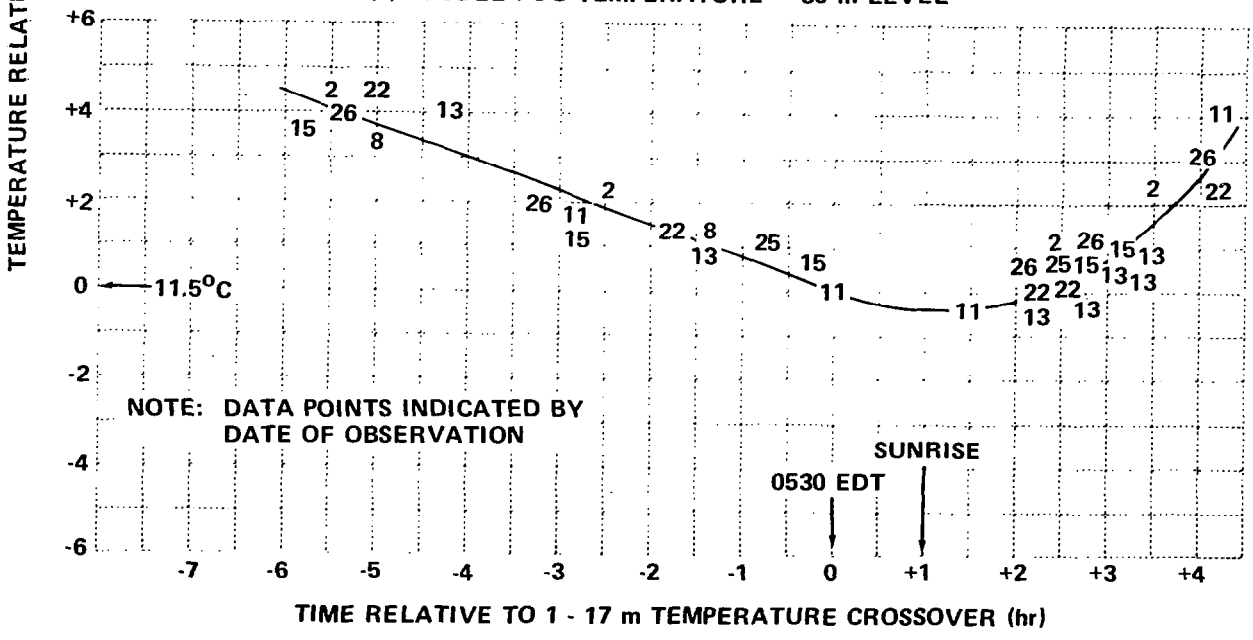

(b) MODEL FOG TEMPERATURE – 60 m LEVEL

Figure 17 SUMMARY OF TEMPERATURES AT 30 AND 60 m AS A FUNCTION OF TIME (8 FOGS) (CORRECTED FOR SUNRISE EFFECT)

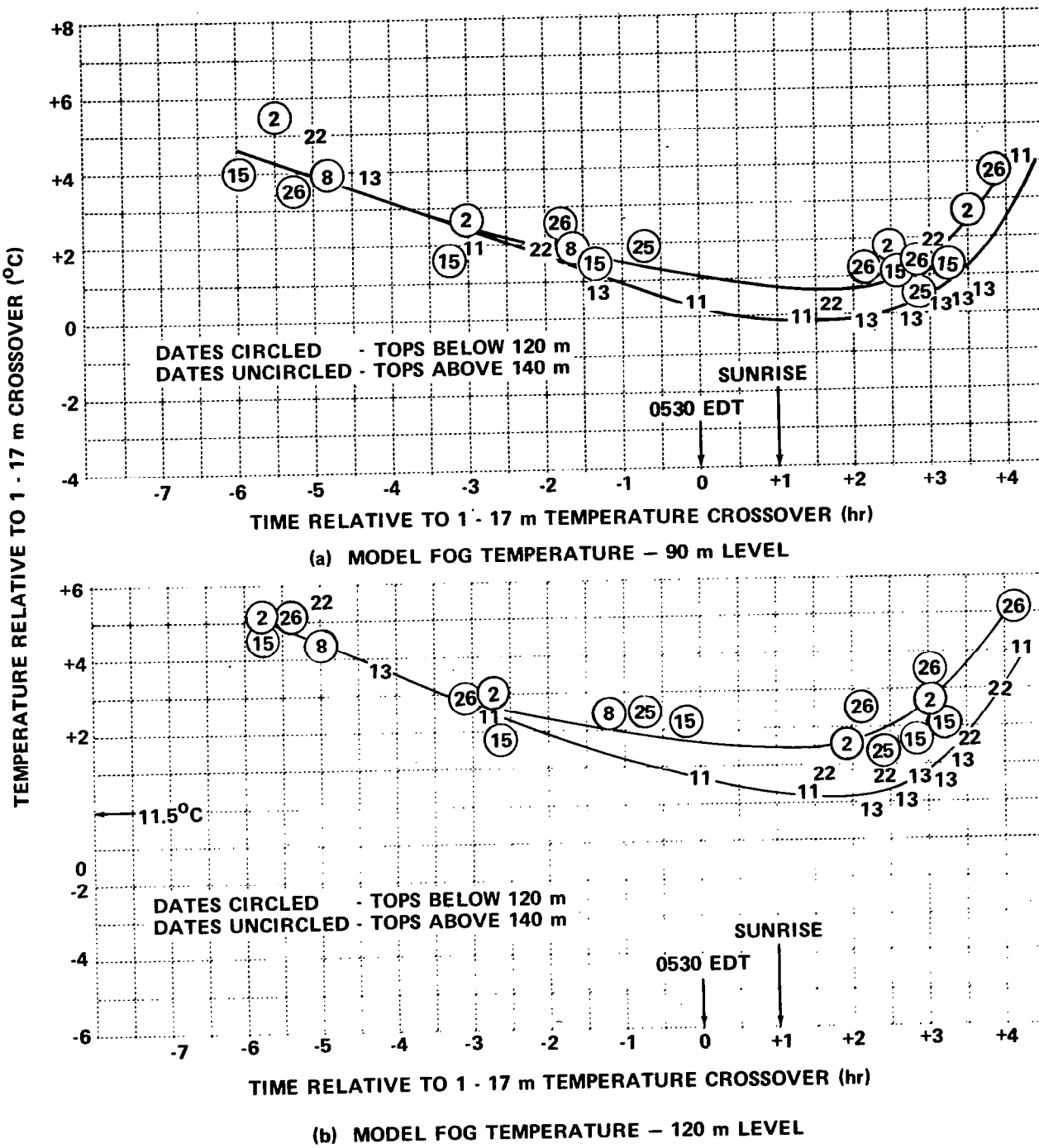

Figure 18 SUMMARY OF TEMPERATURES AT 90 AND 120 m AS A FUNCTION OF TIME (8 FOGS) (CORRECTED FOR SUNRISE EFFECT)

It is apparent from Figure 17 that the consistent temperature behavior noted in the low-level data persists to at least the 60 m altitude. No data point differs from the best mean fit by more than 1.5°C. Substantially greater spreads are evident in the data for 90 and 120 m shown in Figure 18. Here, the data are split into two groups, with normalized temperatures for 11, 13, and 22 August averaging more than a degree colder than those of other dates. Examination of other data shows that the temperature grouping is consistent with a grouping of the data in accordance with fog height. With the exception of a single observation in one fog, the maximum height of the fog on each of the circled dates in Figure 18, representing the warmer group, was less than 120 m while the maximum height of the fog on each of the uncircled dates, the colder group, exceed 150 m. Apparently, the maximum pre-fog cooling rate occurs at a level which is slightly below (about one-third of the eventual fog depth) the eventual fog top, and from the convergence of the data, the atmosphere beneath that level is very nearly isothermal at the time of fog formation.

Attempts to perform this kind of analysis for altitudes above 150 m were fruitless because of the wide scatter in the data. In the belief that this scatter may be associated with the wide distribution of height of the fog top, we examined the temperature distribution about the fog top. Results are presented in Figure 19. It is apparent that the distributions are all reversed "S" shaped with the point of inflection within 15 m of the fog top. For a given fog, the steepness of the inversion remains approximately constant with time, but there is significant variability from fog to fog. The average strength of the inversion at fog top is approximately 2.5°C per 100 m.

- Summary of Temperature Data

The results of these various analyses of temperature distribution with time are summarized in the family of temperature profiles presented in Figures 20 and 21. The curves shown in Figure 20 were obtained by replotting points taken from the curves in Figures 11, 17, and 18. In Figure 21, the data for lower levels were obtained from Figures 11, 17, and 18, and the data for upper levels were obtained by averaging the data at each height in Figure 19 and faired into the lower curves.

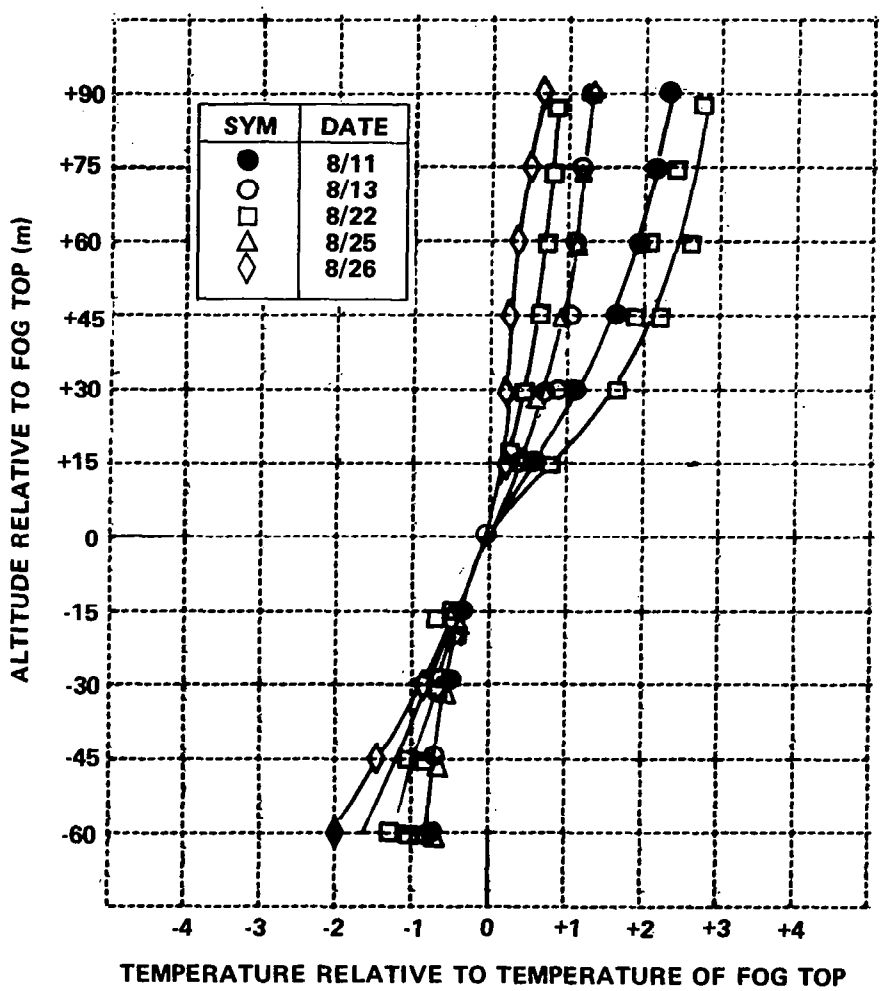

Figure 19 VERTICAL DISTRIBUTION OF TEMPERATURE RELATIVE TO TEMPERATURE OF FOG TOP

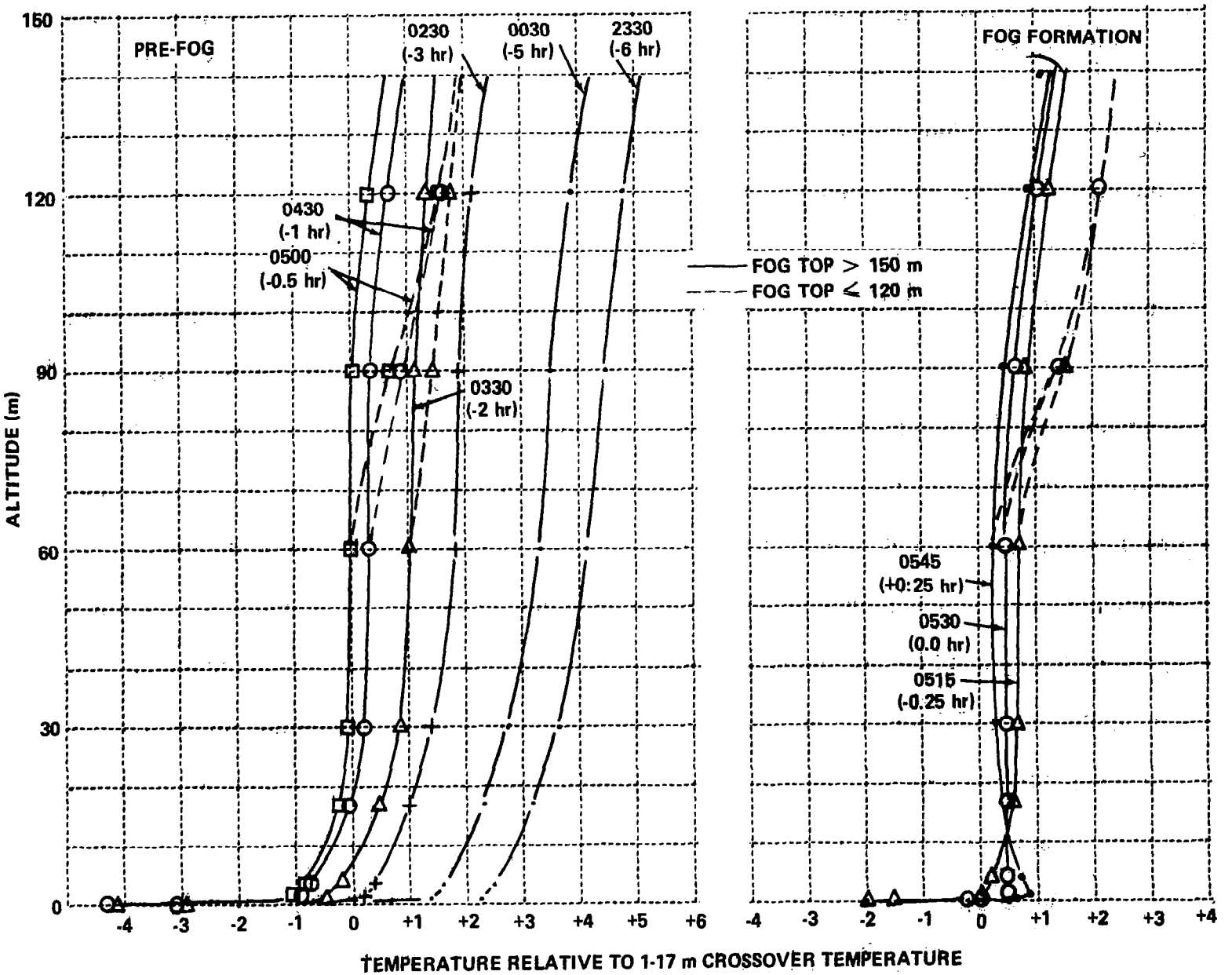

Figure 20 MODEL TEMPERATURE PROFILES – PRE-FOG AND FOG FORMATION PERIODS

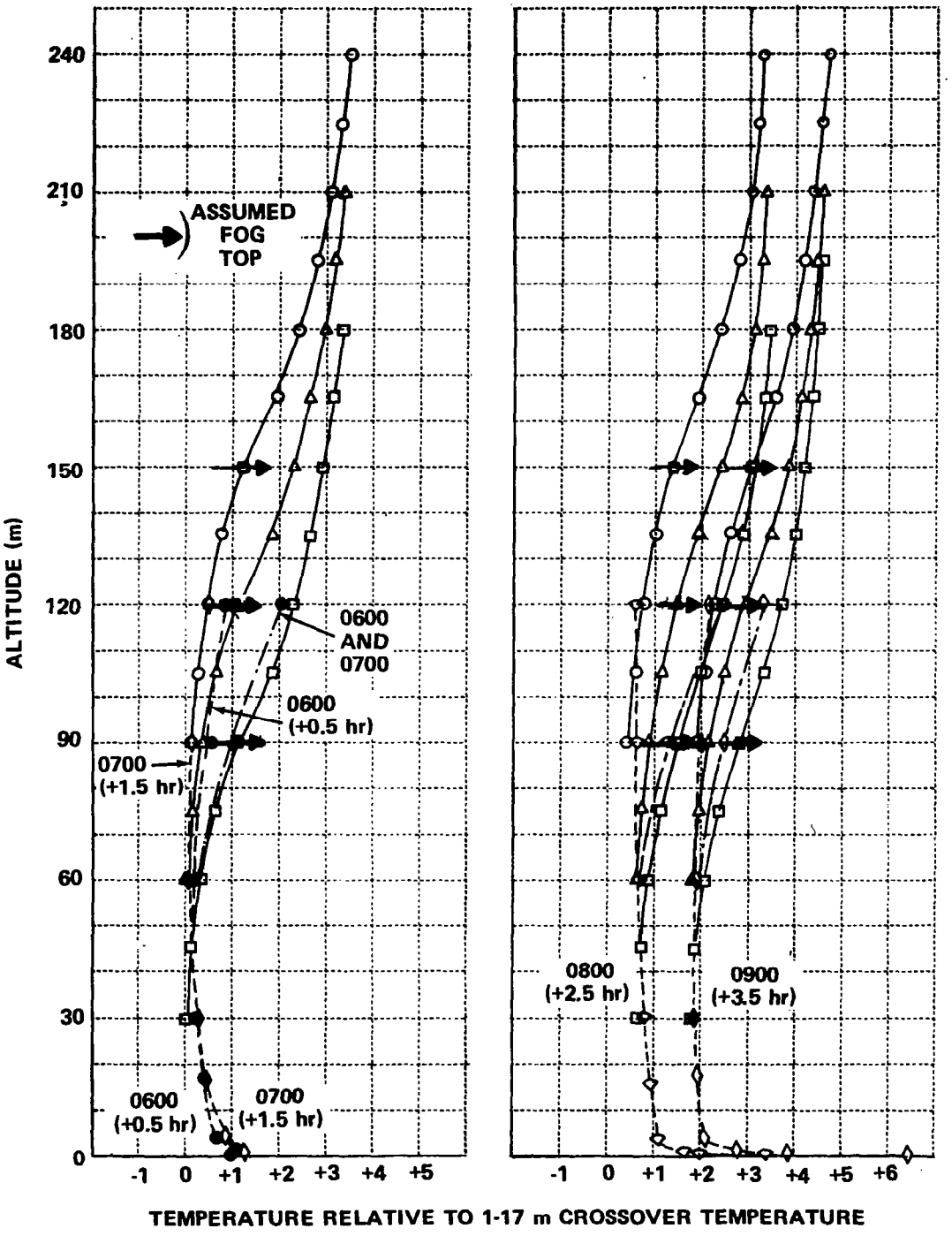

Figure 21 MODEL TEMPERATURE PROFILES IN FOG

Average curve from Figure 19 adjusted in height to correspond to three possible fog top heights (arrows) and faired into curves obtained from Figures 13, 18 and 19.

The important information evident from this presentation is as follows:

1. The intensity of the pre-fog inversion gradually decreases between 30 and 90 m altitudes during the last six hours before fog formation. At lower levels, the inversion intensity remains about constant until approximately one-half hour before fog formation.

2. During the last half hour before fog, the low-level inversion breaks. At the time of fog formation, the atmosphere is approximately isothermal in the lowest two-thirds of the fog depth. The temperature is inverted at higher levels.

3. Within 15 minutes after fog formation, temperature distribution in the lowest 17 m becomes superadiabatic; and above that level, it is approximately wet adiabatic through the lowest two-thirds of the fog depth. An inversion, with maximum intensity slightly above the fog top, exists at higher levels. This condition persists without significant change until sunrise. Surface warming after sunrise causes the temperature lapse to increase at low levels until fog dissipation. Similar observations of the existence of a near wet adiabatic lapse rate in fog have been reported by Fleagle et al. (1952) and Heywood (1931).

4. The rate of temperature increase of the fog after sunrise increases from 0.2°C/hr in the first hour, to 0.7 and 1.2°C/hr in the second and third hours, respectively.

Other pertinent conclusions which are more evident in earlier presentations are:

1. The surface and low-level temperatures decrease at a constant average rate of 0.6°C/hr until one hour before fog formation. Between one-half and one hour before fog, the surface temperature begins to increase rapidly. Shortly thereafter, warming begins in the lowest 3 m of atmosphere but cooling persists at higher altitudes until the atmosphere in the center-valley region is isothermal.

2. Between the time of fog formation and sunrise, the temperatures at the surface and all levels of the fog remain constant or decrease at the same very low rate of 0.1 to 0.2°C/hr.

3. Surface heating begins immediately after sunrise and increases with time. Low-level temperatures follow with time lags that increase with altitude. Above 17 m, the temperature of the entire fog increases at the same rate.

4. A substantial horizontal temperature gradient exists between the center-valley region and the adjacent hills at the same level.

- Low Level Dew Point Data

Dew points were measured at the 1 m, 3 m, and 17 m levels and the data recorded continuously using a Foxboro dew point measuring system.* Before entering discussions of the data validity, it is necessary to illustrate certain characteristics of the records that are typical for different times in the fog life cycle. These illustrations are presented in Figure 22.

A consistent pattern of short-period (2- to 10-minute) fluctuations in indicated dew point that is characteristic of all outdoor records is evident in the samples shown in Figure 22. The fact that many of the indicated fluctuations are correlated on the three separate instruments indicates that in many cases at least the fluctuations are real. It is apparent, however, that in order to obtain representative values for a given time interval, some form of averaging is required. For ease in data reduction, we elected to do the averaging over 7.5-minute intervals by eye. With the care taken in the data reduction, we believe that data points presented in subsequent figures represent the true average of recorded data to $\pm 0.25^{\circ}C$.

When the three dew cells are operated simultaneously in our 600 m^3 experimental chamber, the records show none of the fluctuations that are characteristic of the field environment. By altering the amount of ventilation to the dew cells with a 48-inch fan, short-term fluctuations amounting to approximately $1/2^{\circ}C$ can be induced. The three dew cells always agree to within $0.25^{\circ}C$ when operated simultaneously in the chamber. In a relative sense, therefore, the data presented are quite accurate.

*Model 2701 RG Dynalog Dewcel Element and associated electronics with ERB 6 Multipoint Recorder.

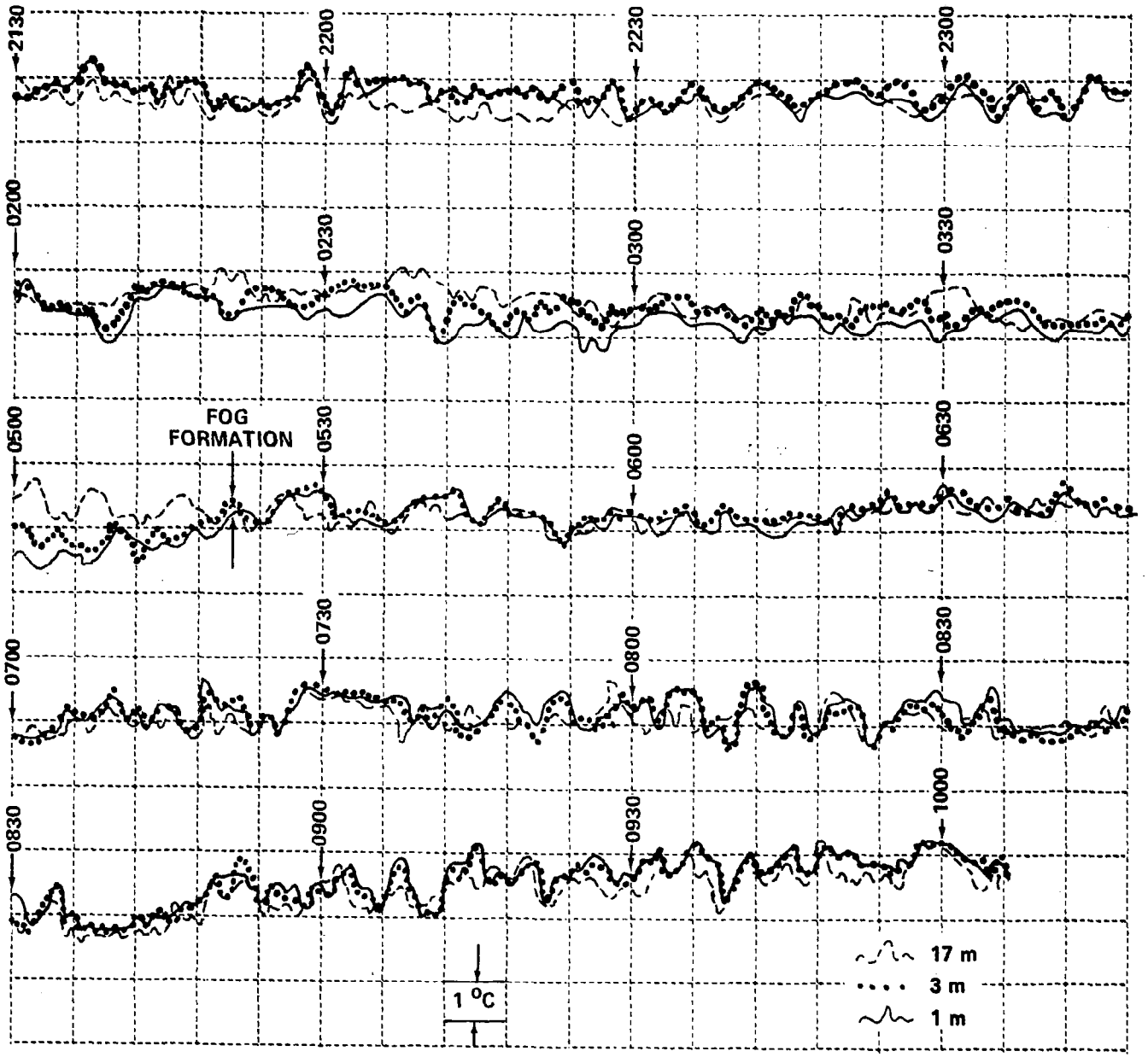

Figure 22 TRACINGS OF TYPICAL DEW POINT DATA AT DIFFERENT TIMES IN FOG LIFE CYCLE (8/21 - 22/70)

The Foxboro system was factory calibrated about a year before going into the field. Attempts to obtain absolute calibrations in the field using wet and dry bulb thermometers usually resulted in agreement to within the recorded dew point fluctuations that were occurring at the time. Because of these fluctuations, and because of the inherent insensitivity of the wet and dry bulb method at very high humidities, we suspect that the Foxboro system provided the best measurement of humidity available to us in the field. Perhaps the best indication of the absolute accuracy of this system rests in the observation that the mean difference between indicated temperature and indicated dew point at the time of fog formation was $0.3^{\circ}C$ for the eleven cases available. The maximum indicated difference was $1.0^{\circ}C$ and in all other cases the difference was less than $0.6^{\circ}C$. Purely on the basis of internal consistency of the data, it appears that the dew points are accurate to $\pm 0.5^{\circ}C$ in an absolute sense and probably better in a relative sense.

Typical dew point data reduced in the manner described above are presented in Figures 23, 24, and 25, which correspond to the temperature data presented in Figures 10, 11, and 12, respectively. From these data sets, it is apparent that there is a gradual decrease in dew point at low levels in the first few hours after sunset, but no consistent change of dew point with height is evident until near midnight. At about midnight, a rather consistent dew point inversion forms and, with the exception of short-term fluctuations that appear to be associated with short-term wind fluctuations and surface temperature increases, gradually increases in intensity until approximately one-half hour before fog formation. At that time, probably because of the sharp increase in surface temperature, the dew points at the 1 m and 3 m levels begin to increase rapidly.

As with the temperature inversion, the breakdown of the dew point inversion is complete at the time of the first visibility minimum. From that time until sunrise, the dew point fluctuates about a constant value and thereafter, until fog dissipation, the dew point increases gradually. As evident in Figure 22, the period and magnitude of short-term fluctuations

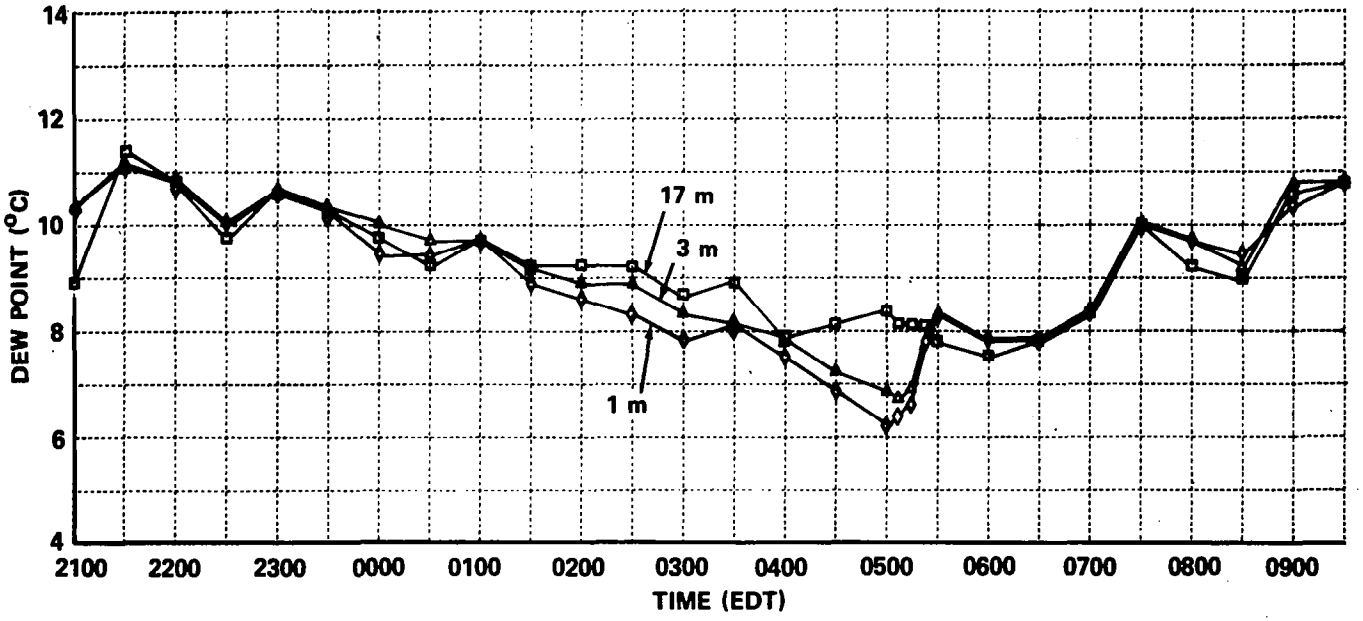

Figure 23 DEW POINTS AS FUNCTIONS OF TIME 8/22/70

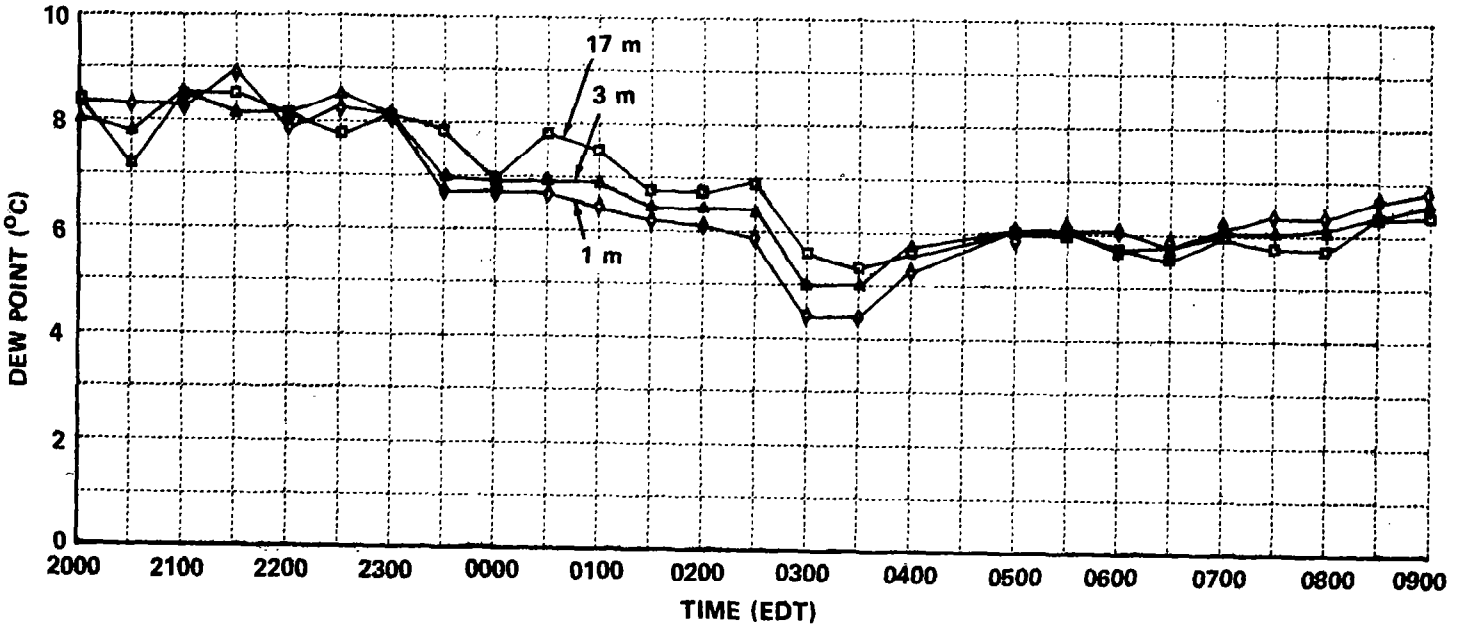

Figure 24 DEW POINTS AS FUNCTIONS OF TIME 9/12/70

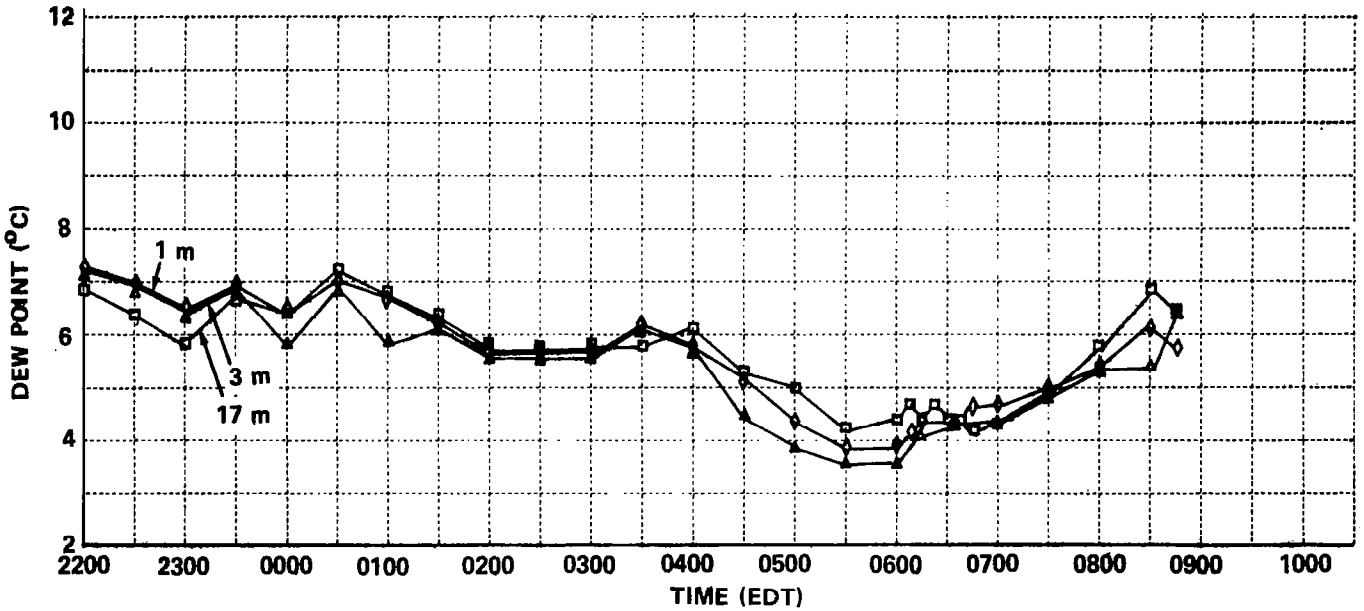

Figure 25 DEW POINTS AS FUNCTIONS OF TIME 9/2/70

decrease significantly immediately after fog formation. With the gradual increase in dew point that follows, these fluctuations also increase and achieve maximum magnitude at about the time fog dissipates.

This typical behavior is summarized in the dew point model presented in Figure 26, which was constructed according to the same rules used for constructing the low-level temperature model; i.e., averages were computed from six hours before actual fog formation to one hour after fog formation for each half-hour interval. These averages were arbitrarily assigned times relative to a 0530 EDT fog formation. To account for the effect of sunrise, the differences between dew point at 0630 and that at each subsequent time were averaged to obtain the shape of the curves after sunrise. The curves obtained for the first seven-hour interval were then extrapolated according to these shapes.

The model indicates that on the average the dew point inversion is already established in the lowest 3 m six hours before fog formation but that dew points are nearly equal at 3 m and 17 m until three to four hours before fog formation.

The deepening of the dew point inversion from four hours to one-half hour before fog formation appears to be due to a decrease in the rate at which the net water vapor is lost at the 17 m level. Throughout the pre-fog period (-6 to -1 hours), the rate of decrease in dew point below 3 m is approximately $0.5^{\circ}C\ hr^{-1}$, which is slightly less than the rate of temperature change.

It is readily apparent from the average data that the breakdown of the low-level inversion in the last half hour before fog is due to an increase in low-level humidity.

The average data indicate that to within the accuracy of the measurements the low-level dew points remain constant and independent of altitude from fog formation until sunrise. When fog forms many hours before sunrise, however, low-level dew point decreases at the same rate as temperature, i.e., about $0.2^{\circ}C\ hr^{-1}$ between fog formation and sunrise. This is illustrated in the data for 14 August 1970 presented in Figure 27, which was not included in the model.

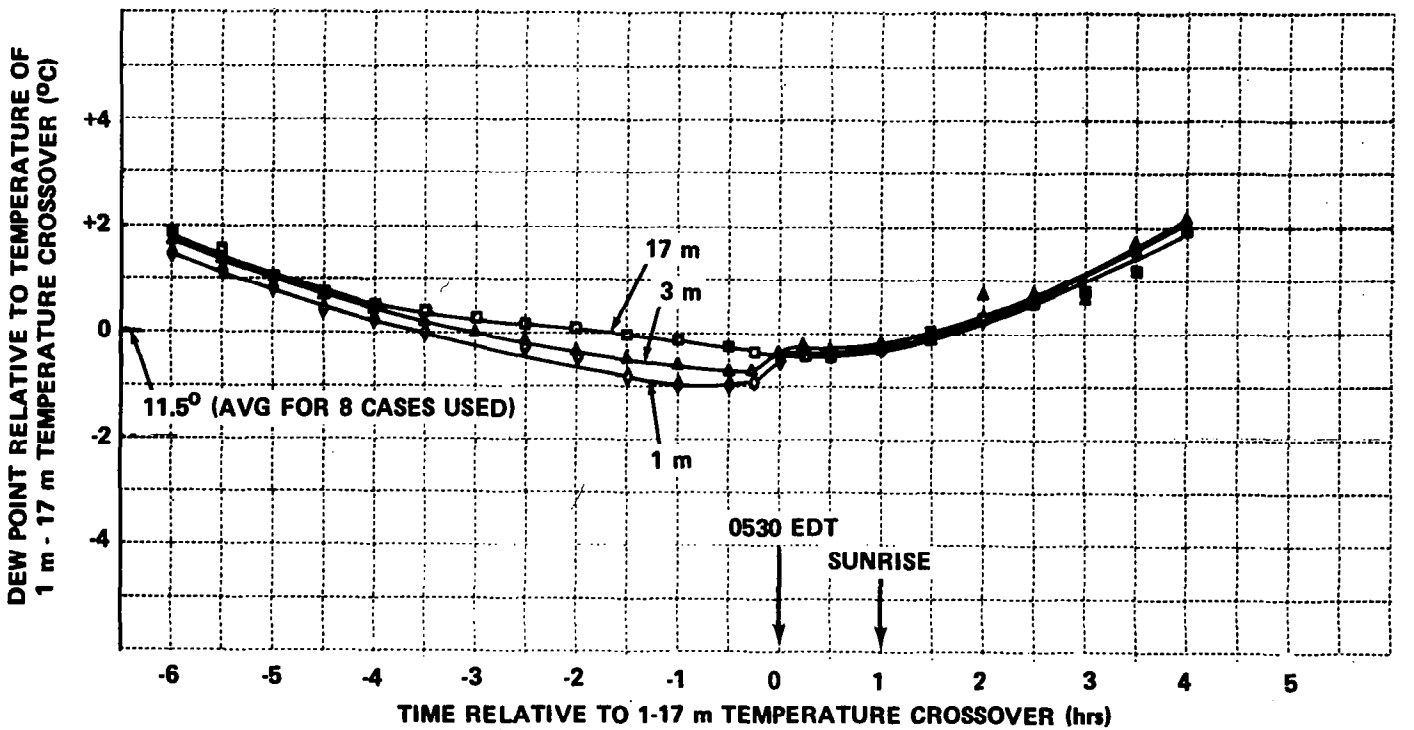

Figure 26 DEW POINT MODEL

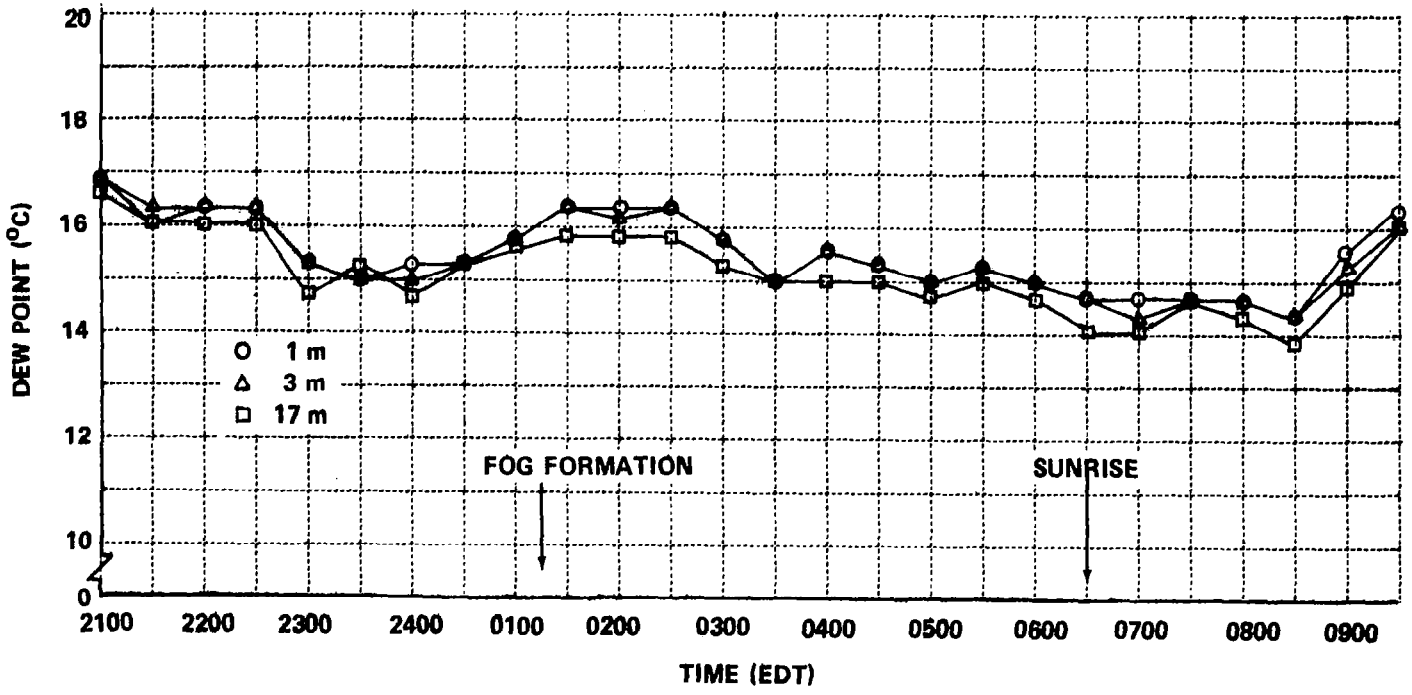

Figure 27 DEW POINT AS FUNCTION OF TIME 8/14/70

The low-level dew point begins to increase shortly after sunrise and within an hour is increasing at a near constant average rate of about $0.8^{\circ}C\ hr^{-1}$. This rate is maintained until fog dissipation.

- Dew Deposition and Evaporation Rates

During the first few fog nights, we became intrigued with the heavy deposition of dew on all vegetation on the valley floor. In an attempt to obtain a quantitative estimate of the amount of dew on the ground, we mounted a $0.1\ m^2$ aluminum plate on a laboratory balance (0.1 g least count), placed the balance on the ground, and weighed the plate at half-hour intervals. Changes in weight resulted from dew deposition on the plate.

To reproduce the long-wave radiation characteristics of grass, we painted the plate black. This may not have been important since the surface of the plate was usually coated with dew within an hour after being placed in the field; and the radiating surface of the plate, like that of the grass, was usually water. Even so, the exact relationship between the dew deposition rates measured with this apparatus and deposition rates on the valley floor are unknown. Important differences probably include the six-inch height of the plate above the ground and the ratio of surface area exposed to the atmosphere to unit area of valley floor. Grass on the airport ranged from four to six inches high; in the meadows, however, which constitute most of the valley in the vicinity of the airport, weed height sometimes exceeded a foot. The surface area of vegetation in a meadow is given by Geiger (1965, Chapter V) as 20 to 40 times the area of the ground. For the plate, of course, this ratio was very nearly two.

Another source of error was dripping of water from the edges of the plate when the amount of dew on the plate exceeded 15 g ($150\ g/m^2$). Since we never observed more than a single drop at a time, errors due to dripping were probably quite small--certainly less than 10%--and only occurred very late in the measurement period.

Our measurements of dew deposition and evaporation rates must be interpreted with these uncertainties in mind. They are certainly indicative of the processes that occur during the life cycle of fog. Quantitatively, our measurements of total dew deposition through a night lie about midway in the range of measured values discussed by Geiger (1965, Chapters, II, VI). We suspect that they represent what happens on the valley floor to within a factor of about two.

Typical dew deposition and evaporation data are presented in Figures 10, 11, and 12. In general, dew was first observed on the grass (and on the plate when it was out early enough) between 2030 and 2230 EDT on all clear nights with low wind speed. Deposition rate on the plate was consistently 25 ± 5 g m^{-2} hr^{-1} until one hour before fog formation. Within the last hour before fog, deposition rates usually decreased to near zero. From that time until sunrise ± one-half hour, the amount of dew remained constant. The total mass of dew deposited depended primarily on the time of fog formation and ranged from 100 g m^{-2}, when fog formed at 0100 EDT, to 220 g m^{-2} when fog formed at 0640 EDT. Once evaporation began, the average evaporation rate during the first half hour was 30 g m^{-2} hr^{-1} and for the next two hours was 55 g m^{-2} hr^{-1}.

All available data were used to generate the dew cycle model presented in Figure 28. To construct this model, it was assumed that the fog formed at 0530 EDT when the dew mass was 200 g m^{-2}. Dew deposition rates as a function of time prior to fog formation were averaged to generate the curve prior to fog formation and evaporation rates after 0630 EDT were averaged to generate the curve for post-sunrise periods. Mass of dew was assumed to be constant in fog prior to sunrise. This model is consistent with the temperature and dew point models presented earlier.

- Wind Speed and Direction

The primary measurements of wind speed and direction were made at the 3 and 17 m levels at the tower site using Packard Bell W/S 100 (B series) wind systems. Factory performance characteristics for the anemometers in these systems are 0.25 m sec^{-1} threshold speed and

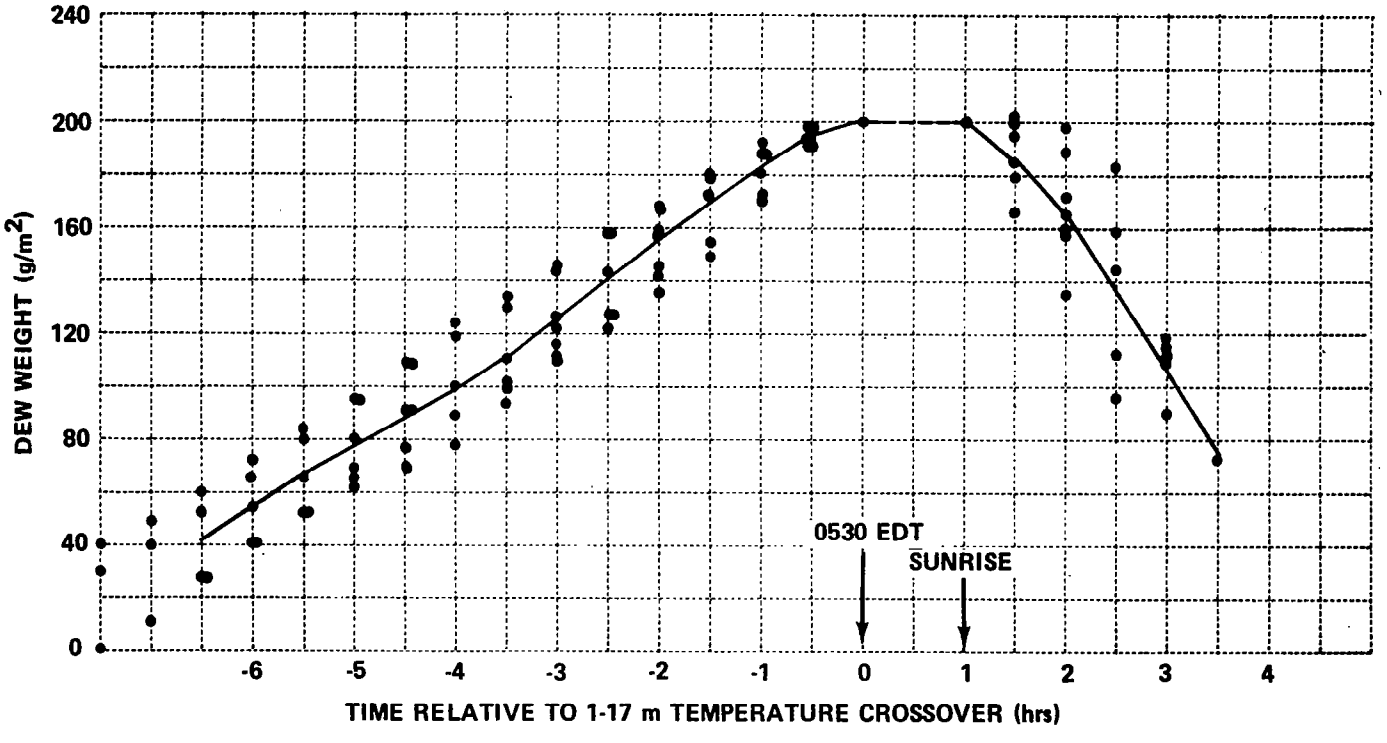

Figure 28 DEW FORMATION-EVAPORATION MODEL – SPREAD IN DATA POINTS IS SHOWN.

0.1 m sec^{-1} accuracy. Quoted characteristics for the wind vanes are 0.35 m sec^{-1} threshold and an accuracy of $\pm 3^{o}$. The vanes were field adjusted to $\pm 1^{o}$ relative to true north using a transit with a runway orientation as reference.

Secondary measurements of wind speed and direction were made with a Danforth wind system mounted on a 2 m mast on top of a hangar at the Harris Hill Airport (see Figure 1). The instrumentation was approximately 250 m above the valley floor. Quoted characteristics for the system are 1 m sec^{-1} threshold and ± 0.5 m sec^{-1} at $\pm 5^{o}$. All of the above accuracies apply only to the speed range of interest.

The data were reduced to half-hour averages estimated by eye to the nearest half mile per hour ($\sim$0.25 m sec) and 22.5^{o}. Typical results are presented in Figures 29 and 30. Data from all fogs may be summarized as follows:

Low-level winds on fog nights were always light. Speeds never exceeded 4 m sec^{-1} at any of the three sites and averaged substantially less. Prior to fog formation, these averages were 1 m sec^{-1} at the 3 m height, 1.6 m sec^{-1} at 17 m and 2.2 m sec^{-1} on Harris Hill. On the average, there is a slight speed increase in the valley (approximately 1 m sec^{-1}) in the one-hour period centered on fog formation. Harris Hill data, on the other hand, show no change in average wind speed at that time.

Wind directions at the 3 and 17 m levels frequently fluctuated by as much as 180° prior to 0200 EDT. By that time, the WSW mountain wind usually became well-established and half-hour averages at both levels did not deviate by more than 22.5^{o} from that direction. On only one occasion did the ambient winds maintain a NNE valley wind direction (up the valley) until fog formation and on that occasion, a 180° wind shift occurred as fog formed.

The wind direction on Harris Hill was controlled primarily by the relative locations of larger-scale systems, with occasional 90 to 180° shifts occurring gradually through the night. On the five fog nights for which good data are available, there was a minimum directional shear

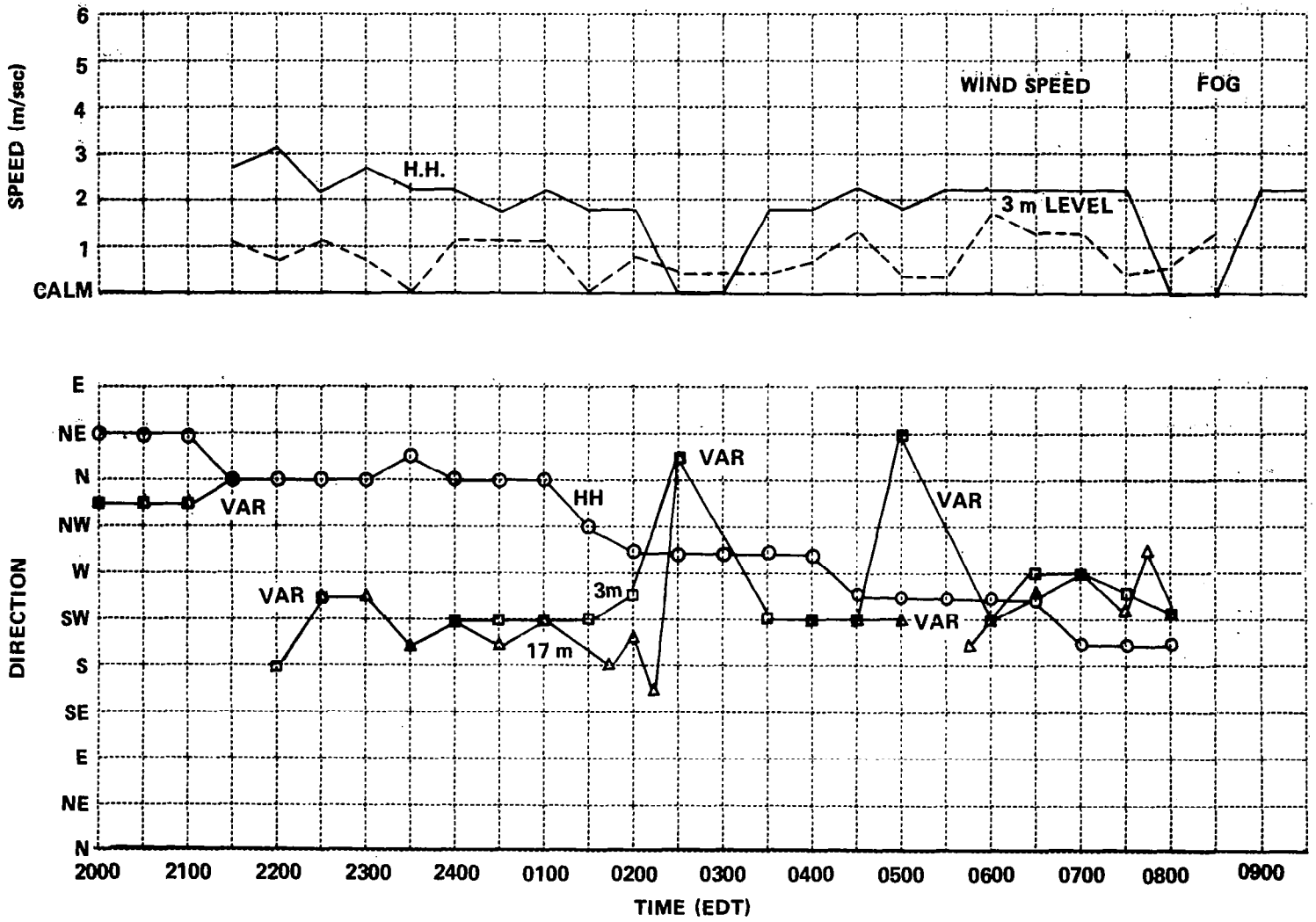

Figure 29 WIND DATA 8/22/70

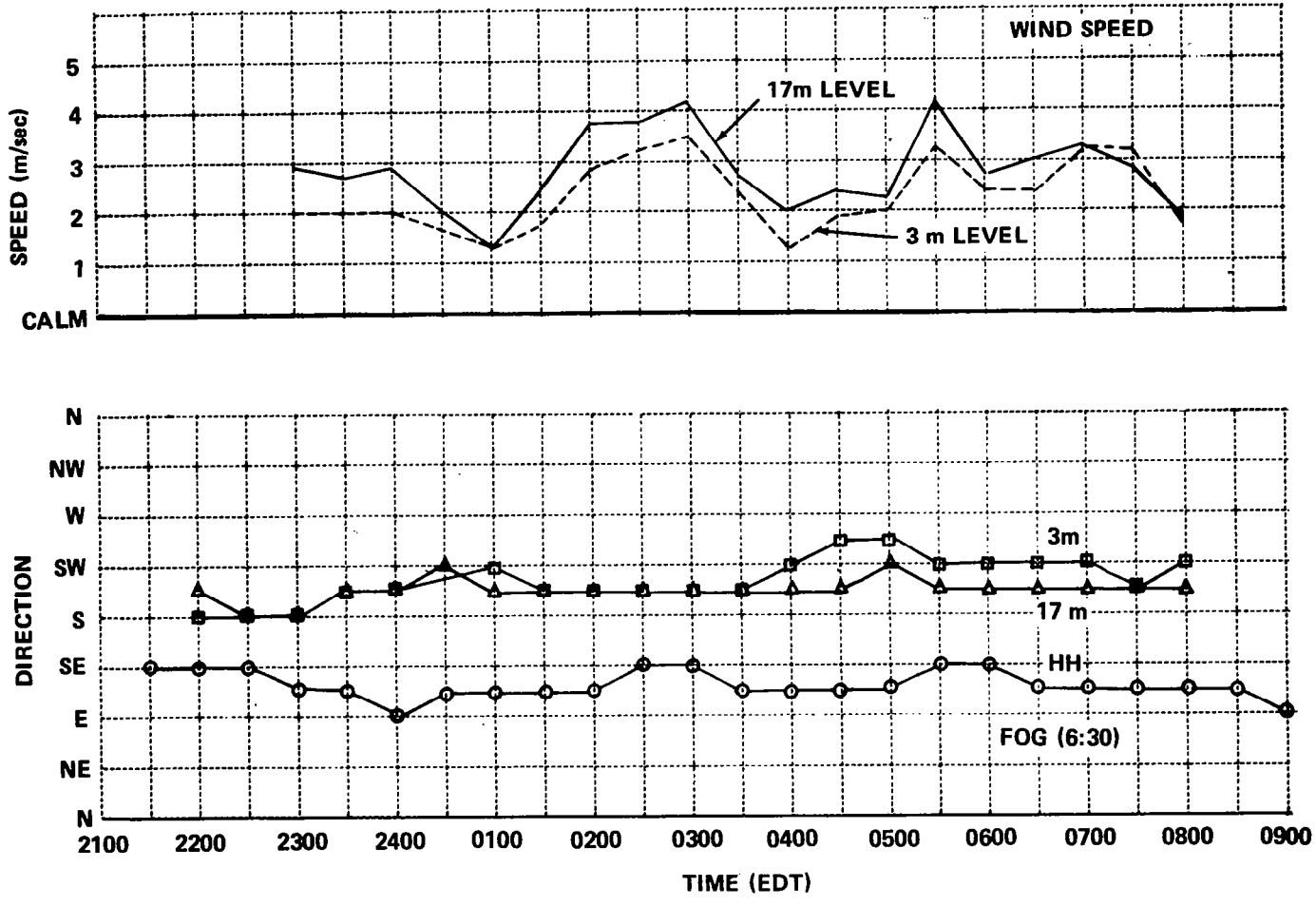

Figure 30 WIND DATA 9/2/70

of 45° between ambient and mountain wind before fog formation and 22.5° thereafter. Maximum directional shear was 150° under both circumstances. Maximum vector difference between the Harris Hill and the mountain wind was 7 m sec^{-1}.

- Vertical Wind Speed and Direction

One of the unanticipated results from the Elmira investigations came from our measurement of vertical wind velocity. As with the surface and 10 cm temperature measurements and dew weight measurements, these measurements were not planned before the field trip. When the lightweight propeller anemometer* (intended for spot measurements of drainage winds) was mounted in the vertical position at 17 m on the tower, up- and downdrafts of the order of 2 m sec^{-1} were observed. A decision was then made to adapt an existing strip chart recorder to the instrument so that continuous data could be acquired for at least one fog.

The single record obtained on 12 September 1970 provides a vivid description of the large-scale fluctuations ($\sim$ 20-second period and greater) in vertical air velocity. The data acquired are in agreement with spot measurements made during other fog situations and are readily correlated with other events that have been shown to affect the fog life cycle.

Segments of the record of vertical wind during the night are reproduced in Figure 31. The general behavior is illustrated by the envelope of vertical speeds presented in Figure 32. To avoid overemphasis of isolated events, such peaks were neglected when drawing the general contour.

Early in the evening, measurable vertical velocities occurred only intermittently. With minor exceptions, peak recorded speeds were less than 0.1 m sec^{-1} in either direction. Measurable fluctuations occurred in bursts of 20- to 30-minute durations separated by calm periods of 5 to 10 minutes. Peak velocities during these bursts of activity increased gradually through the night until about 0100 EDT when gusts exceeding 0.25 m sec^{-1} occurred frequently.

*Gill model No. 27100

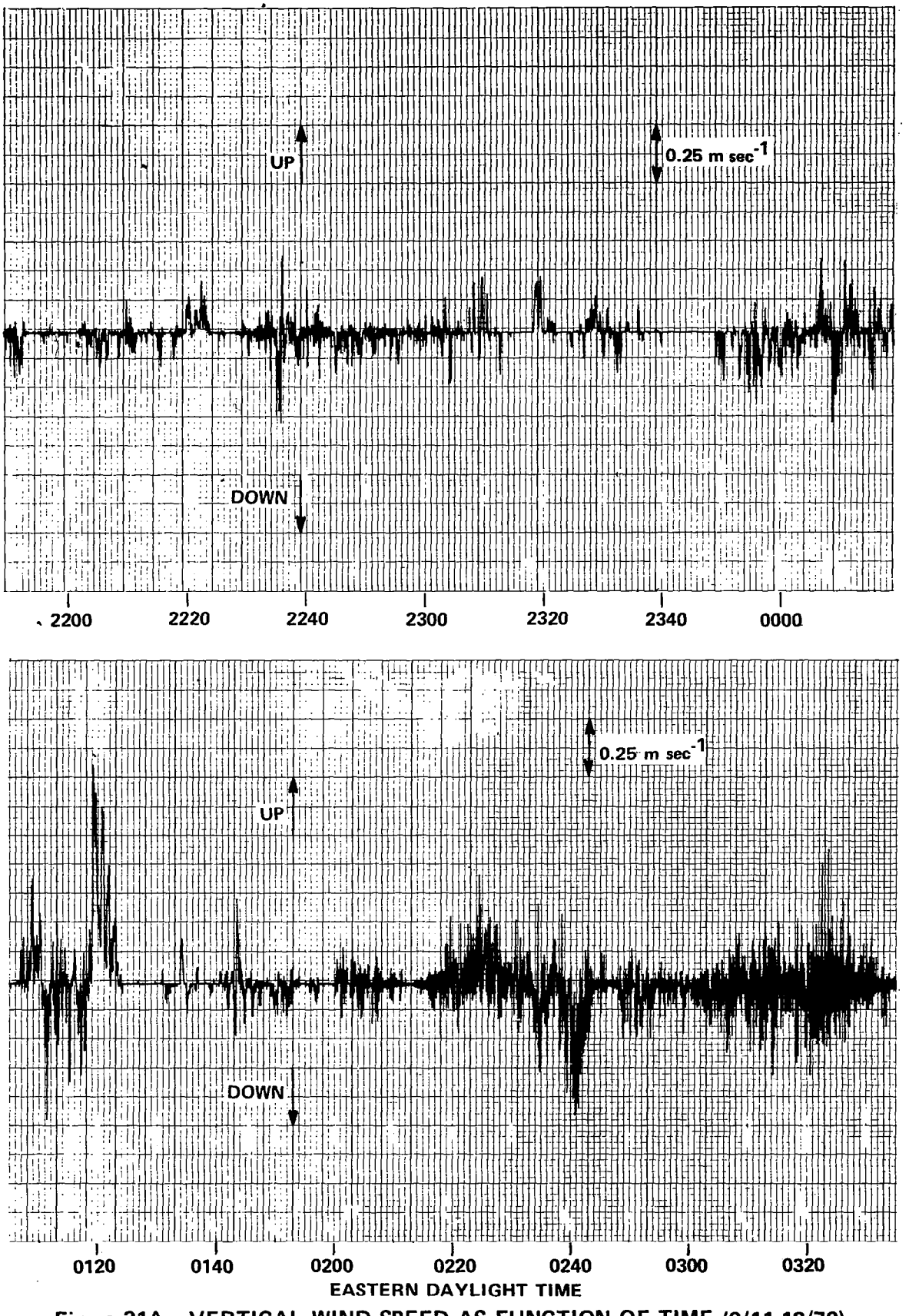

Figure 31A VERTICAL WIND SPEED AS FUNCTION OF TIME (9/11-12/70)

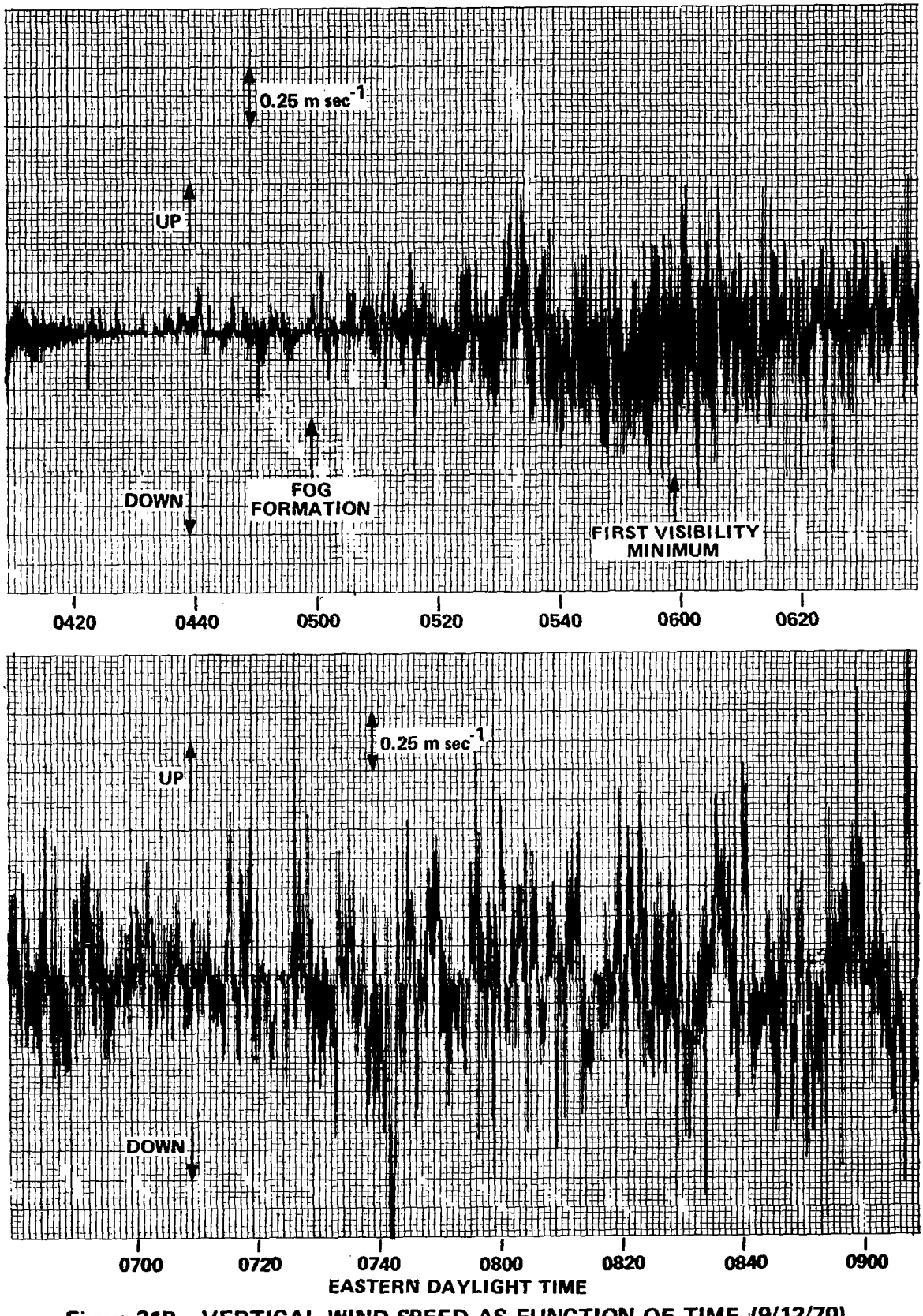

Figure 31B VERTICAL WIND SPEED AS FUNCTION OF TIME (9/12/70)

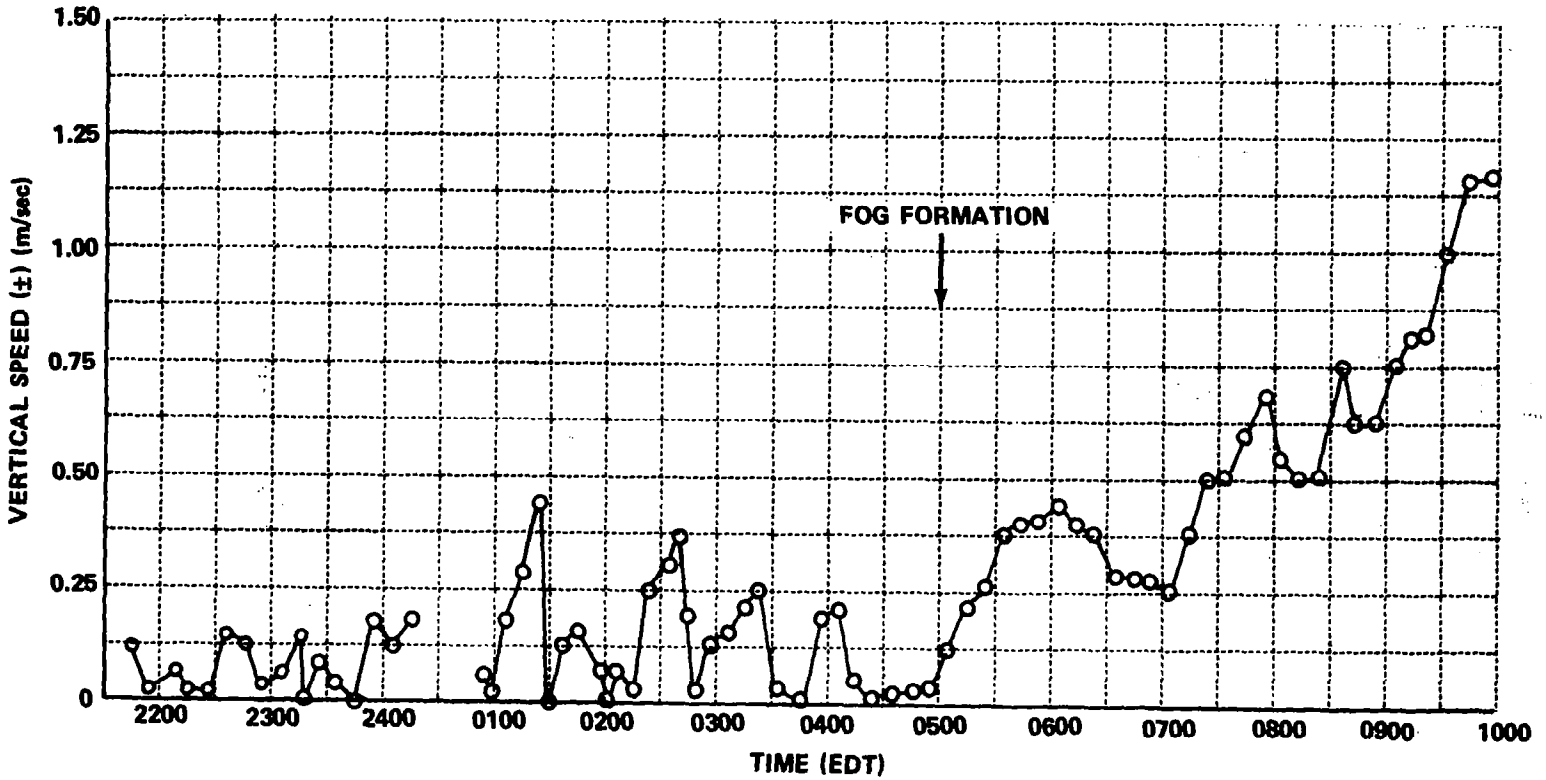

Figure 32 GENERAL ENVELOPE OF PEAKS IN VERTICAL WIND SPEED (ISOLATED PEAKS NEGLECTED) 9/12/70

At 0120 EDT, a 6-minute long period of sustained updraft occurred averaging approximately 0.35 m sec^{-1} and with a peak speed of 0.9 m sec^{-1}. At the same time, the anemometers at 3 m and 17 m indicated near calm (<1 m sec^{-1}) horizontal winds. A similar, though less pronounced, period of persistent downdraft occurred at 0240 EDT. Similar events had been noted on previous nights before the recorder was installed.

The bursts of vertical wind fluctuations and the persistent up- and downdrafts are probably associated with a shifting pattern of the classical nocturnal circulation in a valley, in which the down slope wind stimulates an upward return flow near the valley center before the mountain winds are well-established (see Defant, 1951).

Between 0200 and 0400 EDT, the fluctuation rate of vertical winds increased, but no significant changes in peak velocity occurred. Shortly after 0400, during the period of pre-fog surface temperature rise, peak vertical velocities decreased (with occasional exceptions) to less than 10 cm sec^{-1}. After reaching a minimum at 0430, no significant changes occurred until fog formed at the surface.

A sharp increase in vertical gustiness occurred at 0500 EDT when the inversion broke and fog formed. Maximum pre-sunrise gustiness was noted at about 0600, when peak up and down motions exceeding 0.5 m sec^{-1} occurred at intervals of less than a minute. This condition persisted until shortly after sunrise when the frequency of the fluctuations began decreasing and occasional peak velocities exceeding 1 m sec^{-1} in either direction began to occur. By the time of fog dissipation at 1000 EDT, typical maxima exceeded 1 m sec^{-1} and occasional peaks of 2 m sec^{-1} occurred.

- Radiation

Radiative flux measurements were obtained at half-hourly intervals on eleven fog days and seven no-fog days using a Suomi and Kuhn (1958) net radiometer at the 17 m level. In addition, radiative flux measurements as a function of altitude were acquired using a similar radiometer secured to a tethered balloon (kytoon).

These radiation data were generally contaminated by the formation of dew on the polyethylene windows of the radiometer. For this reason, much of the data cannot be interpreted quantitatively and are not presented here. However, clear evening tower measurements before dew formation and kytoon measurements before fog formation both show net upward fluxes of infrared radiation on the order of 0.1 cal cm^{-2} min^{-1} in good agreement with values in the literature.

The radiation data contaminated by dew formation show a strong reversal in the direction of the net radiative flux about one hour after sunrise, even in dense fogs, supporting the sunrise effects noted in the temperature data, the dew point data, and the dew deposition data.

While the radiation data acquired from kytoon flights were generally too noisy to analyze for radiative flux divergence, measurements obtained in the 12 September 1970 fog at 0630 show a large radiative flux divergence near the measured fog top at 120 m. This flux divergence corresponds to a radiative cooling rate of approximately $4^{o}C$ hr^{-1} in good agreement with values computed from the recently developed dynamic fog model.

FOG MICROPHYSICS DATA

- Drop-size Distributions

Measurements of fog drop-size distribution were obtained using a modified Bausch and Lomb slide projector to expose gelatin-coated slides to a stream of foggy air. In operation, droplets in the air stream were impacted on the treated slides to leave permanent, well-defined "replicas" that could be accurately measured under a microscope. Previous work had established that true droplet diameter is very nearly equal to one-half the diameter of the crater-like impressions left in the gelatin.

The apparatus used at the tower site was constructed to permit control of exposure time from less than 0.1 sec to periods of several minutes and selection of air stream velocity (by a speed control on the blower motor) between 10 and 70 m sec^{-1}. To provide for greater accuracy in applying collection efficiency corrections, air velocity was measured for

each exposure of the four millimeter wide slides. A similar drop sampler was installed in the nose of the Aztec to permit collection of drop samples aloft.

Data reduction was performed manually from photomicrographs obtained with a phase contrast microscope. Where possible, a minimum of 200 droplets was measured for each distribution. In some cases with very low droplet concentration, all replicas on the slide were measured directly through the microscope. A total of approximately 200 surface (3 ft level) drop-size distributions from eight fogs was analyzed. A similar number of samples obtained aloft was analyzed.

Inspection of the drop-size distribution data obtained at Elmira suggests that droplets smaller than 1 μm radius could not be detected in the field even though smaller droplets can be detected in the laboratory. The principal known sources of error in these measurements are statistical in nature and imposed by the time required to measure larger numbers of replicas for each distribution. These errors are particularly important for small droplet sizes (< 3 μm radius) where the number of replicated droplets is limited by small collection efficiencies and consequently collection efficiency corrections are large (Langmuir and Blodgett, 1946). Similar problems occur for large drop sizes where natural concentrations are small. A second type of statistical error is due to the lack of "representativeness" of the sample. A fog that occupies several tens of cubic kilometers is often characterized by a few tens of samples, each containing the droplets from five to ten cubic centimeters.

While exposure time for a given sample is controllable, short exposure times (<0.5 sec) are not reproducible to within a factor of about three from slide to slide. Therefore, normalized drop-size distribution data can be obtained directly but it is not feasible to obtain direct measurements of drop concentration from the droplet samples. Drop concentrations were obtained by combining the normalized distributions obtained at the surface (3 ft) with simultaneous measurements of extinction coefficient obtained from the tower transmissometer (at the 4 ft level ~ 100 ft away) according to the following expression.

$$\beta_{transmissometer} = 2\pi n \sum_{i=0}^{\infty} N(r_i)\, r_i^2 \qquad (3)$$

where N(r) is the normalized distribution and n is the concentration.*

In all cases in which drop samples were obtained from shallow ground fog, the transmissometer was above the fog top. The visibility within the ground fog was therefore always much less than the transmissometer indicated. The size distributions are therefore presented only in normalized form. Data for later periods in the fog life cycle are presented as absolute size distributions.

If measured values for N(r) are used to compute n with typical visibilities measured when GF exceeds the transmissometer height (4 ft), values of n ranging from 100 to 200 cm^{-3} are obtained. These values are in good agreement with the model for radiation fog developed on this program (Jiusto, 1964) which was based solely on published data. Measured N(r) is also in agreement with model size distributions.

The surface drop-size distribution data obtained on fog nights between the time of formation of shallow ground fog (GF) and the time of the first visibility minimum after the formation of deep valley fog reveal a strikingly consistent behavior. Normally, two or three GF samples were taken randomly when GF was first observed. When deep fog began to form, samples were usually acquired at 5- to 15-minute intervals. On 2 September 1970, however,

*Attempts were made to obtain drop concentration data directly using a photographic technique similar to that used with the thermal diffusion cloud chamber. In this apparatus, a 70 μ sec long, 200 watt second pulse of light from a xenon flash tube was focused into a 2 mm wide ribbon in the camera field of view. The flash tube was triggered synchronously with the camera so that point images were obtained from light scattered by droplets in the 0.2 cm^3 sampling volume. Difficulty in maintaining operation of the instrument in the saturated atmosphere prevented acquisition of extensive data. Furthermore, with the small sampling volume, the number of images obtained per sample was so small (1 to 5) that the data were statistically poor. The data available were in general agreement with concentration data obtained in the above-described manner.

it was recognized from the real time display of temperature variations with height and time that formation of deep fog was imminent and therefore a sequence of closely-spaced drop sample collections were initiated before substantial visibility changes were observable. As a result, the most complete data on the evolution of the drop-size distribution in valley fog were obtained on that date. The results are presented in Figure 33.

The drop-size distributions obtained prior to 0632 are characteristic of all distributions obtained in shallow ground fog (i.e., a fairly large number of very small droplets). At 0630, we observed the initial formation of fog aloft and began sampling at 2-minute intervals. Seven minutes later, the first decrease in surface visibility was noted and the sample interval was decreased to one minute or 30 seconds when possible.

The distribution obtained at 0637:30 is characteristic of the distributions obtained at the time of the initial surface visibility decrease on all fog days. Data obtained between 0634 and 0637 show the transition from characteristic GF distributions to what we have named the "fog formation distribution". On this date, the fog formation distribution persisted for only a few minutes. On one occasion, 26 August 1970, however, that distribution persisted for 45 minutes before dense fog formed.

Data obtained between 0638:30 and 0650 illustrate the changes in drop-size distribution that occur between the initial visibility decrease and the first visibility minimum. These changes include (1) the disappearance of droplets smaller than 3 or 4 μm radius, (2) the gradual increase in drop concentration to maximum, and (3) an increase in the maximum drop size to the largest values observed throughout the fog life cycle.

The very small droplets reappear shortly after the first visibility minimum. From that time on, however, the behavior of the drop-size distribution with time is not always completely consistent. In three of the eight fogs sampled, all distributions obtained at the surface after the first minimum were similar to those shown for 2 September 1970 between 0700 and 0810. On three other occasions, surface drop-size distributions obtained after the first minimum were predominantly bimodal, with a maximum near 2 to 3 μm radius and a second maximum in the 6 to 12 μm region.

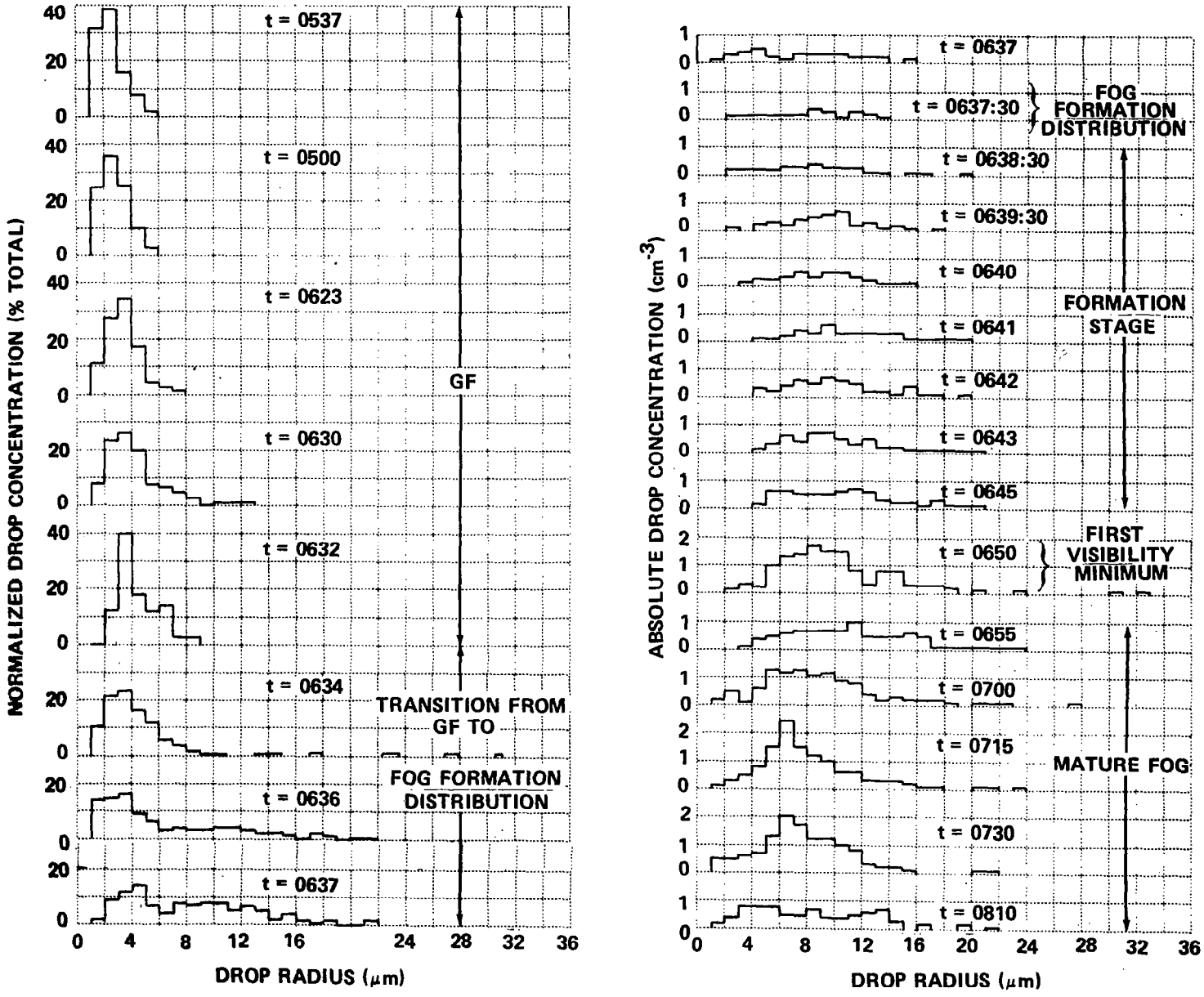

NOTE: DATA OBTAINED AT 0637 ARE PRESENTED IN NORMALIZED AND ABSOLUTE FORM FOR COMPARISON.

Figure 33 DROP SIZE DISTRIBUTIONS OBTAINED ON 2 SEPT 1970

Typical distributions of this kind are illustrated in Figure 34 (for times after 0538). On two occasions, distributions of both kinds seemed to occur randomly through the fog life cycle.

There appeared to be no consistent change in the shape of the surface drop-size distribution associated with fog dissipation. As indicated in Figure 34, the concentration of droplets in each interval simply decreased as visibility improved. These characteristics are further illustrated in Figures 35 and 36 which present data acquired on 22 August 1970 and 12 September 1970.

- Liquid Water Content

Liquid water content data were acquired by integrating the absolute drop-size distribution ($\omega = 4/3\,\pi n \sum_{i=0}^{\infty} N(r_i) r_i^3$) for each drop sample and occasionally (5 to 10 times/fog) by direct measurement using a Gelman* high volume sampler for mechanical collection of the water from 8 m^3 of fog. Cellulose filters were used in the Gelman so that liquid water was absorbed into the fibers. To minimize the error due to absorption of water vapor from the humid atmosphere by the cellulose, the filters were moistened by collection of water and vapor from 2 m^3 of fog prior to the first weight measurement. The increase in weight after exposure to an additional 8 m^3 of fog was used to determine LWC. Simultaneous measurements of LWC by the two methods are compared in Figure 37. In general, the two procedures agree to within ±40 mg m^{-3}, which is quite good for measurement of LWC. Variability appears to be random and is undoubtedly associated in part with the fact that Gelman data were obtained from an average of 8 m^3 of fog acquired over a 7-minute interval while the drop-size distributions were acquired from a few cubic centimeters of fog collected essentially instantaneously.

Complete summaries of the surface microphysics data, including drop concentration, liquid water content and mean, mean squared, and mean volume

*Gelman Model No. 16003

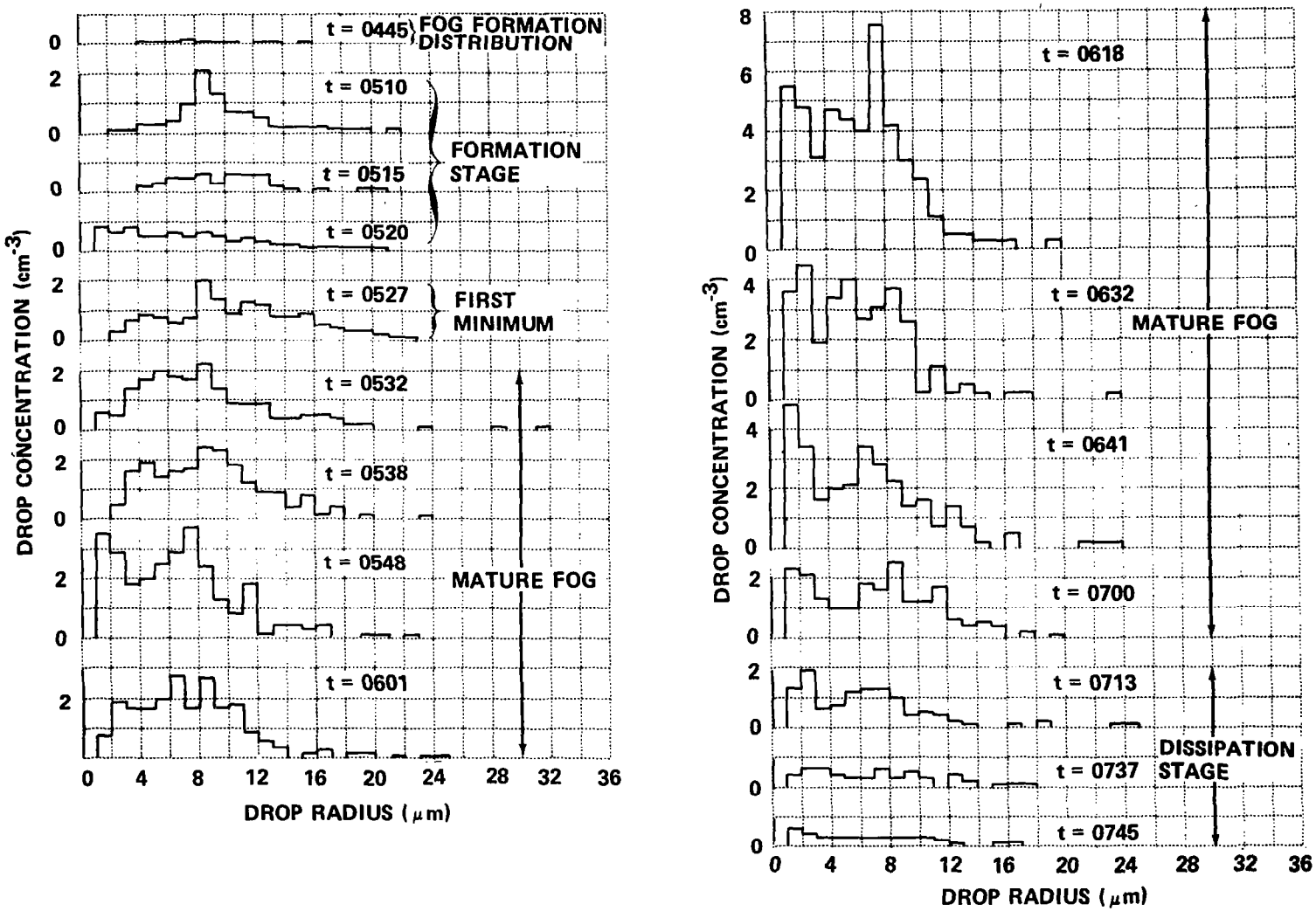

Figure 34 DROP-SIZE DISTRIBUTIONS OBTAINED ON 8/25/70

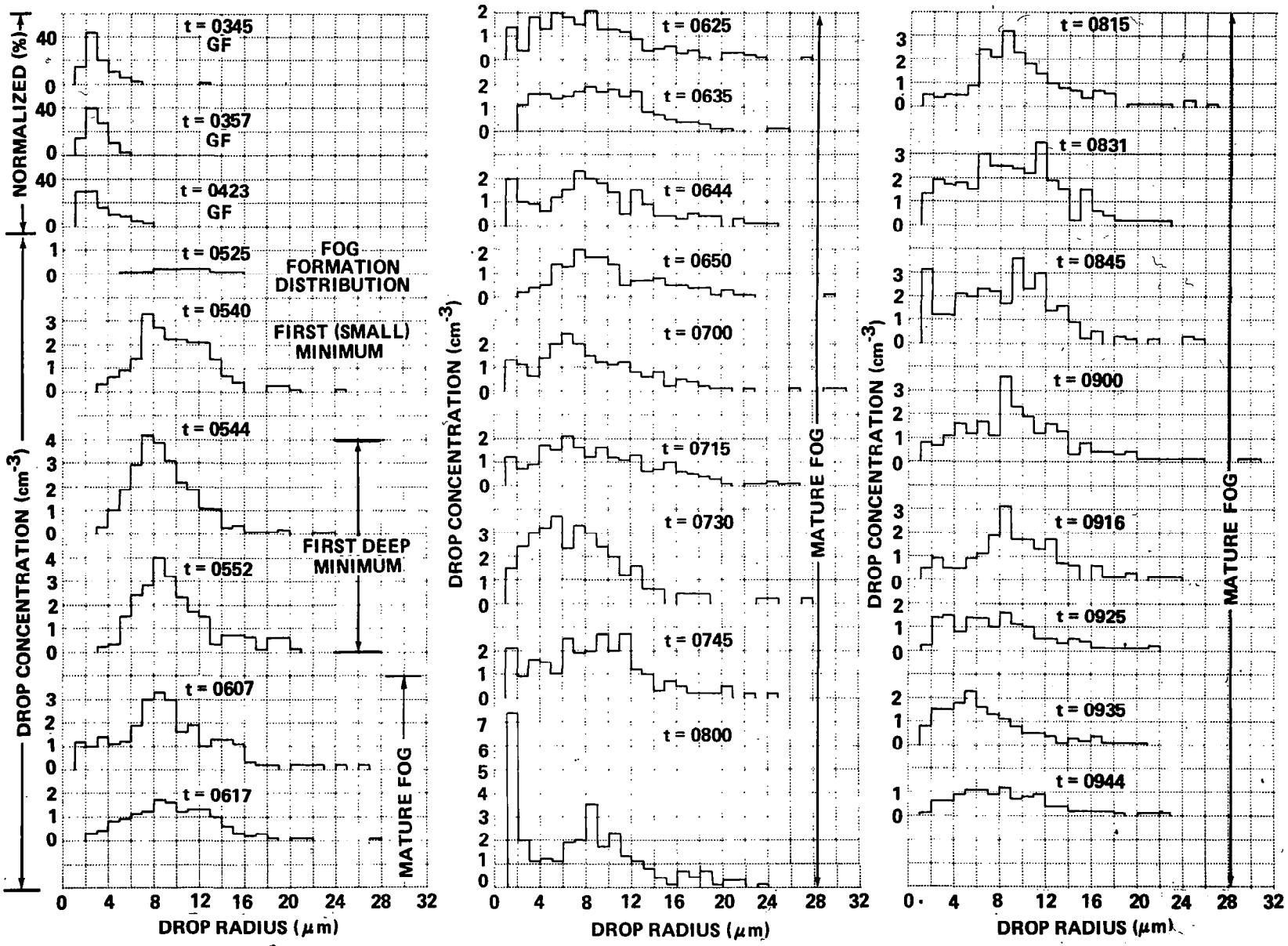

Figure 35 DROP SIZE DISTRIBUTIONS OBTAINED ON 8/22/70

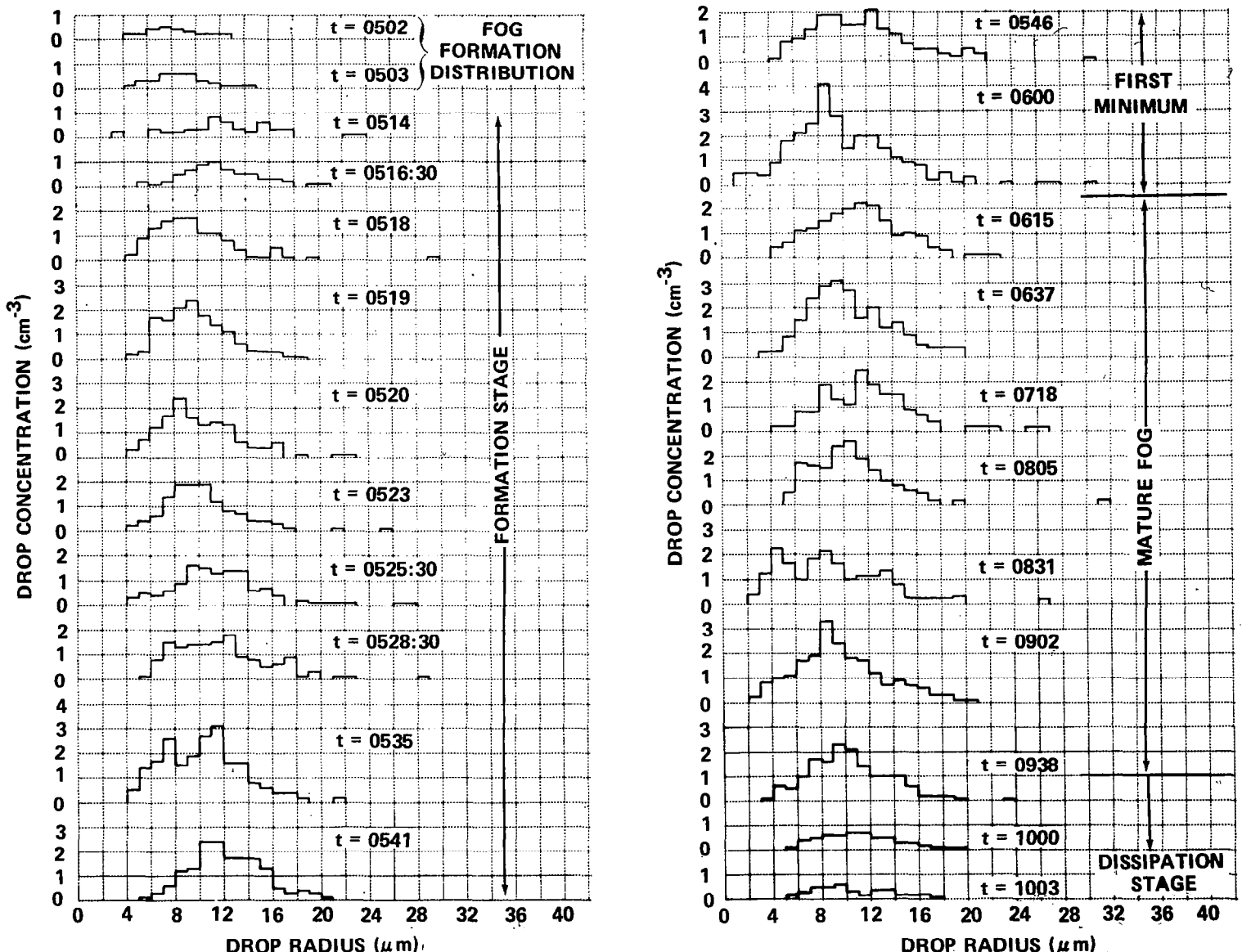

Figure 36 DROP SIZE DISTRIBUTIONS OBTAINED ON 9/12/70

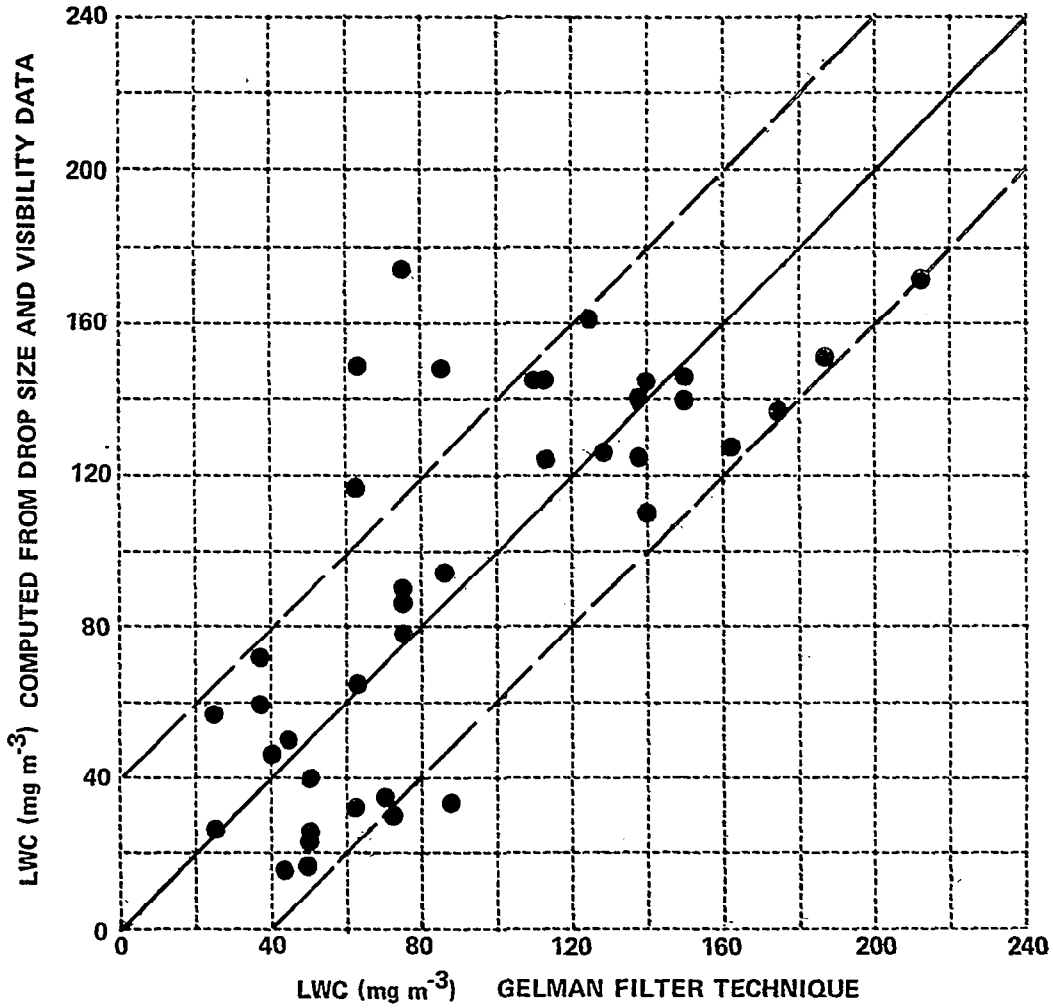

Figure 37 COMPARISON OF LIQUID WATER CONTENT MEASUREMENTS MADE WITH A GELMAN HIGH VOLUME SAMPLER AND SIMULTANEOUS VALUES OBTAINED BY INTEGRATING THE ABSOLUTE DROP-SIZE DISTRIBUTION

droplet radii with time are presented for the three sample fogs in Figures 38, 39, and 40. The tower site visibility trace is reprinted on each figure. Note that in Figure 40 (2 September 1970) the time scale has been expanded.

These three figures taken together illustrate the pertinent features that are characteristic of the microphysical data throughout the life cycle of most Elmira valley fogs. These may be summarized as follows:

1. Visibility decreases to a minimum during the first quarter of the life cycle and then increases somewhat. Through the middle half of the life cycle (the mature fog), visibility may remain nearly constant or undergo large fluctuations. The dissipation stage accounts for the last quarter of the life cycle.

2. Droplet concentration and liquid water content increase to a maximum at the time of the first visibility minimum, fluctuate synchronously with visibility during the mature stage and decrease drastically during the dissipation stage.

3. The mean, mean square, and mean volume radii of the drop-size distributions increase to a maximum approximately midway between the first observable visibility decrease and the first visibility minimum. The mean sizes then decrease slightly at the time of the first visibility minimum and retain near constant values through the mature stage. There appear to be no consistent changes associated with the dissipation stages.

- Summary of Surface Microphysical Properties of the Fog

Since the principal variations in fog microphysical characteristics at the surface occur during the first and last quarters of the life cycle regardless of total fog duration, we attempted to model all microphysical data on a time scale defined by fractions of total fog duration. Averages of all available data from <u>each fog</u> were computed for each phase of the life cycle, with the first visibility minimum placed at t = 1/8 total life, a reasonably representative time. These data, together with the overall averages for <u>all fogs</u> are presented in Figures 41 and 42. The figures therefore summarize all surface microphysical data obtained during the program with the exception of that for the

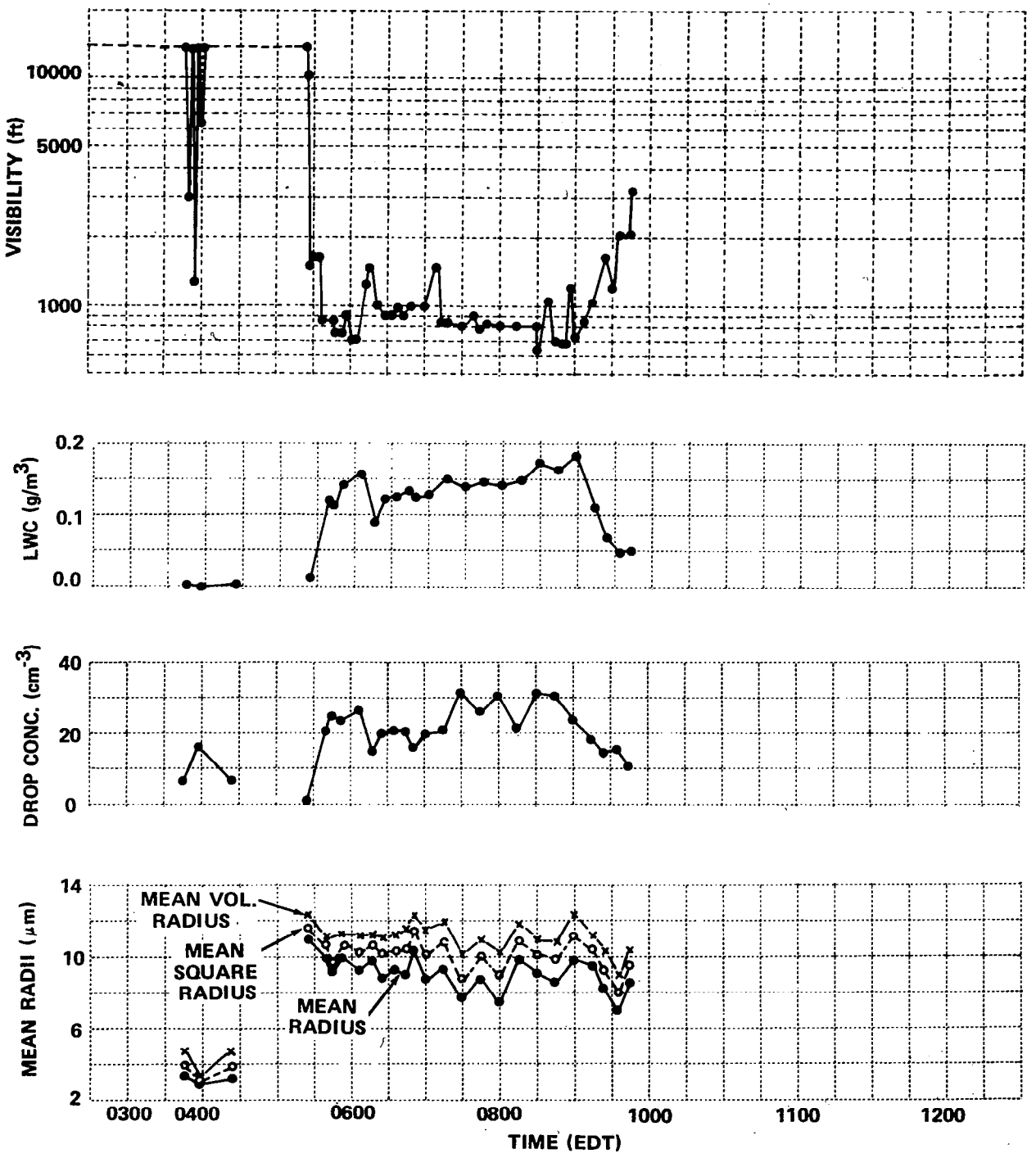

Figure 38 VISIBILITY AND MICROPHYSICS DATA OBTAINED ON 8/22/70

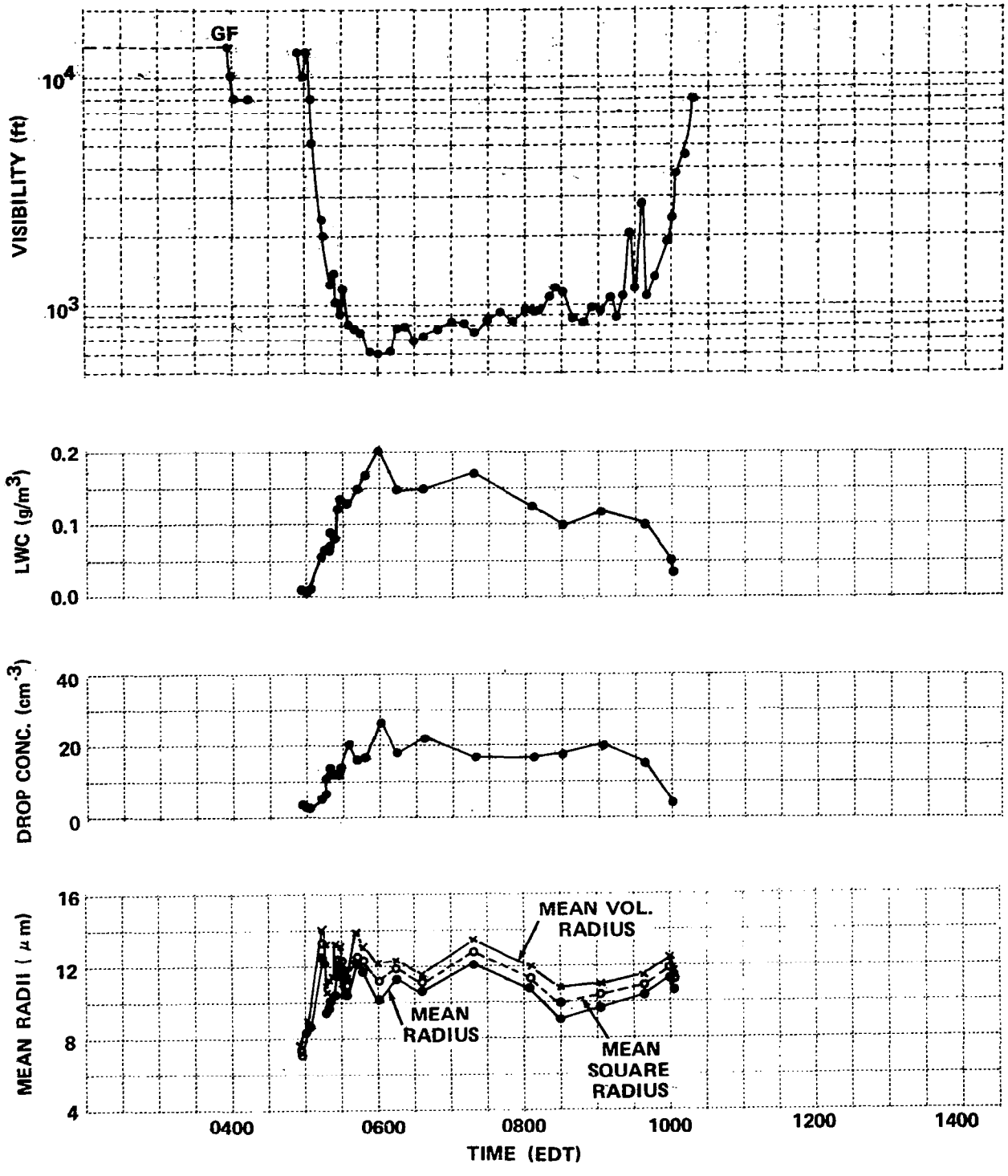

Figure 39 VISIBILITY AND MICROPHYSICS DATA OBTAINED ON 9/12/70

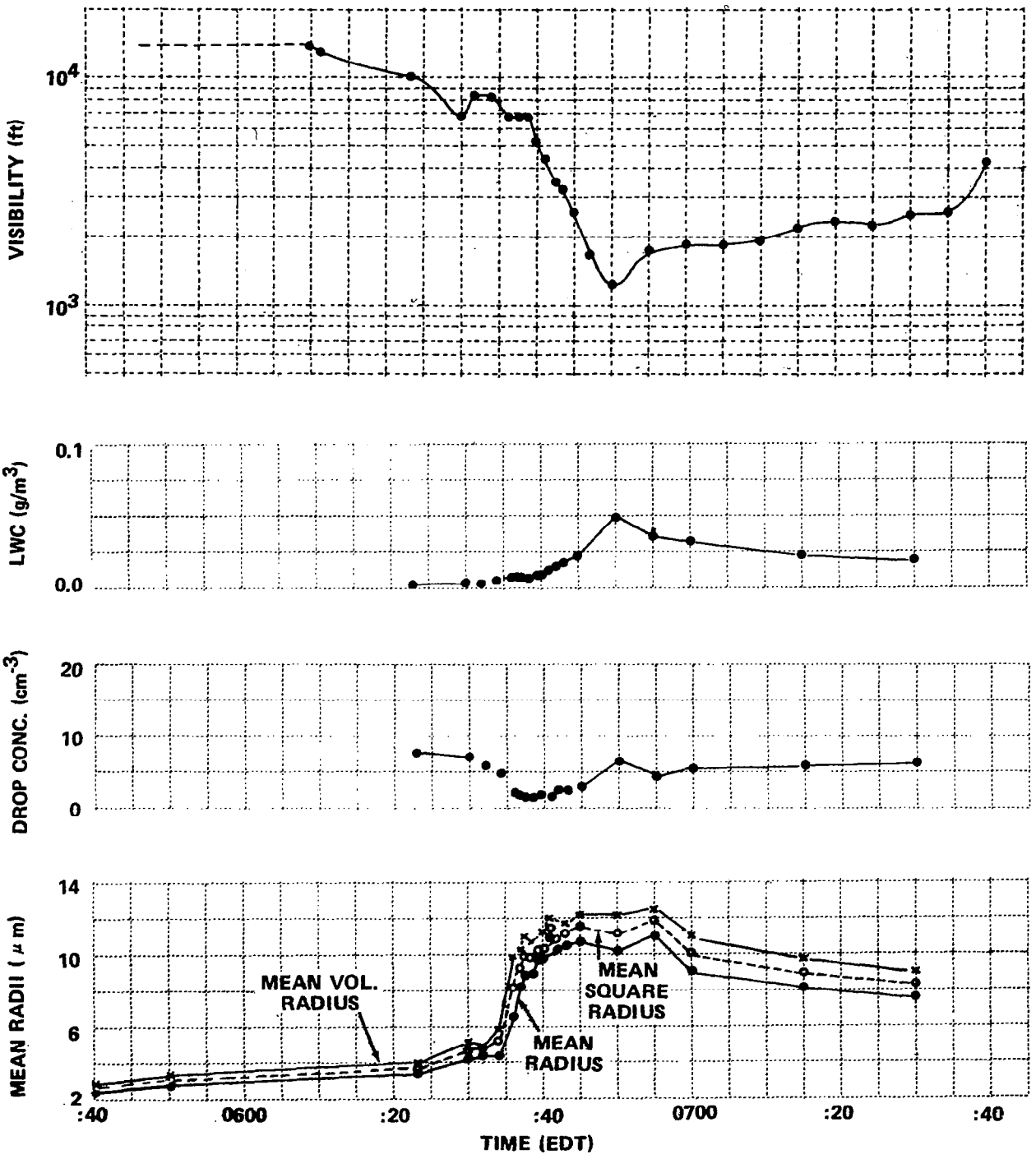

Figure 40 VISIBILITY AND MICROPHYSICS DATA OBTAINED ON 9/2/70

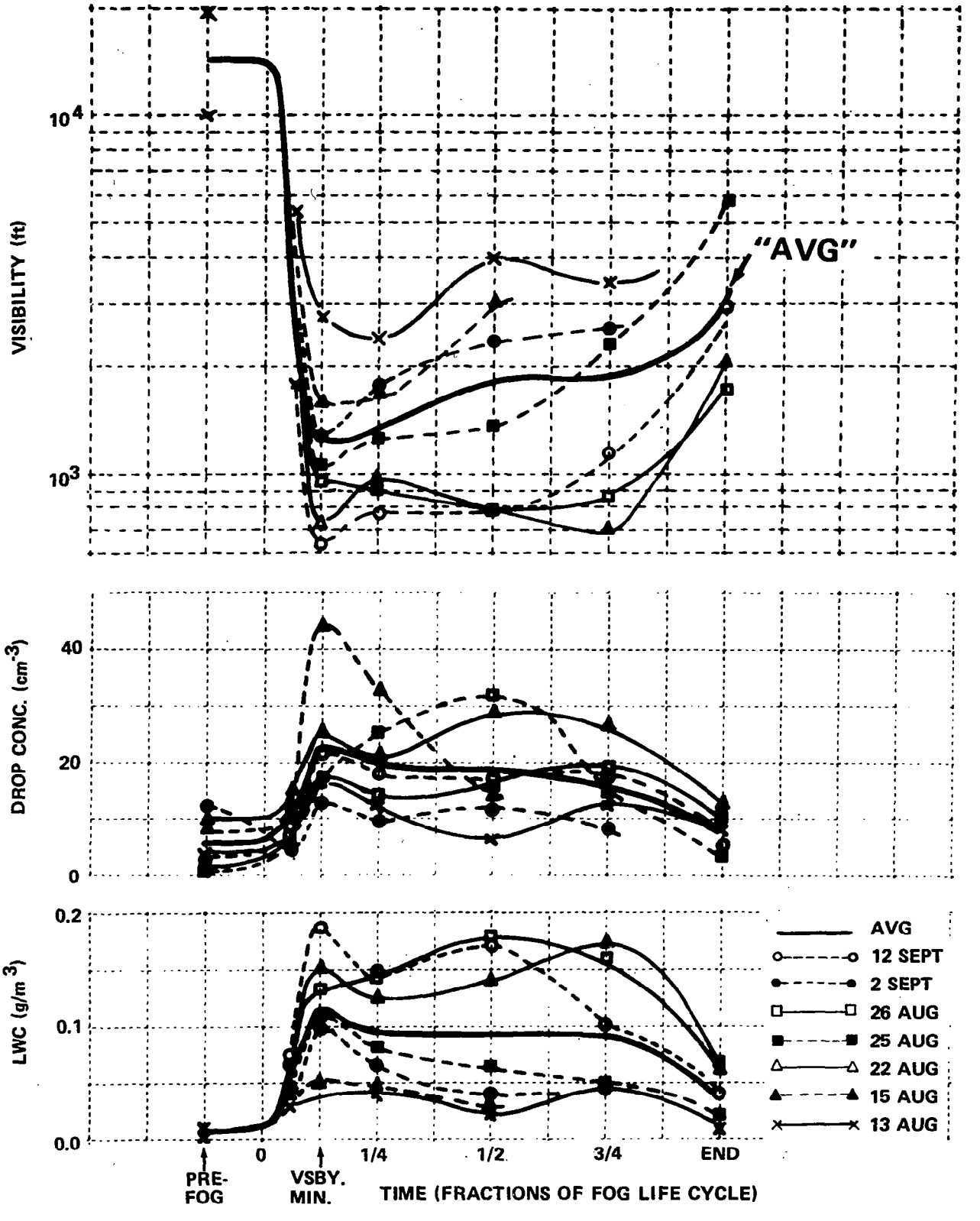

Figure 41 VISIBILITY AND MICROPHYSICS DATA FOR SEVEN FOGS

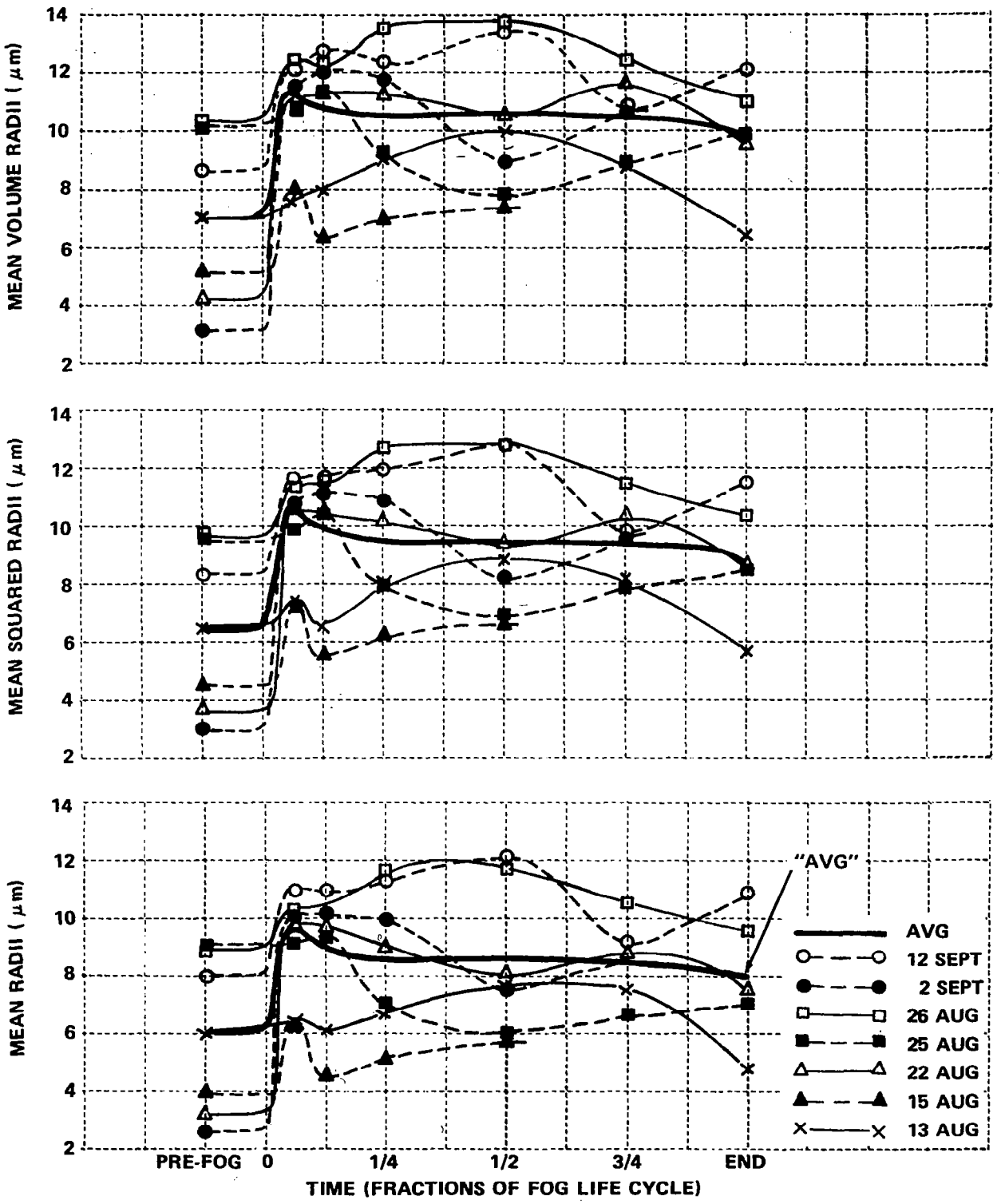

Figure 42 MEAN DROP SIZES AS FUNCTIONS OF TIME FOR SEVEN FOGS

anomalous fog of 14 August 1970. The figures show that, with some exceptions in given fogs, the microphysical characteristics for individual fogs follow a reasonably consistent pattern. There is a wide variability from fog to fog in the absolute values of each of these properties.

- Drop-Size Distributions Aloft

Because of flight restrictions limiting takeoff under zero-zero conditions to daylight hours, we were unable to obtain drop-size distribution data aloft at times prior to the first visibility minimum. The data acquired after daybreak, however, display a very consistent behavior with both height and time. This behavior is illustrated by the data acquired on 22 August 1970 and 12 September 1970 presented in Figures 43 and 44.

Since there are no visibility data aloft, all distributions are presented in normalized form. Note from the figures that the broadest drop-size distributions were observed at or near the surface at all post-daybreak times during the fog. During the earliest sounding, there was always a slight decrease in width of the distribution with altitude but as time progresses, the distributions became more and more peaked in the small size range. The exception to this rule occurred at 60 m on the last sounding on 22 August 1970, which was made on the final landing approach. This naturally was at the end of the dissipation stage when surface visibility exceeded one-half mile and the ceiling exceeded 60 m. Distributions that were more typical of surface distributions were occasionally obtained under these conditions.

The general trend toward smaller drops aloft with increasing altitude and time is best illustrated by the plots of mean radius against altitude for successive soundings. That format is used in Figure 45 to present data acquired during four fogs that are representative of all fog types sampled (22 August and 12 September 1970 - persistent fogs; 13 August 1970 - patchy fogs; and 2 September 1971 - short fogs that form after sunrise). The decrease in radius with increasing height is evident in all cases. Unfortunately, we never made enough soundings in fogs that formed after sunrise to determine if, in those fogs, radius aloft decreased with fog age. The comparison cannot be made in the 2 September 1970 data shown because of the large change in fog top height--45 m at 0735 EDT to 105 m at 0810 EDT.

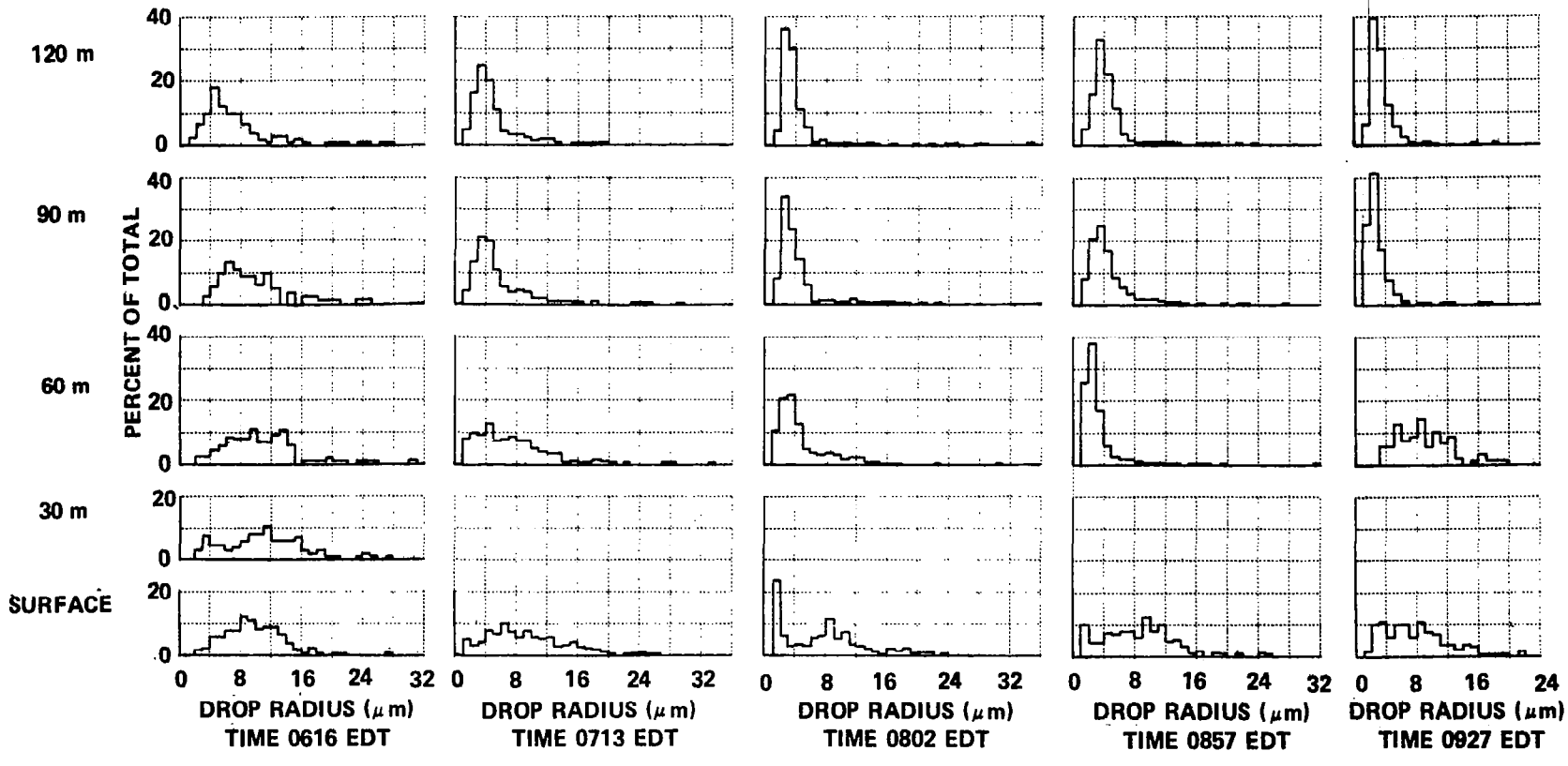

Figure 43 NORMALIZED DROP SIZE DISTRIBUTIONS OBTAINED ALOFT ON 8/22/70

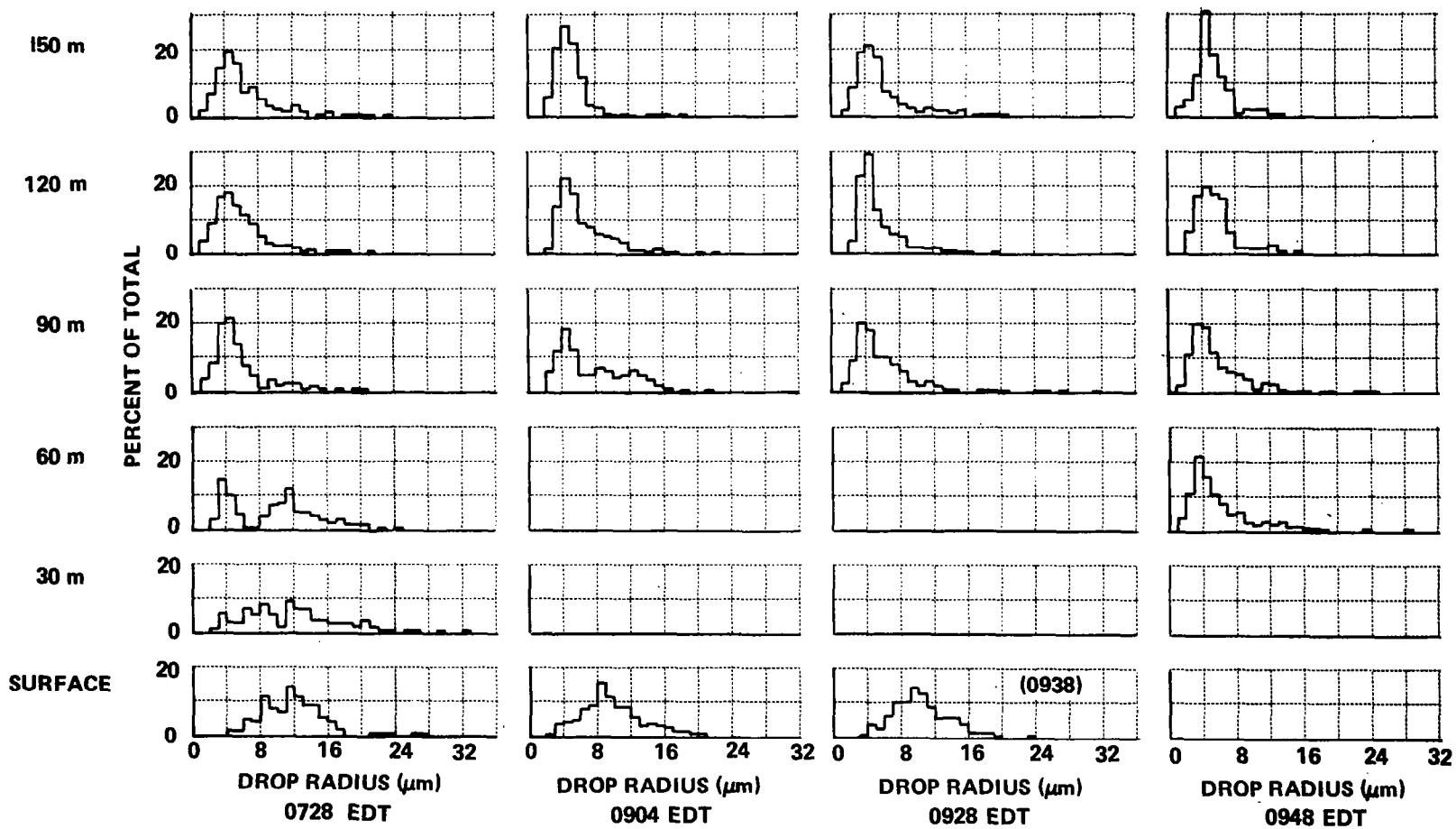

Figure 44 NORMALIZED DROP-SIZE DISTRIBUTIONS OBTAINED ALOFT ON 9/12/70

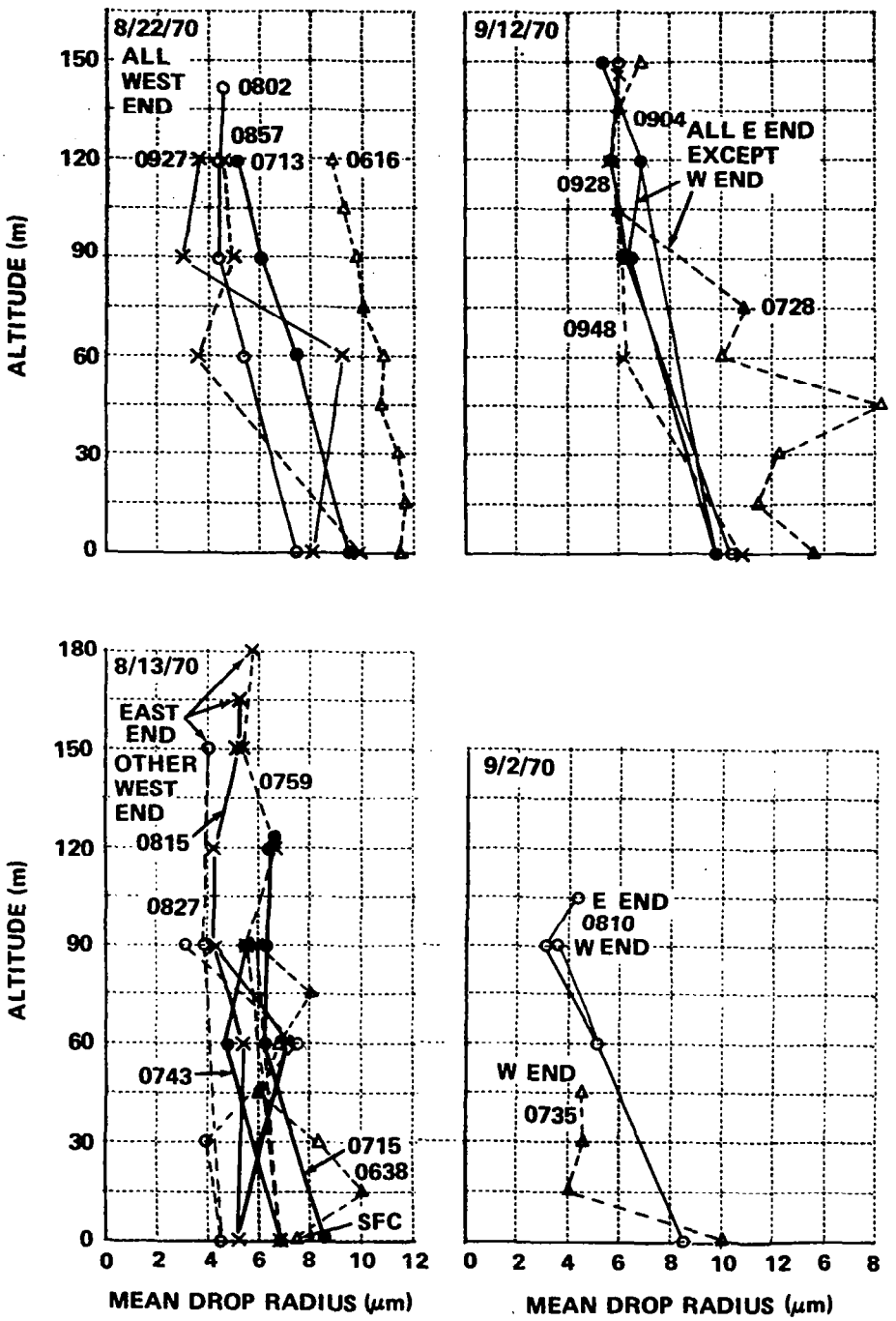

Figure 45 VARIATIONS OF MEAN DROP RADIUS WITH TIME AND HEIGHT

- Cloud Nucleus Observations

The CAL aircraft was used to obtain measurements of cloud condensation nuclei (CCN) at several selected altitudes prior to fog formation. Observations of CCN at 0.3%S* were made at the surface and at altitudes of 30, 90, 150, and 300 m. Flights normally were scheduled at midnight, 0300 and also 0600 if fog had not already formed.

In Figure 46, average cloud nucleus data are shown for the three flight times. Data obtained on 12 flights were used in tabulating the averages although fewer flights were possible at 0600 due to some early occurrences of fog. The data show that cloud nucleus concentration is highest near the ground and systematically decreases at higher altitudes in the valley. It is of some interest to note the abundance of cloud nuclei that are present even in the relatively clean rural environment near Elmira, New York. By comparison, measurements of average CCN in the vicinity of the industrial area of Buffalo, New York over a three-year period were nearly the same or about 1000 cm^{-3} at 0.3%S (Kocmond and Jiusto, 1968). No large differences in the CCN concentrations were found between the fog and no fog flights. Since the population of fog drops is always much smaller than the population of nuclei activated at 0.3%S, this result is not surprising. We did not attempt to measure CCN in fog since there is reason to doubt the accuracy of such observations at high relative humidities (Saxena et al., 1969; Fitzgerald, 1970).

Possibly a more sensitive indicator of variations in the spectrum of "large" and "giant" nuclei that participate in fog formation can be found from the use of the haze chamber. This device, which received only limited use in the field this summer, is similar in most respects to the thermal diffusion cloud chamber, the only difference being that saturated solutions of KNO_3 are used in place of the upper and lower water reservoirs. It is possible, therefore, to produce controlled relative humidities in the range of 95%-100%, thereby "activating" only the largest and most favorable cloud nuclei.

The data in Figure 47 show results of observations of haze and cloud nuclei on 10 and 12 September 1970. The wide differences in haze nucleus concentration on these two dates is particularly noteworthy, especially since

*S = supersaturation

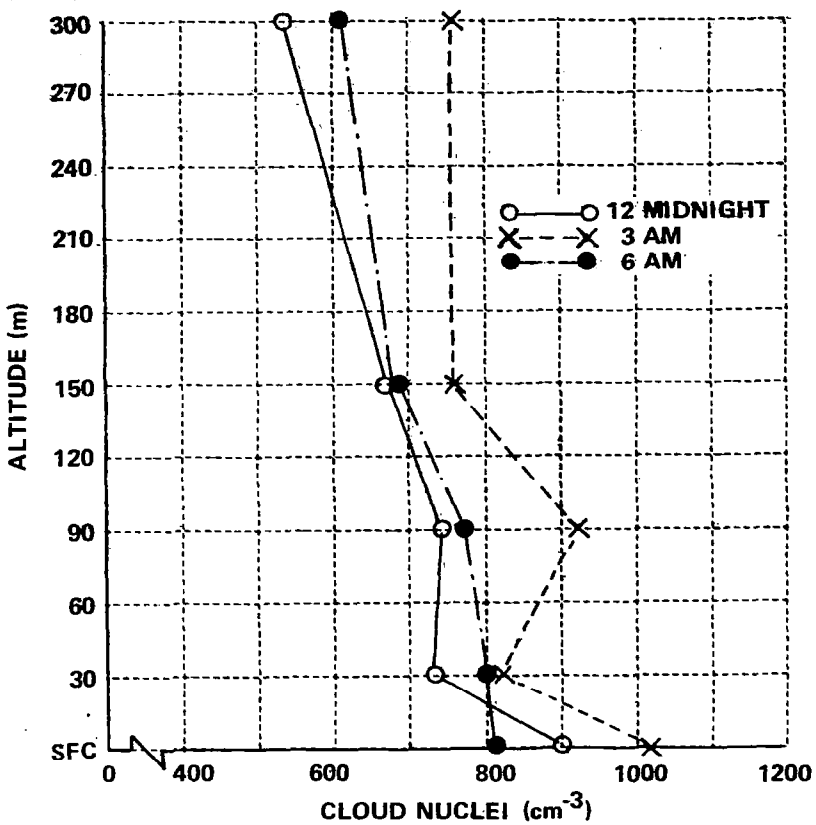

Figure 46 VERTICAL PROFILES OF CLOUD NUCLEUS CONCENTRATION AT THREE TIMES – AVERAGE DATA FROM 12 FLIGHTS AT S = 0.3%

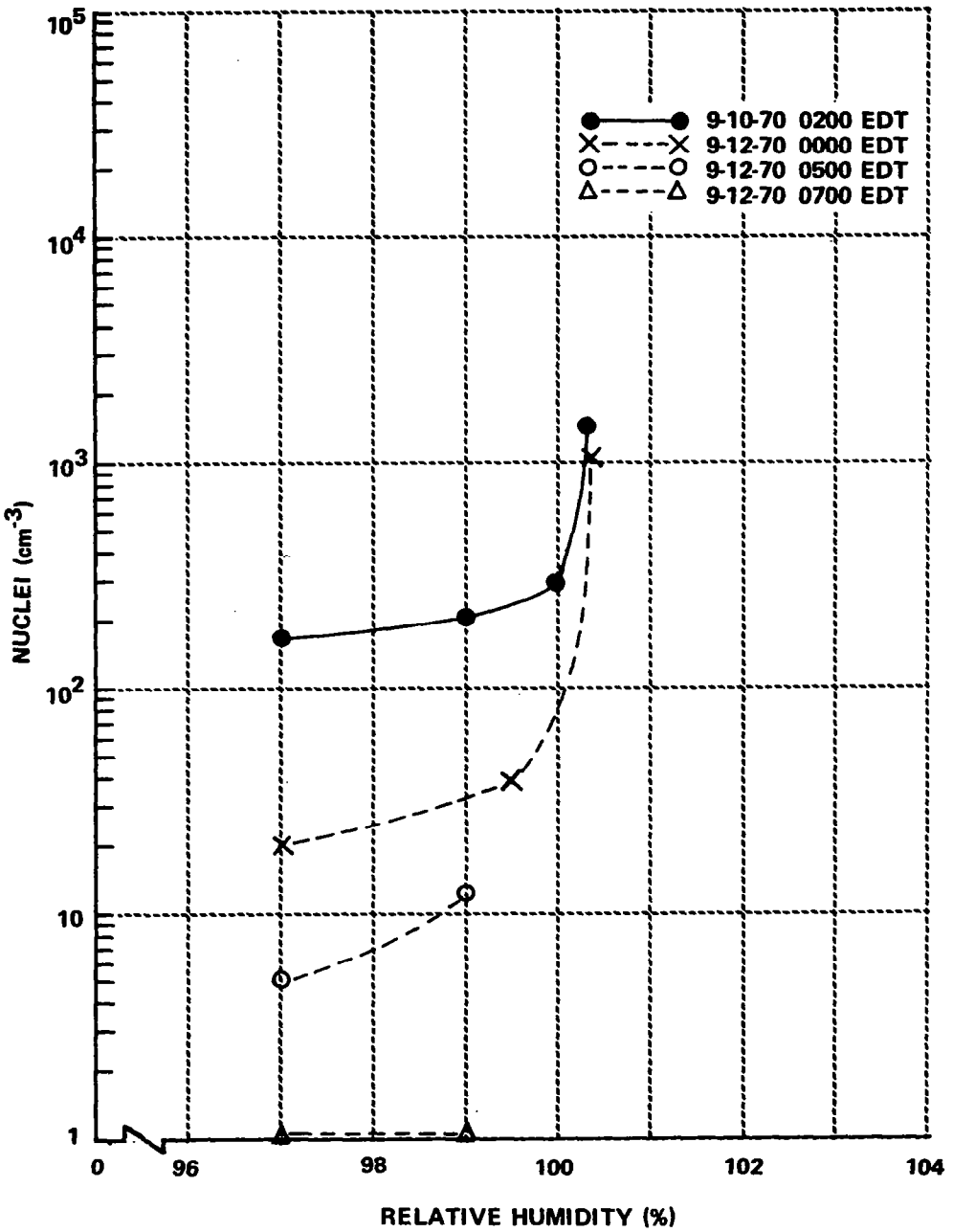

Figure 47 HAZE NUCLEI DATA

the CCN count at 0.3%S was nearly the same on both days. On one of the days, 12 September, ground fog formed at about 0350 EDT and widespread dense fog developed by 0500 EDT. Prior to fog formation, the haze concentration at 99% RH was about 40 cm^{-3}; later, after fog had developed, the count fell to <10 cm^{-3}. Still later in the period, after fog had persisted for several hours, no haze nuclei at all were observed in the chamber. These data suggest to us that many of the haze nuclei observed earlier in the day contributed to the formation and persistence of droplets in the dense fog that later developed at the airport. Unfortunately, no additional observations were made after fog dissipation. In future field programs, we intend to examine the haze nucleus concentration more carefully prior to, during, and after fog formation. The hope is that, for the first time, measurements can be made of the concentration of those nuclei that actually produce fog droplets.

CHAPTER III

DISCUSSION OF EXPERIMENTAL RESULTS

- Fog Formation Processes at Elmira

Numerous authors have concluded that deep fog cannot be produced by cooling from below. Taylor (1917) concluded that turbulent transfer of heat to a cold surface could not form fog and explained some advection fogs on the basis of mixing of warm and cold air masses. Several authors, for example Emmons and Montgomery (1947), Lyons et al (1962), concluded that fog was formed as a result of radiational cooling of the moist air. Rodhe (1962) emphasized the importance of turbulence in fog formation but showed how radiation also contributes. He suggested that two or more processes are usually involved in the formation of deep fog.

The observations made in Elmira and the computer model experiments discussed in Chapter IV suggest that two or more processes are indeed involved with the formation of deep fog in the Chemung River Valley. The model and the data both suggest that the ground fog, ranging in depth from a few centimeters to a few meters, results from cooling of the air by diffusion of heat to the cold ground. The fact that the deep fog forms first aloft, with its base at least 30 to 60m above the surface, indicates that some process other than the turbulent transport of heat to the surface is involved.

Examination of the Elmira data, together with the model calculations and previously-published information, provides some insight into what these mechanisms may be. We can not describe these mechanisms in a precise manner, however.

Several authors who concluded that eddy diffusion could not produce sufficient cooling to cause deep fog have already been referenced. In our modeling experiments, we were unable to produce significant cooling above a few tens of meters without assuming unreasonably high transfer coefficients. In fact, those conditions which produced even slight cooling at the 100m level produced unrealistic low-level temperature profiles and never produced even a thin ground fog. The empirical data show, however, that the maximum cooling rates during the last six hours before fog formation occur in the vicinity of 100m. Obviously, some other cooling mechanism must be responsible.

It seems most reasonable that the temperature distribution leading to the formation of a valley fog is a result of the nocturnal valley circulations described by Defant (1951) on the basis of the work of Wagner (1931, 1932, 1938). Radiative cooling of the slopes stimulates the downslope wind and its upward return flow in the center valley region as illustrated in Figure 48. This process, which begins within an hour after sunset (Geiger, 1965, Chapter VII) certainly contributes to the formation of the deep nocturnal inversion. Several hours after sunset, the so-called mountain wind is established by drainage of the cool air in the direction of the axis of the valley. The speed of the mountain wind is usually maximum (2 to 4 m sec^{-1}) at levels ranging from 40 to 200 m. As the mountain wind is generated, the upward motion in the center of the valley dies, but the downslope wind persists as shown in Figure 49. During the late night hours, the downslope winds cease so that the mountain wind occupies the entire valley and persists until after sunrise.

It is attractive to speculate that the cooling at all levels within the valley until approximately three hours before fog formation results from the upward flow of cool surface air in the center valley region. At about that time, the mountain wind is initiated (see Geiger, 1965, Chapter VII) and retards the upward motion in the center valley region so that the cooling rate at higher levels is decreased without significantly affecting cooling at lower and mid levels. This is reasonable, since the downslope wind must provide the most cold air at the altitude of maximum mountain wind speeds. Qualitatively, therefore, the temperature-time relationships depicted in Figures 17 and 18 should result.

If we postulate further that the dew point inversion extends to significantly higher altitudes than the highest measurements made in Elmira (i.e., 17m), fog would form first aloft. Justification for this assumption is presented in the next subsection. Further justification was found by Schuepp (1945) in the only known simultaneous investigation of temperature and moisture distributions and valley circulations. He reported that on the average, a tongue of moist air extended from the slopes to the center of the Davos Valley in Switzerland at an average height of 40m, the same altitude

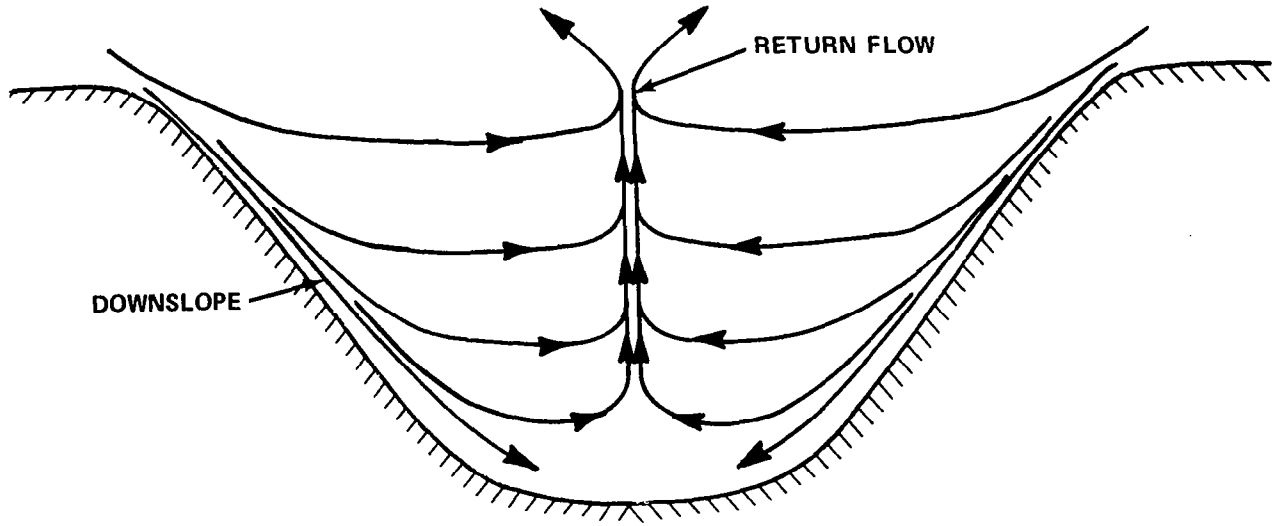

Figure 48 NOCTURNAL CROSSVALLEY CIRCULATION (AFTER WAGNER)

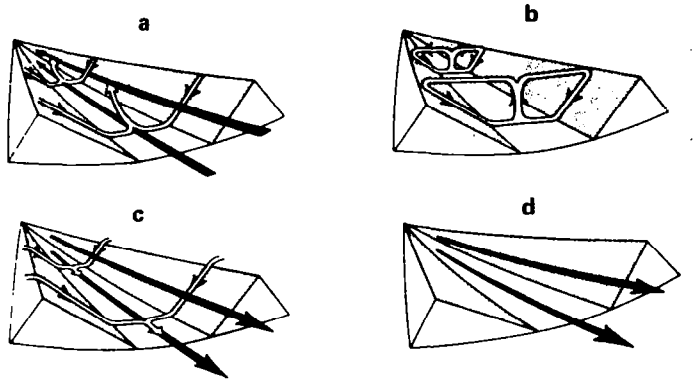

a. DOWNSLOPE WIND BEGINS SHORTLY AFTER SUNSET BEFORE UP-VALLEY MOUNTAIN WIND DIES.
b. IN LATE EVENING UP-VALLEY WIND DIES AND ONLY DOWNSLOPE WIND AND RETURN FLOW AT CENTER OF VALLEY EXIST.
c. RETURN FLOW AT CENTER OF VALLEY CEASES AND DOWN-VALLEY MOUNTAIN WIND BECOMES ESTABLISHED.
d. LATE AT NIGHT THE DOWNSLOPE WIND CEASES AND THE DOWN-VALLEY MOUNTAIN WIND PERSISTS.

Figure 49 THE NOCTURNAL MOUNTAIN WIND (AFTER DEFANT)

as the maxima of the valley wind for the experimental period. Schuepp's data are presented in Geiger (1965, Chapter VII)

Once fog has formed aloft, the propagation of its base downward is readily explained by an extension of the ideas suggested by Fleagle et al. (1952) concerning changes in stability that occur as a result of radiative flux divergence at the fog top. Assuming that no heat transfer occurs at the fog boundary, Korb and Zdunkowski (1970) calculated the cooling due to the flux divergence of a 1.6 m thick fog layer with a LWC = 0.1 g/m^3 to be approximately 9°C/hr. Such a cooling rate tends to increase the stability at and immediately above the fog top and causes an unstable lapse to exist within the fog. In the case of fog aloft, the instability must eventually extend beneath the fog base. As a result, the cold foggy air mixes predominantly with the clear, almost saturated air beneath to cause saturated conditions to propagate downward.

As mixing causes the supersaturated region to grow downward and fog forms at lower levels, condensation and evaporation that accompany up and down motions must cause the lapse rate beneath the level of maximum radiation divergence to approach wet adiabatic.

To summarize, therefore, we believe that the manner in which deep valley fog forms is as follows: (1) Nocturnal radiation from the surface and subsequent turbulent heat transfer from air to ground which produces an initial low-level temperature inversion stimulates the downslope wind and the upward return flow near the valley center. During this period, dew deposition at the cold surface creates the low level dewpoint inversion. The upward motion at the valley center carries the cool and somewhat dry air aloft to cause the inversion to deepen. (2) Approximately three hours before fog formation, the mountain wind forms and restricts the upward motion of air near the valley center. Cooling is therefore restricted to low and mid-levels of the valley; i.e., those levels in which fog will eventually form. The continuing downslope wind, which provides cold air for the mountain wind, mixes with existing, warmer air at mid-levels in the valley and causes the cooling rate to maximize in that region. Through this period, the dewpoint inversion persists. Temperature and dewpoint,

therefore, converge at mid-levels, and two to three hours after formation of the mountain wind, a thin layer of fog forms aloft. (3) The divergence of radiation in the fog simultaneously increases the stability at the fog top and promotes unstable conditions at the base of the thin fog layer aloft. Cool, foggy air therefore mixes with the clear air immediately below and causes supersaturation to propagate downward. This process continues until the fog base reaches the surface.

When fog forms before sunrise, the surface warming that begins between one half and one hour before sunrise is a result of a decrease in net radiation from the surface caused by the fog forming aloft and the continued conduction of heat from subsurface levels. The warming is reproduced quite well by the computer model.

When fog has not yet formed by sunrise, the surface warming and accompanying dew evaporation is caused by the sun. The instability that results at low levels stimulates vertical motions which apparently cause the now moist air from low levels to mix with cooler air aloft and produce the supersaturation that results in fog formation. Apparently this process produces fog after sunrise only when nocturnal processes have produced a very delicately balanced set of atmospheric conditions in the valley, since post sunrise fog formation occurred at the airport on three occasions and formed in other parts of the valley but not at the airport on two other seemingly identical occasions.

In reviewing the processes of fog formation, other mechanisms were examined in attempts to explain the observed temperature changes that occur in the valley. The mechanisms include direct long-wave radiative flux divergence from the upper atmosphere, horizontal eddy diffusion to the valley walls, and advection of cool air over the valley from the adjacent hilltops. As indicated in the subsequent paragraphs, these mechanisms are either inadequate to explain the observed cooling rates or produce temperature distributions that are in conflict with the data.

Kondo (1971) estimated the low-level cooling due to long-wave radiation under atmospheric conditions similar to those encountered in Elmira,

i.e., low wind speeds and high humidity at slightly warmer than freezing temperatures. His results indicate that long-wave radiation is indeed important to the heat budget in the lowest 100 m. Maximum cooling rates ($1.2\,^{\circ}C\ hr^{-1}$) occur in the lowest meter of air and cooling rates at the 100 m level between midnight and 0600 are of the order of $0.2\,^{\circ}C\ hr^{-1}$. The observed vertical distribution of cooling at Elmira is therefore reversed from that predicted on the basis of long-wave radiation.

Order of magnitude calculations show that to produce the observed cooling rates through horizontal eddy diffusion to the valley walls with the maximum observed temperature difference between hillside and center valley would require horizontal diffusion coefficients at least two orders of magnitude greater than expected under the stable conditions that exist before fog formation. Hence, horizontal diffusion must be eliminated as a cooling mechanism.

Advection of cold air from near the hilltops with the cross valley component of the ambient wind certainly contributes to cooling aloft. During the early evening, this process may be viewed qualitatively as an eddy diffusion process in which the ambient wind is blowing across an extremely rough surface consisting of the Chemung County hills. Such a mechanism could be responsible for the deep inversions (illustrated in Figures 15 and 16) which form before midnight.

The hypothesis that this cooling mechanism is responsible for fog formation breaks down upon consideration of the observed vertical temperature distribution after midnight and the correlation of that distribution with eventual fog height. Advection of cold air over the valley from the hilltops would cause maximum cooling near the hilltop levels or 200 to 300 m above the valley base. The data show, however, that the rate of cooling decreases at these levels several hours before fog formation, while the maximum cooling persists at or below 100 m in a manner that is correlated with eventual fog height. The data indicate, therefore, that the air in which the fog will form becomes more and more isolated from the air advecting over the valley from the hills in the hours immediately preceding fog formation.

- The Role of Dew in the Fog Life Cycle

The downward transport of moisture on clear nights and the formation of the nocturnal dew point inversion are attributed by numerous authors to the deposition of dew at the surface. See Wells (1838) and Geiger (1965, Chapter II). The first question pertaining to the role of dew in the fog life cycle is whether or not sufficient moisture is extracted by dew to produce the deep inversion postulated in the previous subsection.

Geiger presents empirical and theoretical data from a number of authors indicating that the nocturnal dew point inversion frequently extends to between 40 and 200 meters. The dew point inversions observed by Schuepp to extend to the 40 m level in a valley were already referenced. On the basis of past work, therefore, the assumption seems reasonable.

Our numerical model predicts dew point inversions extending to 40 m only with exchange coefficients too large to permit formation of fog. It must be recalled, however, that these same large exchange coefficients were required to produce temperature inversions extending to the same levels. Obviously, therefore, the numerical model does not simulate the valley situation adequately.

Some direct evidence that the prefog dewpoint inversion extends to upper levels in Elmira may be derived by combining our low-level dew point and dew deposition data.

If the observed dew is formed entirely as a result of extraction of water vapor in the atmosphere at the starting time and air mass changes do not account for observed dew point changes, conservation of mass may be used to provide an order of magnitude estimate of the depth of the dew point inversion if it is assumed that the initial and final dew point profiles are linear. The results of such a calculation based on the average data presented in Figures 26 and 28 and illustrated in Figure 50 indicate an inversion depth of 200 m. Even if 50% of the observed dew was formed from water vapor evaporated from the relatively warm soil (beneath the cold upper surface of grass) during the observation period (see Geiger, 1965, Chapter II) the depth of the inversion is more than adequate to explain

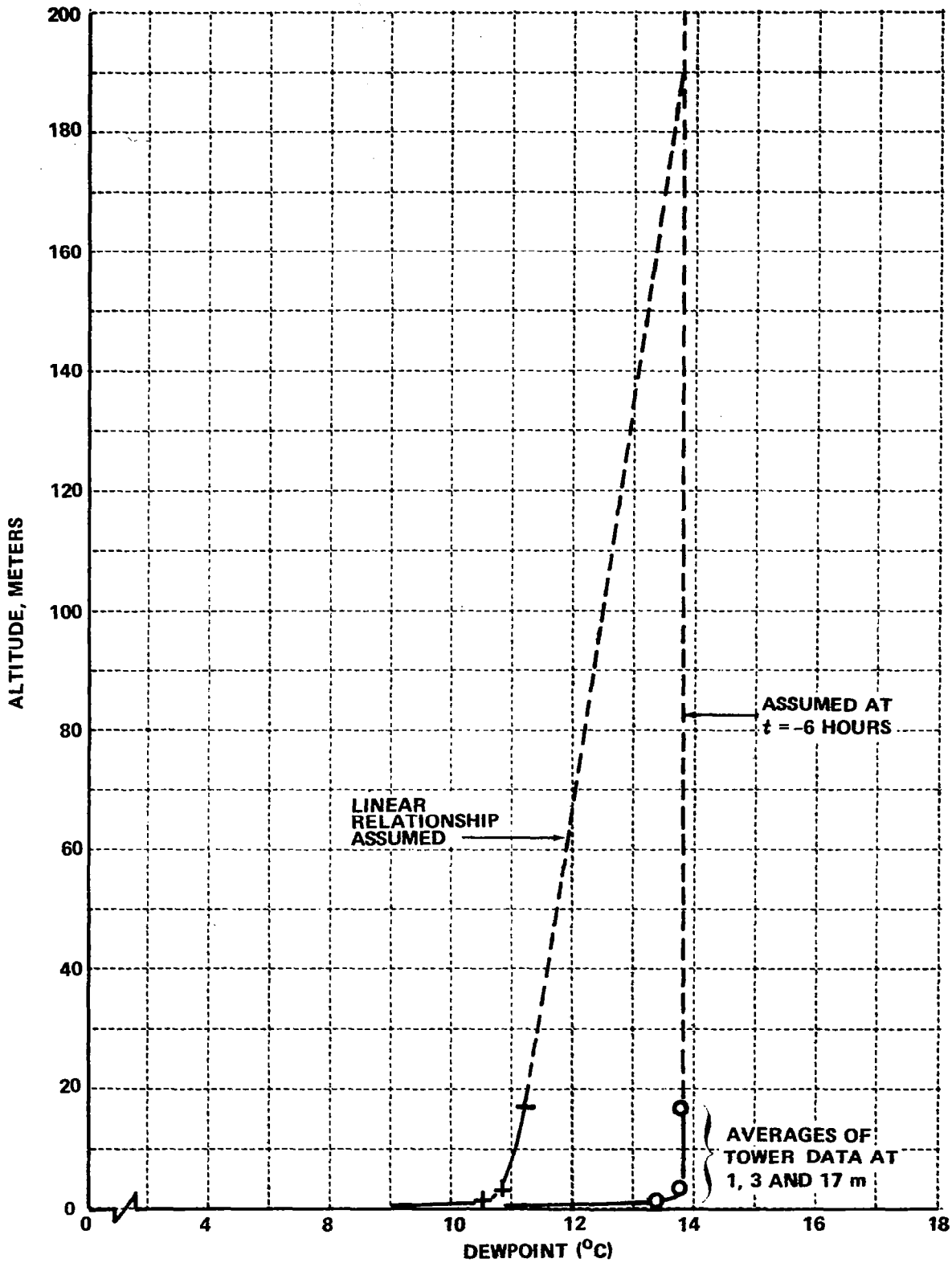

Figure 50 CALCULATED DEW POINT CHANGE BETWEEN t = -6 HOURS AND t = -0.5 HOUR REQUIRED TO PRODUCE MEASURED DEW DEPOSITION IN SAME TIME INTERVAL

inversion heights in the 30 to 60 m range. With the temperature distribution approaching isothermal beneath these levels, fog forms first aloft.

Between the time of fog formation and sunrise, it appears that dew serves no function other than to provide a wet lower boundary for the valley fog. After sunrise, the role of dew is most important.

Shortly after sunrise, the surface temperature begins to increase and stimulate dew evaporation. During the second hour after sunrise, the temperature of the entire fog increases at an average rate of $0.7°C\ hr^{-1}$. It is necessary, therefore, to provide water vapor to the fog at a rate of $0.4\ g\ m^{-3}\ hr^{-1}$ simply to maintain saturation. During the same period, the average dew evaporation rate is $55\ g\ m^{-2}\ hr^{-1}$, which is sufficient to maintain saturation in a fog 140 m thick. The fog, therefore, persists.

During the third hour after sunrise, the average rate of heating of the fog gradually increases to the point where dew evaporation can no longer maintain saturation. One should, therefore, expect fog dissipation to begin between 0830 and 0930 local time. The average observed time of the beginning of dissipation was very near 0900.

From these simple quantitative observations, it is apparent that dew evaporation plays a major role in the persistence of valley fog after sunrise.

As indicated above, natural fog dissipation begins when dew evaporation is not adequate to maintain saturation at a rate consistent with the rate of temperature increase. It is readily apparent from even casual observations that dissipation occurs first at the surface and gradually proceeds upward; a fact which undoubtedly has resulted in the term "fog lifting." For this sequence of events to occur, it is necessary for temperature to increase most rapidly at low levels to establish a lapse rate that is steeper than wet adiabatic beneath the persisting part of the fog. Under these conditions, the fog can be maintained aloft by cooling due to the upward air motions that occur at the time of fog dissipation (Figure 31).

Our tower temperature data indicate a superadiabatic lapse in the lowest 17 meters through fog dissipation. Our aircraft temperature data are not sufficiently accurate to distinguish between a wet adiabatic and the slightly greater lapse needed to explain "fog lifting."

- Evolution of Drop-Size Distributions and Associated Implications

The experimental data presented in Figures 33 and 35 show that the drop-size distributions that exist prior to formation of deep fog are consistently characterized by a mode between 2 and 4 μm radius and a maximum of about 8 μm. Between 65 and 95% of the droplets in each distribution have radii larger than 2 μm, suggesting that the observed droplets were not simply enlarged nuclei; i.e., the nuclei were fully activated to droplet growth. As indicated in the data presentation, these droplets characterize the ground fog which is usually below the level of the transmissometer. For this reason, absolute concentration cannot be established. Calculations based on transmissometer data obtained when the beam passes through the ground fog indicate typical droplets concentrations of 100 to 200 cm^{-3}.

Our notes do not include comments indicating the presence of ground fog immediately preceding the formation of deep fog. Through the early morning hours, we often observed GF to dissipate and reform. We were usually distracted, however, from the ground fog by the formation of deep fog aloft and consequently do not know if the dense ground fog dissipates prior to deep fog formation. From the data presented in Figures 33 and 40 for the fog of 2 September, it appears that the ground fog droplets did persist until deep fog formation but that drop concentration decreased before deep fog formed.

Changes in drop concentration may be due to a combination of the low-level warming that precedes fog formation and to the vertical mixing that increases significantly during the formation period of deep fog. In any case, it is apparent that the supersaturation present in the ground fog is sufficient to support the presence of 60 to 200 droplets cm^{-3} and therefore to produce full activation of those concentrations of cloud nuclei. These concentrations are greater by a factor of 2 to 10 than droplet concentrations observed in the deep fog. If it is assumed that the activation spectrum of the nuclei in the region in which ground fog forms is the same as at higher altitudes in the valley, which is certainly reasonable, it follows that supersaturation at the time of formation of ground fog is significantly greater than during formation of the deep fog.

This conclusion seems quite reasonable upon consideration of the temperature distribution through the two fog depths. Figure 13 shows the mean temperature difference to be approximately 2.5°C between the 1 m and 0.1 m levels during the six hours before fog. As equal air parcels from each of these levels are mixed, the supersaturation developed (before vapor depletion by droplet growth) is approximately 0.3%. Without vapor depletion, our cloud nuclei data (Figure 46) show that approximately 1000 nuclei cm^{-3} would be activated. With the existing vapor losses, the supersaturation attained is less and apparently just sufficient to produce the observed 100 to 200 droplets cm^{-3}.

The data presented in Figure 20, on the other hand, indicate a maximum temperature difference of about 1°C during the interval in which deep fog forms (Δt = one-half hour). Mixing of the two saturated air parcels at the temperature extremes would produce a supersaturation slightly exceeding 0.1% if such mixing could occur. Considering the extreme separation of these air parcels, it is obviously impossible for such mixing to occur without thorough dilution by air from other levels.

While the supersaturation at the time of ground fog formation exceeds that for deep fog, the drop-size distribution in ground fog remains narrow throughout its life cycle. This is partially due to precipitation of the largest drops (e.g., a 5 μm radius droplet falls through the 1 m depth in approximately five minutes) and is also associated with vapor depletion by the high concentration of existing droplets. Available water must be distributed over a higher concentration of nuclei so that no one droplet can grow rapidly. For obvious reasons, these mechanisms are not as effective in deep fog and the equilibrium drop-size distribution is significantly wider.

The consistent pattern of the evolution of the drop-size distribution between the fog formation distribution and the first visibility minimum is intriguing. The fact that droplets smaller than 3 to 4 μm radius are never detected during this period in which the total concentration of droplets is increasing deserves explanation. There appears to be an internal conflict in the data; i.e., large droplets seem to form without going through the small droplet stage.

One hypothesis which was considered in attempting to explain these observations is that the time required for growth of a new droplet from its critical radius (i.e., its radius at the maximum of the relevant Kohler curve) to 3 μm radius is so short and the concentration of drops in the 1 to 3 μm size range at any time is so small that the probability of detection of one of these droplets with our sampling procedure is essentially zero.

Excluding the fog of 15 August 1970, the average maximum rate of increase in drop concentration was 0.6 cm^{-3} min^{-1}. On 15 August 1970, the only case in which small drops were observed during the formation stage of deep fog, the rate was 2.6 drops cm^{-3} min^{-1}. Since droplets smaller than 3 μm radius are seldom observed, the hypothesis stipulates that the average concentration of droplets in this range must be smaller than 0.1 cm^{-3}, which is the minimum concentration that is consistently detected (probably about 50% of the time) with our sampling procedures. If we consider the average concentration to be a time average, it is necessary that the fraction of any long-time interval during which a given cubic centimeter of air is occupied by at least one droplet smaller than 3 μm radius is substantially less than 0.1. Otherwise, droplets in this size range would be detected. This fraction of the time is given by the product of the production rate of droplets and the time τ required for a newly activated droplet to grow to 3 μm radius. To go undetected, therefore:

$$0.1 < 0.6 \text{ cm}^{-3} \text{ minute} \times \tau \text{ minutes}$$

$$\tau < 0.17 \text{ minutes} = 10 \text{ seconds}$$

We may now ask whether or not the supersaturation required to produce such rapid growth can exist near the surface during fog formation. As a test case, we computed the growth at 0.3% supersaturation of drops that form on nuclei with different activation thresholds. The results are presented in Table III.

Table III

Growth of Droplets at 0.3%S
on Nuclei of Different Activation Supersaturations

Radius of dry NaCl Particle	Activation Threshold	Droplet Size at Indicated Time		
		5 Seconds	10 Seconds	20 Seconds
0.020 μm	0.45%	0.12 μm	0.13 μm	0.14 μm
0.025	0.32	0.20	0.20	0.20
0.032	0.23	1.17	1.85	2.82
0.040	0.16	1.31	1.95	2.90

It is obvious from these values that the time required for droplet growth on nuclei with even significantly lower activation thresholds than the existing supersaturation substantially exceeds the ten-second limit established above. Even larger supersaturation would therefore be required to explain the observations on the basis of this hypothesis. Since the data presented in Figure 46 show that the concentration of nuclei activated at 0.3% is of the order of 1000 cm^{-3}, we know that such supersaturations do not exist in the region of the measurement.

We must conclude from this analysis that the increase in concentration of droplets near the surface during deep fog formation is not due to activation of new nuclei in the region where the observations are made.

It is conceivable under some fog conditions that sporadic supersaturations exceeding 0.3% could be produced in small regions by mixing of the two near-saturated air parcels with different initial temperatures. The required temperature differences exceed those which were observed within the fog at Elmira, however.

A more realistic hypothesis for explaining the increase in droplet concentration at the surface during the fog formation stage is that the droplets are transported to the surface by turbulent diffusion from aloft. Under this assumption, the initial appearance of deep fog at the surface could occur

during a period in which the surface atmosphere is slightly unsaturated. With the fog existing aloft for times ranging from one-quarter to one hour before the first decrease in visibility, it is not necessary to postulate such rapid droplet growth and high supersaturations in order to cause most of the droplets to grow to radii exceeding 3.0 μm. The generation of new droplets can proceed continuously at higher altitudes. Upon being trapped in turbulent eddies, the droplets are carried downward. The associated warming promotes evaporation which tends to produce a wet adiabatic lapse. With the driving function for evaporation under a wet adiabatic lapse being a 0.02% supersaturation reduction per meter of descent, evaporation of newly formed small droplets can begin even before the eddy reaches the existing fog base.

If this level is 20 m, for example, evaporation may proceed for periods exceeding 100 seconds at the typical downward velocities observed on 12 September 1970 (Figure 31B) during the fog formation period. With the lower atmosphere already slightly subsaturated, the extremely small droplets can disappear.

The evaporation of droplets in the lower atmosphere plus the evaporation of dew from the warming surface must cause an increase in dew point at lower levels. (Such an increase is evident in the data presented in Figure 26.) When the lower atmosphere becomes saturated, complete evaporation of small droplets no longer occurs and the small droplets reappear in the data.

From the bimodal drop-size distributions in some fogs, it appears that in some cases, the low levels become supersaturated so that additional nuclei are activated. At the very low supersaturations that can exist in the presence of the high droplet concentration, the newly formed droplets grow very slowly so that it is not necessary to postulate continuous activation of nuclei to maintain the bimodal distribution.

CHAPTER IV

NUMERICAL MODELING OF RADIATION FOG

INTRODUCTION

• Brief Description of Model

A numerical model has been developed to investigate the influences of various vertical transfer processes in shaping the life cycle of radiation fogs, i.e., fogs which result from the nocturnal cooling of the earth's surface by infrared radiation. The model has a one-dimensional vertical grid system which extends from one meter below the earth's surface to several hundred meters above the surface. In the atmosphere, starting from various initial conditions, the model predicts the temporal evolution of the vertical distributions of potential temperature, water vapor, and liquid water as determined by turbulent diffusion. Prior to fog formation, radiative flux divergence in the atmosphere is neglected. In the soil, the model predicts the evolution of the vertical temperature distribution under the influence of heat conduction.

The atmosphere and soil are coupled at the surface by maintaining continuity of the temperature and heat flux. During nocturnal cooling, the net upward flux of infrared radiation at the surface is balanced by an upward heat flux from the soil and a downward eddy flux of heat from the atmosphere. A no-flux boundary condition on water vapor content is maintained at the surface until the dew point is reached. After the surface is cooled to the dew point, the water vapor content at the surface is assumed to be saturated at the surface temperature, and dew is allowed to form.

Fog is formed in the model by converting any water vapor content in excess of saturation into liquid water, after accounting for the latent heat of condensation released in the process. The model includes the influences of infrared absorption and radiation by fog, and fog drop sedimentation upon the development and maintenance of fog.

The most difficult area in the model development has proven to be the necessity of providing atmosphere exchange coefficients for turbulent transfer of heat and moisture over wide variations of height and stability.

Some success has been achieved in using exchange coefficients which are functions of friction velocity, height, and the predicted local thermal stability.

Numerical experiments with the fog model have been devoted to delineating the roles of the turbulent transfer of heat and moisture and the radiative transfer of heat in the formation and maintenance of fog. The model has been fairly successful in simulating the formation of radiation fogs (10-40 meters in height) starting from conditions near sundown. It appears, however, that a considerable improvement on the realism of the modeling results might be effected by making the horizontal wind a prognostic variable of the model, and including a dependence of the exchange coefficients on the vertical wind shear.

The model has not been successful in producing the deep fogs (100-150 meters in height) observed near Elmira, New York. It is believed that a two- or three-dimensional model will be required to provide a satisfactory simulation of fog formation aloft and some other characteristic features of the deep valley fogs. The present model, however, constitutes a significant advance in the modeling of the processes which shape the life cycle of fog and provides a sound basis for the development of multi-dimensional models in the future.

- Previous Work

Although the development of the present model was based upon studies of fog, nocturnal cooling, turbulence, and radiative transfer too numerous to cite here, it is appropriate to mention certain studies which had a particularly important influence on the direction of the present modeling investigation.

An investigation of the factors which contribute to the formation of fog is not complete without a careful study of the classical paper by Rodhe (1962) on "The effect of turbulence on fog formation." Rodhe puts the thermodynamics of unsaturated and saturated processes on a common basis and delineates the key role in fog formation of the simultaneous turbulent transfer of heat and moisture. His analytical treatment of the formation of radiation fog, although based on a constant, height independent turbulent exchange coefficient, offers important insights in the physical processes involved.

Fisher and Caplan (1963) demonstrated the feasibility of simulating the formation and dissipation of radiation and advection fogs by means of a numerical model. The present model employs to a large extent the computational procedure used by Fisher and Caplan to solve their differential equations for the changes in potential temperature, water vapor content, and liquid water content produced by vertical turbulent diffusion. Fisher and Caplan use variable turbulent exchange coefficients which depend upon height and local stability, although in a somewhat crude manner. No radiation effects are included in the model.

A study of the Fisher and Caplan results for radiation fogs shows that the principal shortcoming of their model is a predetermined temperature variation at the surface, which does not depend upon the computed variables. Also, their no-flux condition on moisture at the surface precludes the development of a dew point inversion as a result of dew deposition at the surface.

McDonald (1963) proposed a "saturation adjustment" procedure in the numerical modeling of fog to treat condensation and evaporation in a thermodynamically sound manner. This procedure is used in the present model.

Zdunkowski and Nielsen (1969) discuss a fairly sophisticated numerical model of radiation fog. Their model provides a careful, unified treatment of the atmosphere and the soil so that the surface temperature is a prognostic variable of the model. In the Zdunkowski and Nielsen model, the radiative flux divergences produced by water vapor and fog droplets are predicted through unified radiative transfer calculations at every time step. Their turbulent exchange coefficients, on the other hand, are height dependent, but do not vary with time as a function of prognostic variables of the model.

The surface boundary conditions on moisture employed by Zdunkowski and Nielsen conserve the total moisture content of the atmosphere. This again precludes the formation of a dew point inversion as a result of dew deposition of the surface, a phenomena which can significantly delay the formation of fog (see Rodhe (1962)). Nevertheless, the numerical results obtained by Zdunkowski and Nielsen appear sufficiently realistic to indicate the fundamental soundness of much of the model. As noted by the authors,

the principal improvement necessary in the development of a satisfactory radiation fog model is the internal generation of realistic exchange coefficients as a function of the prognostic variables of the model.

The primary improvements attempted in the present numerical fog model are internally generated exchange coefficients, dew formation at the surface, and inclusion of the effects of fog drop sedimentation. Only a crude treatment of radiative transfer is included. The numerical model is described in some detail in the next section entitled Numerical Model, and the results of numerical experiments with the model are discussed in the section entitled Results.

NUMERICAL MODEL

- Major Assumptions

The following assumptions are adopted in the numerical modeling study of radiation fog:

a) The model is one-dimensional in the Z direction. All of the quantities are uniform in an X, Y plane.

b) The turbulent exchange coefficients for heat, water vapor, and liquid water are equal.

c) Prior to fog formation, radiative flux divergence in the atmosphere is neglected.

d) Supersaturated water vapor condenses instantaneously until saturation is achieved. Liquid water in an unsaturated region evaporates instantaneously until saturation is achieved or the liquid water is exhausted.

- Equations

List of Symbols

In order to avoid lengthy explanations in the text, a list of the most important symbols employed will be given first:

T, θ	temperature and potential temperature of air
T_s	soil temperature
r	water vapor mixing ratio
r_s	saturation mixing ratio
w	liquid water mixing ratio
z	height coordinate
z_k	kth vertical grid level
t	time
K	turbulent exchange coefficient for vertical transfer
K_s	thermal diffusivity of soil
ρ, ρ_s	density of air and soil
C_p, C_s	specific heat of air at constant pressure and of soil
R	net upward flux of infrared radiation
σ	Stefan-Boltzmann constant
P	air pressure
L	latent heat of condensation
V_t	mean terminal velocity of fog drops
k_w	mean mass absorption coefficient of fog for infrared radiation ($cm^2 g^{-1}$)
g	gravitational constant
u^*	friction velocity
k	Von Karman constant = 0.4
n	denotes nth time step

Major Equations

The equations employed in the model for the time rate change of potential temperature θ, water vapor mixing ratio r, liquid water mixing ratio w, and soil temperature T_s are:

$$\frac{\partial \theta}{\partial t} = \frac{\partial}{\partial z}\left(K \frac{\partial \theta}{\partial z}\right) + \frac{1}{\rho C_p}\left(\frac{1000}{P}\right)^{2/7}\left(L \cdot C - \frac{\partial R}{\partial z}\right) \tag{4}$$

$$\frac{\partial r}{\partial t} = \frac{\partial}{\partial z}\left(K \frac{\partial r}{\partial z}\right) - C \tag{5}$$

$$\frac{\partial w}{\partial t} = \frac{\partial}{\partial z}\left(K\frac{\partial w}{\partial z}\right) + \frac{\partial}{\partial z}\left(V_t\, w\right) + C \tag{6}$$

$$\frac{\partial T_s}{\partial t} = K_s \frac{\partial^2 T_s}{\partial z^2} \tag{7}$$

Saturation Adjustment

The symbol C denotes a source function for condensation or evaporation. In the actual model, the finite difference approximations to Eqs. (4) through (7) are integrated for a time step, neglecting condensation or evaporation. Then, the saturation adjustment procedure developed by McDonald (1963) is applied to the new values of θ, r, and w. Taking into account the heating of the air by the release of latent heat of condensation, supersaturated water vapor at a grid level is converted into liquid water until saturation is achieved. Similarly, taking into account the cooling of the air, liquid water at a grid level is evaporated into an unsaturated vapor until saturation is achieved or the liquid water is exhausted.

Radiation

The treatment of radiation in the present model is designed to capture the essence of physical processes while avoiding detailed radiative transfer calculations. Prior to fog formation, the radiative flux divergence $\partial R/\partial z$ in Eq. (4) is assumed to be everywhere zero. The net upward flux of infrared radiation at the surface $R(0)$ is assumed to be a constant fraction β of the blackbody radiation at the surface temperature $T(0)$ i.e.,

$$R(0) = \beta \sigma T^4(0) \tag{8}$$

The constant β is typically taken to be .25 (Sutton, 1953), signifying that the back radiation from atmosphere is assumed to be .75 of the full blackbody radiation from the surface.

After fog formation, a radiative flux divergence $\partial R/\partial z$ resulting from absorption and reradiation by the fog drops is introduced in Eq. (4). Representing the influence of fog drops by a single spectrally-averaged mass absorption coefficient k_w and neglecting temperature gradients in the fog, the radiative flux at a height z in the fog is given by

$$R(z) = \beta\sigma T^4(0)\, e^{-1.6 k_w \rho_z \int^{z_t} w(z')\,dz'} \tag{9}$$

where z_t is the top of the fog and the effect of the angular dependence of the radiation field has been approximated by using the diffusivity factor 1.6 (Goody, 1964). Differentiating with respect to z, the radiative flux divergence at height z is given by

$$\frac{\partial R}{\partial z} = \beta\sigma T^4(0)\, 1.6\, k_w \rho\, w(z)\, e^{-1.6 k_w \rho \int_z^{z_t} w(z')\,dz'} \tag{10}$$

In the model, the integrals over w are evaluated numerically.

In the Rayleigh limit $r/\lambda \ll 1$, the absorption cross section of water drops is proportional to r^3 (Batten, 1959). The results of Stephens (1961) show that spectrally-averaged absorption cross sections for blackbody radiation are virtually independent of temperature in the temperature range of interest to this study, and approximately proportional to r^3 for drop sizes up to $r = 5\ \mu m$. Based upon these results of Stephens, a mean mass absorption coefficient $k_w = 1.5 \times 10^3\ cm^2 g^{-1}$ was deduced and was applied in the model.

This treatment of radiative transfer in a fog would not be a satisfactory approximation for a fog which has a significant number of drops with $r > 10\ \mu m$, since the spectrally-averaged absorption cross sections for large drops are approximately proportional to r^2 (Zdunkowski and Nielsen, 1969), and scattering becomes increasingly important in the radiative transfer as the drop sizes increase. It also should be noted that use of a spectrally-averaged absorption coefficient for blackbody radiation is less than accurate for the back radiation from the atmosphere which is deficient in water vapor window near $\lambda = 10\ \mu m$. In spite of these

shortcomings, this simple treatment provides a roughly quantitative simulation of the reduction of the net upward radiation at the surface by fog and of the accompanying radiative cooling of the fog.

Exchange Coefficients

The most difficult area in the development of the model proved to be providing realistic turbulent exchange coefficients for the vertical transfer of heat and moisture over wide ranges of height and stability. The preponderance of useful information in the literature on vertical turbulent transfer is restricted to a few tens of meters above the surface in the "constant flux" layer. Furthermore, during low wind nocturnal inversion conditions, there is a paucity of observational data on turbulence and vertical transfer.

Observational data from Elmira in mature fogs show a transition from unstable conditions near the surface to a capping inversion at fog top, even at night. To treat this situation, it appeared necessary that the turbulent exchange coefficients in the model should be a function of the local stability, not just the surface heat flux as in a constant flux layer. On the other hand, since the horizontal wind is not a prognostic variable in the present model, the friction velocity $u^* = \sqrt{\tau/\rho}$, where τ is the shear stress, is treated as an input parameter in the model.

It is assumed in the model that the exchange coefficients for heat, water vapor, and liquid water are equal. The functional dependence of the exchange coefficients upon local stability and height in the model is based upon the so-called KEYPS formula (Lumley and Panofsky, 1964)

$$S^4 - \gamma \frac{z}{L} S^3 = 1, \tag{11}$$

for the dependence of non-dimensional wind shear

$$S = \frac{kz}{u^*} \frac{\partial v}{\partial z} \tag{12}$$

upon height z and the scaling length

$$L = \frac{-u^{*3} \rho C_p T}{k g H} \tag{13}$$

Here, H is the vertical heat flux and γ is an empirical constant which is assumed to be 14 after Lumley and Panofsky.

The KEYPS formula is an interpolation between free and forced convection and has been shown to be in reasonable agreement with observations in the constant flux layer extending 10-100 meters above the surface, where τ and H are approximately constant. Assuming that the exchange coefficients for momentum and heat are equal and that H is the local heat flux, the KEYPS formula yields an explicit relationship for the exchange coefficients as a function of height and stability. In the present fog model, this relationship is applied throughout the entire depth of the model atmosphere.

By definition of the exchange coefficient for momentum K_m, the non-dimensional wind shear can be written in the form

$$S = \frac{k u^* z}{K_m} \tag{14}$$

By definition of the exchange coefficient for heat K_h, the vertical heat flux is

$$H = -\rho C_p K_h \frac{\partial \theta}{\partial z} \tag{15}$$

Substituting this expression for H into Eq. (13), the scaling length can be written

$$L = \frac{u^{*3} T}{k g K_h \frac{\partial \theta}{\partial z}} \tag{16}$$

Now substituting Eq. (14) and Eq. (16) into KEYPS formula, Eq. (11), and asserting $K_h = K_m = K$, we obtain

$$(kz)^4 \left[\left(\frac{u^*}{K}\right)^4 - \gamma \frac{g}{T} \frac{\partial \theta}{\partial z} \left(\frac{1}{K}\right)^2 \right] = 1 . \tag{17}$$

Solving Eq. (17) for K, we obtain the expression

$$K = \frac{kz}{\sqrt{2}} \left\{ -\gamma \frac{g}{T} \frac{\partial \theta}{\partial z} (kz)^2 + \left[\left(\gamma \frac{g}{T} \frac{\partial \theta}{\partial z} (kz)^2 \right)^2 + 4 u^{*4} \right]^{1/2} \right\}^{1/2}, \tag{18}$$

used in the model for K as a function of z, $\partial\theta/\partial z$, and the parameter u^*.

It can be verified that when $\left|\gamma \frac{g}{T} \frac{\partial\theta}{\partial z}(kz)^2\right| << 2u^{*2}$, Eq. (18) reduces to the expression for a neutral atmosphere

$$K = k u^* z \tag{19}$$

In the limit $\gamma \frac{g}{T} \frac{\partial\theta}{\partial z}(kz)^2 >> 2u^{*2}$ occurring under stable conditions, it can be shown that

$$K = \frac{u^{*2}}{\left[\gamma \frac{g}{T} \frac{\partial\theta}{\partial z}\right]^{1/2}} \tag{20}$$

independent of z.

In the limit $-\gamma \frac{g}{T} \frac{\partial\theta}{\partial z}(kz)^2 >> 2u^{*2}$ occurring under unstable conditions, it can be shown that

$$K = \left[-\gamma \frac{g}{T} \frac{\partial\theta}{\partial z}\right]^{1/2} (kz)^{3/2} \tag{21}$$

independent of u^*.

To permit the incorporation of a dependence upon roughness length z_0 into the values of K near the surface, the constant $k u^* z_0$ is added to the computed values of K in the model. Since the K dependence for neutral conditions (Eq. (19)) prevails near the surface, regardless of stability, the K dependence near the surface now becomes $K = k u^*(z + z_0)$, in agreement with velocity profiles under neutral conditions (Lumley and Panofsky, 1964).

In a cloud or fog, a moist adiabatic lapse rate is neutrally stable rather than a dry adiabatic lapse rate. Therefore, when K is evaluated in fog, $\partial\theta/\partial z$ in Eq. (18) is replaced in the model by the expression

$$\frac{\theta}{T}\left(\frac{\partial T}{\partial z} + \Gamma_m\right), \tag{22}$$

where Γ_m is the local moist adiabatic lapse rate. In practice, the model fogs are sufficiently close to surface so that the ratio θ/T can be replaced by unity.

Terminal Velocity of Fog Drops

In the model, the sedimentation of the fog drops is simulated through the mean terminal velocity V_t in Eq. (6). Preliminary experiments with the model in which V_t was maintained at a constant 1.2 cm/sec corresponding to a drop 10 μm in radius, showed that this value of V_t served to unrealistically inhibit the upward development of a model fog after formation at the surface. Consequently, V_t in the model was made a function of the local liquid water mixing ratio through the assumption that the drop concentration remains constant. Under this assumption, V_t is negligible until the liquid water content approaches values observed in well-developed fogs.

The liquid water mixing ratio w can be written

$$w = N \frac{4\pi}{3} \frac{\rho_w}{\rho} r^3 \tag{23}$$

where N is the number of drops per unit volume, r is the mean volume radius of the drop-size distribution, ρ_w is the density of liquid water, and ρ is the air density. Eq. (23) can be solved for r and the result substituted in the Stokes relationship (Fletcher, 1966)

$$V_t = 1.2 \times 10^6 r^2 (cgs\ units) \tag{24}$$

for terminal velocity of water droplets under 20 μm in radius. The resulting expression is

$$V_t = 5.3 \times 10^3 \left(\frac{w}{N}\right)^{2/3} \tag{25}$$

where N is number drops cm^{-3}.

Assuming a constant drop concentration $N = 50\ cm^{-3}$, Eq. (25) reduces to the expression

$$V_t = 4 \times 10^2 w^{2/3}\ cm/sec \tag{26}$$

employed in the model. For a liquid water mixing ratio $w = 1.22 \times 10^{-4}$ corresponding to liquid water content of approximately $0.15\ gm^{-3}$, typical of well-developed Elmira fogs, Eq. (26) yields $V_t = 1.0\ cm/sec$

- Boundary Conditions

Upper and Lower Boundaries

At the upper boundary of the vertical grid system in the atmosphere, the values of the potential temperature θ , water vapor mixing ratio r , and the liquid water mixing ratio w are maintained equal to their initial values throughout a numerical experiment. The normal boundary condition on w is $w = 0$. At the lower boundary of the vertical grid system in the soil, the soil temperature T_s is maintained equal to its initial value throughout a numerical experiment.

The Surface

The earth's surface ($z = 0$) represents an internal boundary in the model between the atmosphere and the soil. The boundary conditions invoked in the model at this internal boundary in order to couple the atmosphere and soil are continuity of temperature and heat flux. The former condition merely asserts $\theta = T = T_s$ at the surface (assumed to be at $p = 1000\ mb$). The latter condition can be written in the form

$$-\rho_s C_s K_s \left(\frac{\partial T_s}{\partial z}\right)_{z=0} = -\rho \left[C_p \left(K \frac{\partial \theta}{\partial z}\right)_{z=0} + L \left(K \frac{\partial r}{\partial z}\right)_{z=0} \right] + R(0) \tag{27}$$

where the upward flux of heat from the soil equals the sum of the upward fluxes of sensible heat, latent heat, and infrared radiation in the atmosphere.

Before the dew point is reached at the surface, a no-flux boundary condition $\left(K \frac{\partial r}{\partial z}\right)_{z=0} = 0$ on the water vapor mixing ratio r is maintained at the surface. After the surface is cooled to the dew point, r at the surface is assumed to be saturated at the surface temperature, and dew is allowed to form. The boundary condition $w = 0$ is maintained on the liquid water mixing ratio at the surface under all conditions.

Denoting the first grid level below the surface in the soil by -1, the surface by 0, and first grid level above the surface in the atmosphere by +1, Eq. (27) is represented in the model by the finite difference equation

$$-\rho_s C_s K_s \frac{(T(0) - T_s(-1))}{\Delta z_{-1}} =$$

$$\rho K(+\tfrac{1}{2})\left[\frac{C_p(\theta(+1)-T(0)) + L(r(+1)-r(0))}{\Delta z_{+1}}\right] + \beta\sigma T^4(0)\, e^{-1.6 k_w \rho \int_0^{z_t} w(z')dz'} \tag{28}$$

where Δz_{-1} and Δz_{+1} are the grid distances from the surface and $K(+1/2)$ denotes K evaluated at a point midway between the surface and grid level +1 in the atmosphere.

Given values of $T_s(-1)$, $\theta(+1)$, $r(+1)$ and the integral over w, Eq. (28) can be solved for the surface temperature $T(0)$, provided some assumption is made about $r(0)$. The procedure adopted in the model is to assume that $r(0) = r(+1)$, and solve Eq. (28) numerically for $T(0)$ using the Newton-Raphson method. It should be noted that this can be accomplished either when $T_s(-1)$, $\theta(+1)$ and $r(+1)$ are known explicitly or through some known functional relationships between $T_s(-1)$ and $T(0)$, $\theta(+1)$ and $T(0)$, and $r(+1)$ and $r(0)$. Both situations are encountered in the model.

After solving for $T(0)$, assuming $r(0) = r(+1)$, a saturation adjustment procedure is carried out at the surface, which is similar in philosophy to that carried out in the model atmosphere after each time step. If $r(0) = r(1) > r_s(T(0))$ or dew is already present, $T(0)$ and $r(0)$ are adjusted to satisfy the boundary condition

$$r(0) = r_s(T(0)), \tag{29}$$

while accounting for the adjustment of the surface heat balance as a result of the latent heat flux introduced into Eq. (28) by the procedure.

- Computational Procedure

Grid System

In the vertical grid system employed in the model, the separation between adjacent grid levels expands upward from the surface in the atmosphere and downward from the surface in the soil. The expanding grid system

provides high resolution near the surface where the variables of the model change rapidly with height and removes the upper and lower boundaries from the region of primary change, without requiring a prohibitively large number of grid levels.

In the soil, there are 16 grid levels. The grid separation expands downward by a factor of 1.5 per level from the highest level 1 mm below the surface to the lower boundary at 1.31 meters below the surface. In the atmosphere, various expanding grids have been employed with the lowest level at 1 cm or 10 cm above the surface. At highest resolution, 50 atmospheric grid levels have been used, with the grid separation expanding by a factor of 1.2 per level from the lowest level 1 cm above the surface to the upper boundary 379 meters above the surface.

Implicit Integration

Since the grid system has very fine grid spacing near the surface, it was necessary to adopt an implicit method of solution of the partial differential equations of the model (Eqs. (4)-(7)) in order to obtain stable solutions using reasonably large time steps. The implicit method used in the model is almost identical to that employed successfully by Fisher and Caplan (1963) with a similar group of equations. The basic integration scheme for diffusion equations of the type

$$\frac{\partial Q}{\partial t} = \frac{\partial}{\partial z}\left(K\frac{\partial Q}{\partial z}\right) \tag{30}$$

is

$$\frac{Q_{n+1} - Q_n}{\Delta t} = \frac{\frac{\delta}{\delta z}\left(K_n \frac{\delta Q_n}{\delta z}\right) + \frac{\delta}{\delta z}\left(K_n \frac{\delta Q_{n+1}}{\delta z}\right)}{2} \tag{31}$$

where n and $n+1$ denote values known at the end of successive time steps. In Eq. (31), the Q_n's and K_n's are known explicitly, while the Q_{n+1}'s are known only implicitly.

Denoting three adjacent grid levels by $k-1$, k, and $k+1$, Eq. (31) can be placed in the general form,

$$D_n(k) = -A_n(k)\,Q_{n+1}(k+1) + B_n(k)\,Q_{n+1}(k) - C_n(k)\,Q_{n+1}(k-1) \tag{32}$$

where A, B, C, and D are known quantities from the previous time step. There is an equation of this type involving $Q_{n+1}(k+1)$, $Q_{n+1}(k)$, and $Q_{n+1}(k-1)$ for each vertical grid level k. In order to determine the Q_{n+1}'s, this system of simultaneous linear equations must be solved. This is the essence of implicit integration methods.

The general method of solution adopted by Fisher and Caplan (1963) is based on the techniques of Richtmyer (1957) and will not be discussed in detail here. Basically, it involves scanning the grid system in one direction, making use of the boundary value at the start, to develop linear relations between the Q_{n+1}'s at adjacent grid levels, e.g.,

$$Q_{n+1}(k) = E(k)\,Q_{n+1}(k+1) + F(k) \tag{33}$$

or

$$Q_{n+1}(k) = E'(k)\,Q_{n+1}(k-1) + F'(k) \tag{34}$$

Then, making use of the boundary value at the other end of the grid system to start, the grid system is scanned in the opposite direction, successively determining all the Q_{n+1}'s.

Summary of Computational Sequence

Suppose all the variables are known at the vertical grid levels z_k and at the surface $(z = 0)$ after the nth time step. The $n+1$ time step of the integration is accomplished in the following manner:

1. Starting from the invariant boundary values at the upper boundary of the grid system in the atmosphere, initiate the implicit integration by proceeding down the grid system to first grid level above the surface $(k=1)$ and computing the $E'(k)$'s and $F'(k)$'s (see Eq. (34)) for θ, r, and ω. Starting from the invariant boundary value at the lower boundary of the grid system in the soil, proceed up the grid system to the first grid level below the surface $(k=-1)$ computing the $E(k)$'s and $F(k)$'s (see Eq. (33)) for T_s.

2. Using the relationships,

$$\begin{aligned} \theta(1) &= E'_\theta(1) \cdot \theta(0) + F'_\theta(1) \\ r(1) &= E'_r(1) \cdot r(0) + F'_r(1) \\ T_s(-1) &= E_{T_s}(-1) \cdot T_s(0) + F_{T_s}(-1) \end{aligned} \tag{35}$$

and $\theta(0) = T(0) = T_s(0)$, solve the surface heat balance relationship for $T(0)$ and $r(0)$.

3. Given $\theta(0) = T(0)$, $r(0)$, and the boundary value $\omega(0) = 0$, proceed up the atmospheric grid system, computing the new values of θ, r, and ω using the previously determined relationships (Eq. (34)). If necessary, perform a saturated adjustment on the values of θ, r, and ω to account for condensation or evaporation. Compute integrals over ω for the computation of radiative flux divergence $\partial R/\partial z$. Given $T_s(0) = T(0)$, proceed down the soil grid system, computing new values of T_s using the previously determined relationships (Eq. (33)).

4. If necessary, recompute $T(0)$ and $R(0)$ based on the adjusted values of $\theta(1)$ and $r(1)$ and the new value of integral over ω in the expression for the net radiation flux at the surface $R(0)$.

5. Proceed up the atmospheric grid system, computing new values of the turbulent exchange coefficient K and the radiative flux divergence $\partial R/\partial z$. The change in the amount of total dew deposition at the surface during the time step is computed by averaging the moisture fluxes at the surface at the beginning and end of the time step. This completes the time step.

Timing

The fog model was programmed in FORTRAN and run on CAL's IBM 370/165 digital computer. It was found that 60 sec time steps provided stable integrations during nocturnal cooling and initial fog formation. Based upon a 50 level atmospheric grid and a 16 level soil grid, a simulation of 14 hours of meteorological time with the fog model using 60 sec time steps requires 20 sec of computer time on the 370.

If a fog is formed in the model which has sufficient liquid water in a unit column, the net radiative flux at surface $R(0)$ is reduced as the fog top takes over as the effective radiating surface. Under these conditions, the surface temperature rises and the temperature stratification in the lower part of the fog becomes unstable. With time, the unstable region builds upward toward the top of the fog. It is found in this situation that the time step must be reduced to approximately 10 sec to eliminate computational instabilities which develop in unstable regions of the fog.

- Initial Conditions and Constants

The fog model permits initialization with observed distributions of the four variables of the model. All numerical experiments which have been carried out with the model, however, have been based upon idealized initial distributions of the model variables.

The initial distributions of potential temperature θ have been either adiabatic (θ = const.) or isothermal (T = const.). The soil temperatures have always been initialized to be isothermal at the temperature of the first grid level above the surface in the atmosphere.

The most common initial condition on water vapor mixing ratio was a uniform distribution with height. The liquid water mixing ratio was always initialized to zero, everywhere.

These initial conditions are assumed to be approximately representative of conditions prevailing near sundown. The initialization procedure is completed by solving the surface heat balance relation for the surface temperature $T(0)$ and setting $\theta(0) = T_s(0) = T(0)$. This results in an initial $T(0)$ that is 0.1 to 0.2°C cooler than $T_s(-1)$ and $\theta(+1)$ and sets up the nocturnal cooling process.

The soil parameters, $K_s = 3 \times 10^{-3} cm^2/sec$ and $h_s = \rho_s C_s K_s = 1.5 \times 10^{-3} cal. cm^{-1} (^oC)^{-1} \cdot sec^{-1}$ are treated as constants. They are typical of a soil of average thermal characteristics, say, a sandy clay (Johnson, 1960; Geiger, 1965).

The roughness length z_0 in the expression for the turbulent exchange coefficients K in the model was varied between 0 and 3 cm. The latter value of z_0 corresponds to an average height of the roughness elements of approximately 20 cm (Plate, 1971), thought to be rather typical of the Elmira field site. Variation of z_0 between 0 and 3 cm had a profound effect on the predicted temperature stratification in the lowest 10 cm of the model atmosphere during nocturnal cooling, reducing the temperature discontinuity between the surface and the first grid level at 1 cm from $0.4^{\circ}C$ to less than $0.1^{\circ}C$. However, since the variation of z_0 had no other important effect upon the results of the numerical experiments with the fog model, it will not be discussed further.

The friction velocity u^* was the most important parameter to be varied in the numerical experiments with the fog model, since it controls the degree of turbulent diffusion in the model. For various initial conditions, u^* was varied between 3 cm sec^{-1} and 30 cm sec^{-1}, to delineate the important factors which influence the formation and properties of radiation fog.

RESULTS

• General Characteristics of Model Fogs

Fog formed by this model is a relatively shallow type of radiation fog. Figure 51 shows typical behavior of fog top height with time; steady state fog top heights vary from six to forty meters.

The model in its present form does not reproduce deep fogs with tops around 100-150 m as frequently observed in Elmira, New York and reported for Handford, Washington (Fleagle et al., 1952). Formation of deep fogs at Elmira is related to the influence of the valley on atmospheric processes. The exact nature of the valley effect is not known, although the discussion in Chapter III provides considerable insight into this problem. The inability of the present model to form these deep fogs stems, in part, from its one-dimensional character and the assumption of a constant U^*. In subsequent sections, these limitations of the model are discussed in somewhat more detail.

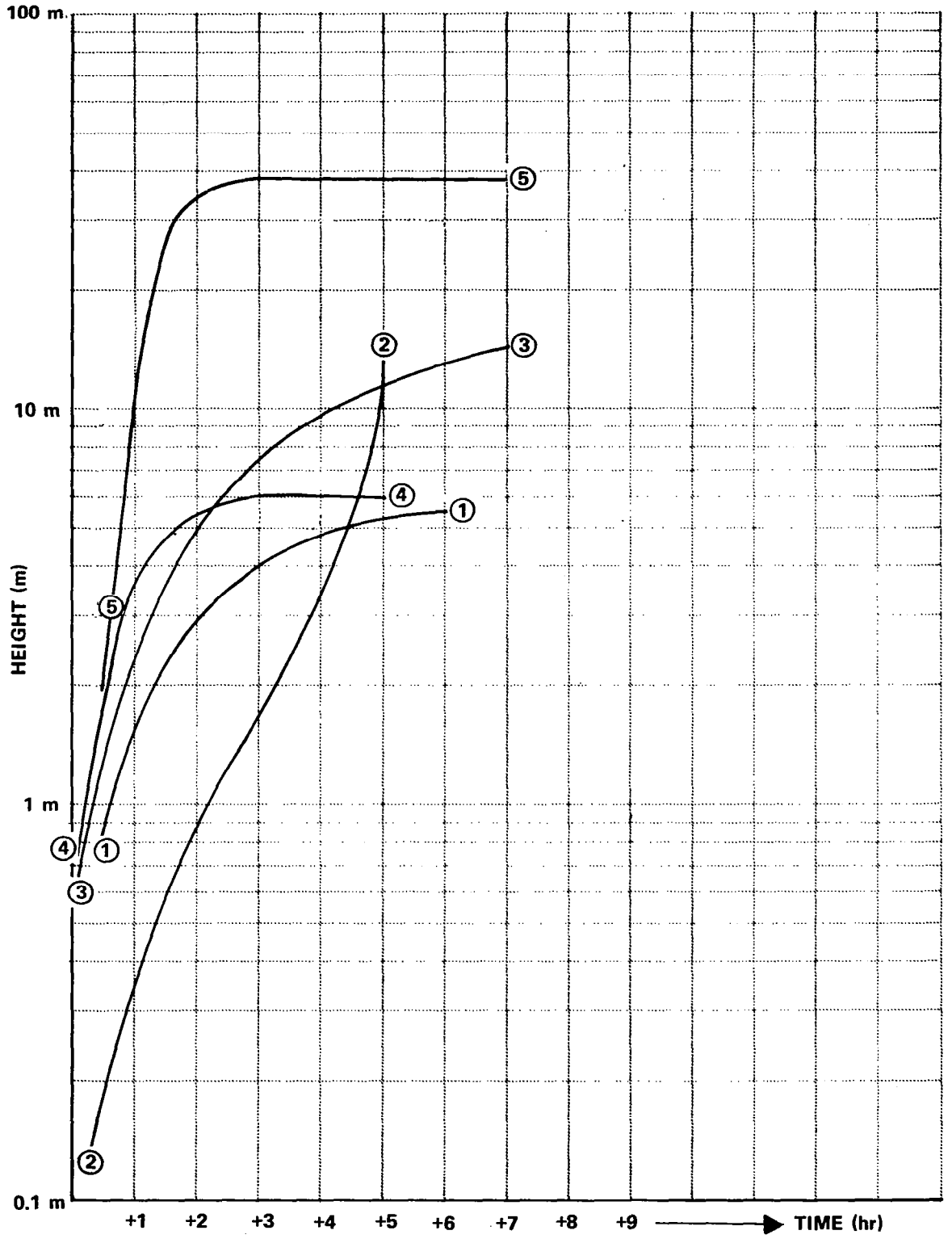

Figure 51 MODEL FOG TOP HEIGHTS vs TIME, NUMBERING LABELS PARTICULAR NUMERICAL EXPERIMENT FOR WHICH DATA ARE ALSO SHOWN IN FIGURE 52

As shown in Figure 51, the model fog top heights are similar to those observed for shallow radiational fogs; however, the liquid water content (LWC) is generally too large. Figure 52 shows the time variation of a characteristic LWC for the model fogs. In general, the LWC reaches a steady value around 300÷500 mg m^{-3}, which is much larger than the average 150 mg m^{-3} observed at Elmira for the deep valley fog. The generation of larger LWC by the model is not completely understood but appears to be partly the result of a small initial dew point spread (1-2°C) near the fog top. If a larger dew point spread is used, fogs having the desired LWC can be simulated but they are too shallow compared to observed depths. One such simulation (case 1) in which the LWC was approximately 150 mg m^{-3} is discussed in detail below and illustrates the behavior of this model in forming fog.

- Example of Model Fog Formation

In the example to be discussed, the initial temperature conditions chosen for the simulation were an adiabatic lapse rate and a surface temperature of 288°K. The initial moisture distribution was represented by a mixing ratio invariant with height; for the mixing ratio value chosen, the dew point spread was 4°C at the surface and smaller aloft. A time-height profile of the fog produced during this simulation is shown in Figure 53. As shown, fog formed after eight hours of integration and then grew, at first rapidly and then more slowly, both in height and LWC until the integration was terminated.

Temperature Structure Prior to Fog Formation

The manner in which the temperature structure evolved during this simulation is shown in Figure 54. In the figure, the temperature profile is shown at two-hour intervals along with an indication of the fog top height. The characteristics of the temperature field are: cooling with time at the surface, a weak temperature gradient in the lowest meter, a strong temperature inversion near 10 m, and absence of cooling at 100 m.

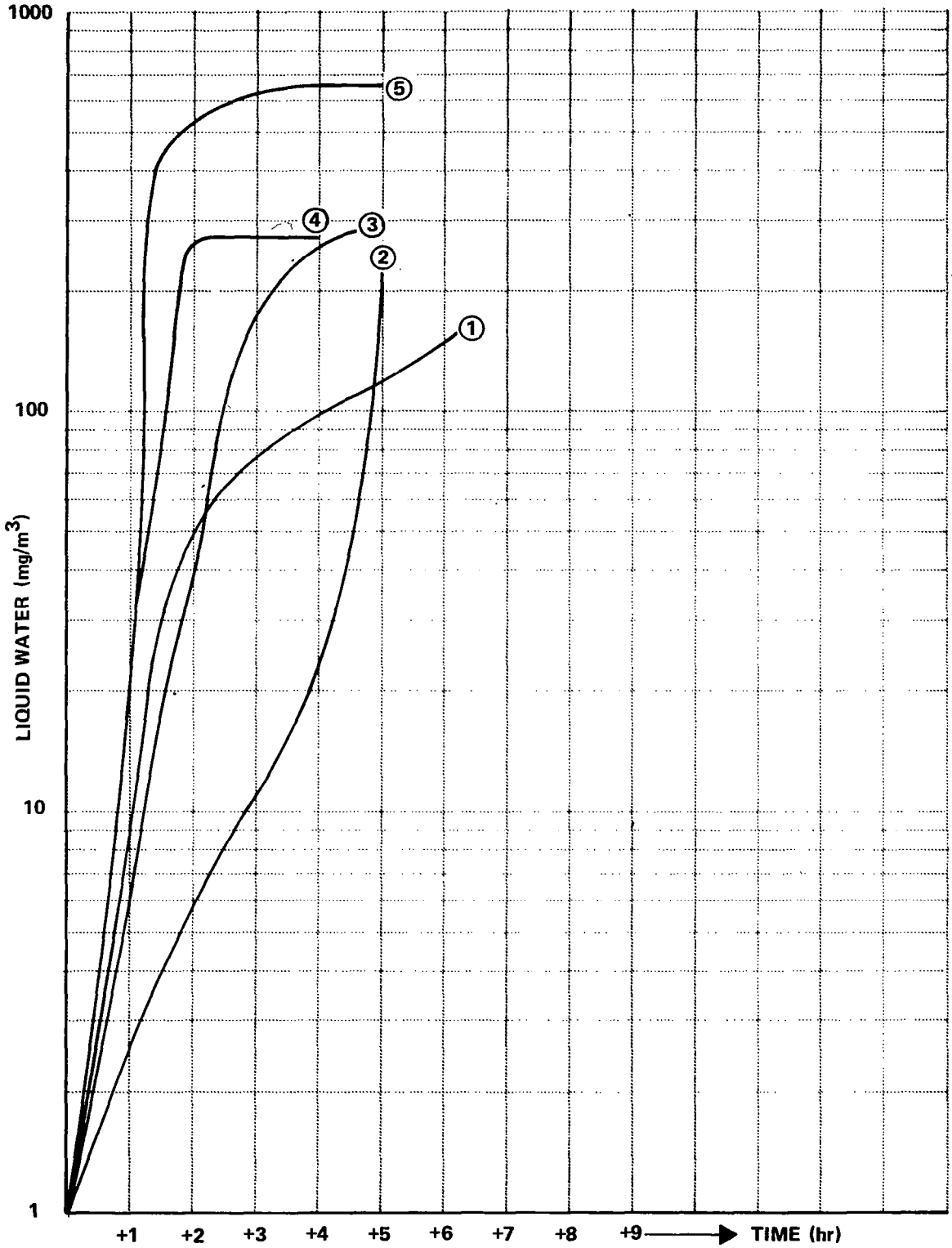

Figure 52 MODEL FOG LIQUID WATER CONTENT vs TIME

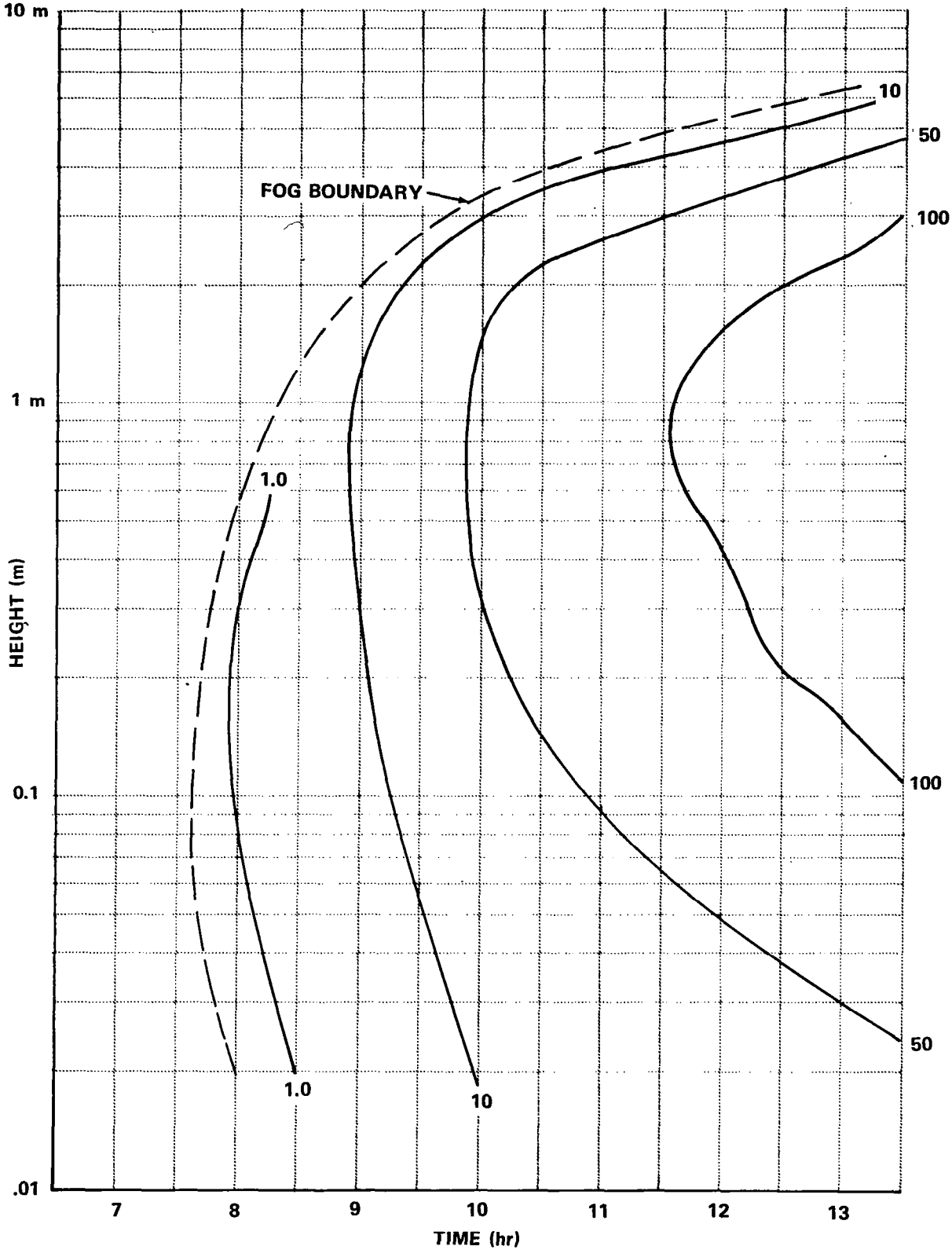

Figure 53 EXAMPLE OF MODEL TIME-HEIGHT VARIATION OF LIQUID WATER CONTENT (IN mg/m^3) – CASE ① IN FIGURES 51 AND 52

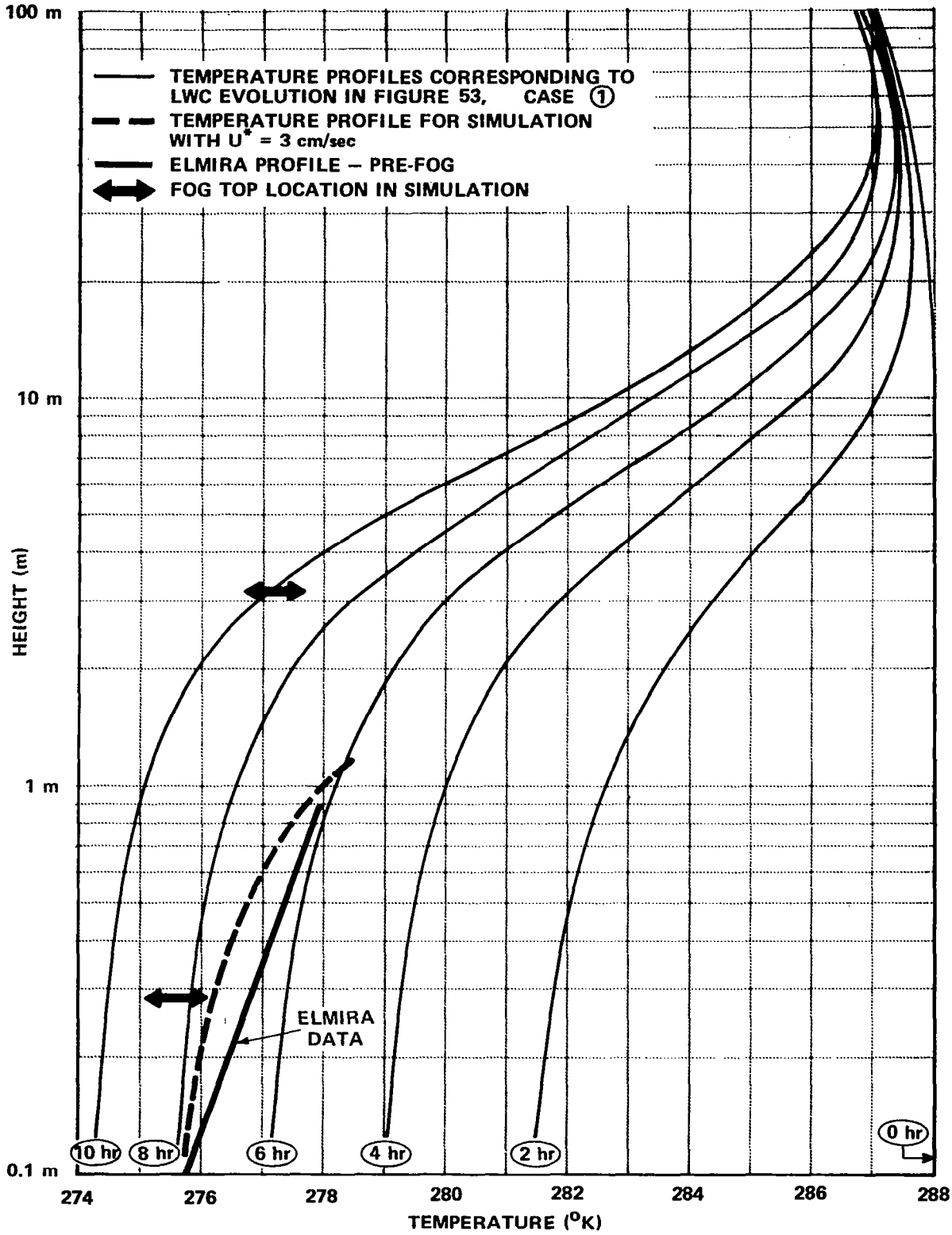

Figure 54 PRE-FOG TEMPERATURE PROFILE IN MODEL AND OBSERVATIONS

In order to properly model the formation of fog, it appears important to produce the pre-fog temperature profile. It is felt that this feature is particularly important in simulating vertical growth of fog. Temperature profile data covering the life cycle of the type of radiation fog produced by this model do not exist in the readily available literature. Other data are available for situations somewhat similar to those under which radiation fog forms. For example, Best et al. (1952) shows the average temperature behavior in the lowest 100 m for 19 clear summer nights. Temperature and wind observations are available from Elmira for fog situations in 1970, but this fog type primarily builds down to, rather than up from, the ground. Since data such as these are the only type available, in the following discussion model temperature profiles are compared to these observations, and any important differences in general atmospheric conditions between the model and observations are described.

We can assume that the valley temperature structure near Elmira, New York under light wind conditions prior to valley fog formation provides a good representation of the low-level temperature profile. The model results are, therefore, compared with data obtained in Elmira during the summer of 1970. From a review of the average Elmira temperature behavior at 10 cm (see Figure 13), the cooling rate for the period midnight to 0300 was found to be $0.67^{\circ}C/hr$, which is similar to values obtained from measurements by Best et al. (1952). For a comparable level and period in the model simulation, the cooling rate is $0.85^{\circ}C/hr$, showing fairly good agreement with observations in the field.

In Figure 54, the average 0.1 m to 1 m temperature profile is shown for pre-fog conditions in Elmira. The data are matched to the model profile by plotting the observed 0.1 m temperature at the value obtained in the model. The Elmira value of $2^{\circ}C$ increase between 0.1 m and 1 m is comparable to that measured by Thornthwaite (1948-52). Comparison of temperature profiles shows that the model does not produce a large enough temperature inversion in the lowest meter.

The Elmira observations are representative of light wind and stable temperature conditions and hence weak turbulent transfer in the low levels. Within our treatment of turbulence, the $u^* = 5\ cm\ sec^{-1}$, which was used for the above simulation, apparently did not give weak enough turbulent transfer in the low levels. A profile from a simulation with $u^* = 3\ cm\ sec^{-1}$, shown in Figure 54, reproduces the strong gradient in the lowest meter.

Observations from Elmira and other sources for the region above 1 m are shown in Figure 55 and documented in Table IV.

Table IV

Description of Temperature Profiles
Observed During Nocturnal Cooling

Profile No.	Source	Local Time	Type of Data
1	Best et al. (1952)	0400	Average
2	Elmira (1970)	0400	Average
3	Fleagle et al. (1952)	?	Single Case
4	Funk (1962)	1800	Single Case
5	Best et al. (1952)	2200	Single Case

Comparison of these observations with the model simulation shows that the model produces too large a temperature gradient in the region around 10 m. In addition, both the Best et al. observations and Elmira observations show cooling during the night at 100 m, whereas the model shows none.

With our model, the solution to obtaining a weaker temperature gradient through 10 m and cooling at 100 m was to increase u^*. A simulation was made in which u^* was set at 20 cm sec^{-1}. The temperature profile produced in this simulation after eight hours is shown in Figure 55. As shown, the agreement is considerably better than in the previous simulation. In addition, at the end of eight hours with $u^* = 20\ cm\ sec^{-1}$, the 100 m temperature cooled $2^{o}C$, whereas previously, there was no cooling. Not too surprisingly, attempts to form fog with u^* this large proved futile since the turbulent transfer of heat was very large.

In summary, the following table illustrates model behavior as a function of u^* :

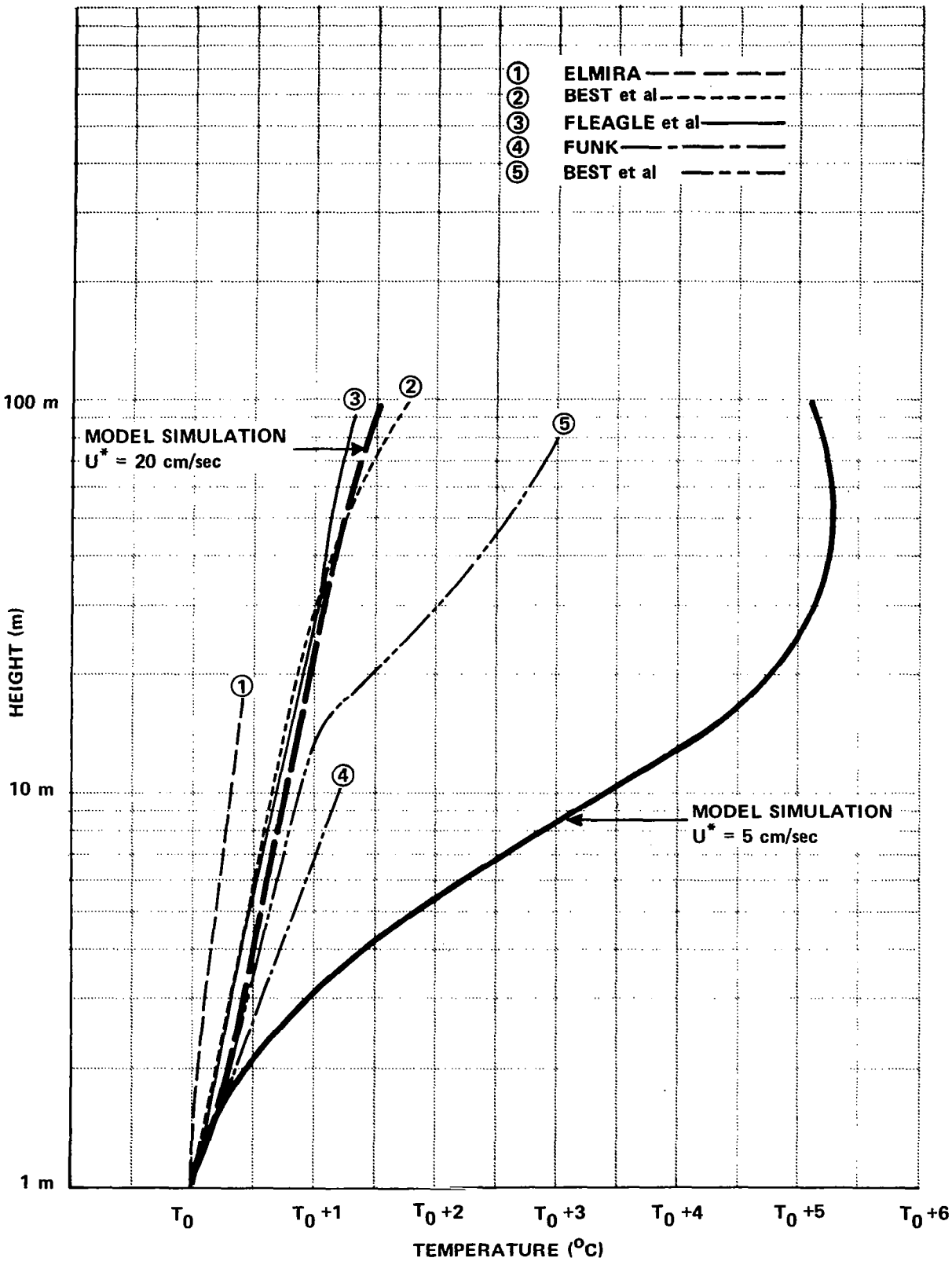

Figure 55 COMPARISON OF MODEL TEMPERATURE PROFILES TO OBSERVED PROFILES FOR PRE-FOG CONDITIONS

Table V

Model Behavior as a Function of u^*

$u^*(cm\,sec^{-1})$	Fog	0.1 m to 1 m Temperature Profile	1 m to 100 m Temperature Profile	100 m Cooling
3	Tenuous ground fog	Yes	No	No
5	Shallow radiation fog	No	No	No
20	None	No	Yes	Yes

With a low u^*, the low-level temperature structure can be duplicated, but only a very shallow (1-2 m) tenuous fog (30 mg m^{-3}) is formed. With somewhat larger u^*, a shallow fog with reasonable LWC can be formed, but none of the desired temperature structure can be reproduced. With still larger u^*, the temperature gradient through 10 m is duplicated and cooling at 100 m is produced; but fog does not form for realistic initial moisture conditions. The conclusion to be drawn is that, with a non-time-varying u^*, the model is not capable of producing a fog with reasonable LWC and the desired pre-fog temperature structure.

Based on this conclusion, it appears a simulation must start with a large u^* so that cooling can be transported to high levels and the temperature profile can be established. Modeling results and observations (Figure 20) show that, once the shape of the temperature profile is established, further cooling produces a generally uniform decrease of temperature at all heights. After the temperature profile is established, then u^* can be reduced so that cooling is concentrated at the lower levels and fog can form. This procedure might result in both fog formation and observed temperature behavior in a single simulation. By including the horizontal wind as an additional prognostic variable of the model and incorporating a dependence of the exchange coefficients upon vertical wind shear, such a variation in u^* can be internally generated in the model (see Kondo, 1971). The diurnal cycle model developed by Kondo also indicates that radiative flux divergence due to water vapor, which is neglected in the present model, can also have a significant influence on the temperature profiles.

Temperature Structure after Fog Formation

Observations show that after thick radiation fog forms, the surface temperature frequently rises and the pre-existing temperature inversion changes to a lapse condition (Figure 10; Fleagle et al., 1952). The mechanism controlling the surface temperature is most likely the balancing of the surface-long-wave radiation by that emanating from the fog, although the LWC and depth of the fog present when balance occurs is not completely known. However, using a LWC of the order of 0.1 g m^{-3}, a value characteristic of the Elmira fogs in which the surface temperature rises, the model results suggest a fog must reach a depth of 40 m before the temperature rises at a rate approaching that observed.

For purposes of demonstrating the capabilities of the numerical model, we would like to show the model temperature behavior after fog forms. Unfortunately, the model does not reproduce fog containing 0.1 g m^{-3} over 40 meters. However, in the model, the surface net radiation is controlled by the integrated LWC in a column; so the net radiation behaves similarly whether LWC is small through a large depth or large through a small depth. Consequently, even though the LWC is unrealistically large in the simulation about to be discussed, the results illustrate the temperature behavior in the model when the surface net radiation is reduced to essentially zero.

Figure 56 shows the temperature profile evolution for a simulation in which the net surface radiation is reduced to essentially zero after fog forms. The values of the net surface radiation are shown in the figure. As the radiation decreases, the temperature profile not only reverses from inversion to lapse, but the surface temperature increases by about 1.5^{o}C. In the model, the surface temperature responds to the surface boundary condition of continuous heat flux across the surface. When the net radiation is reduced by the presence of fog, the surface temperature rises in order to satisfy the boundary condition. Thus, the model treatment of the net surface radiation and heat balance at the surface is sufficiently realistic to raise the surface temperature and to produce a lapse condition after fog forms, which is in qualitative agreement with observations.

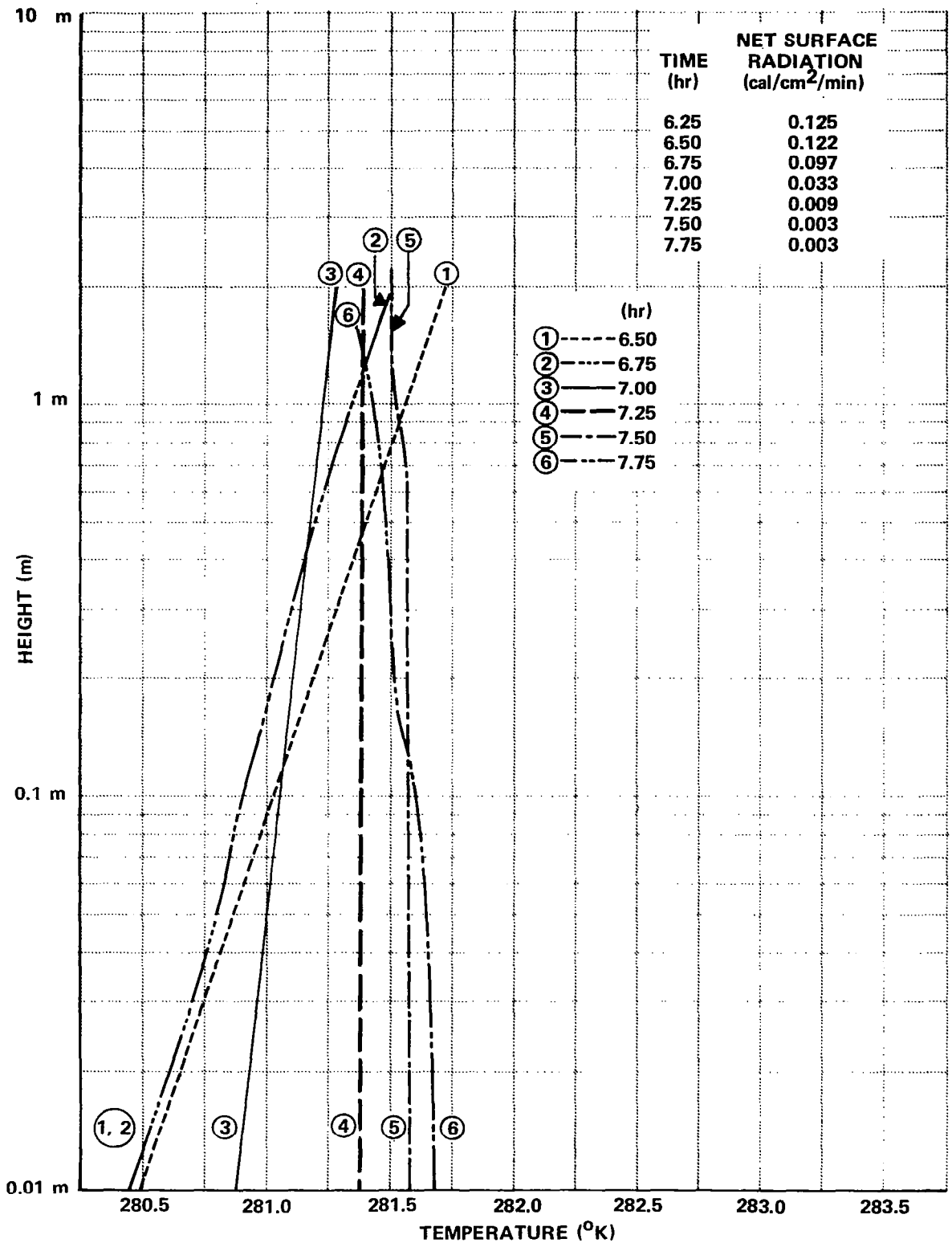

Figure 56 MODEL LOW-LEVEL TEMPERATURE PROFILE EVOLUTION IN FOG AFTER SURFACE NET RADIATION BECOMES NEGLIGIBLE

- Exchange Coefficient as a Function of Thermal Stratification

Even though K, the turbulent exchange coefficient, cannot change during a simulation due to changes in u^*, it can vary as a function of the vertical temperature stratification. An example of this change in K is shown in Figure 57 for a simulation in which the temperature profile is initially isothermal, becomes inverted before fog formation, and then after fog formation, changes to a lapse condition up through 3 m.

From an increase with height at 1 hr, K changes to a profile at 4 hr which shows an increase up to 1 m, essentially constant from 1-10 m and then a slow increase to a maximum around 50 m. The most notable decrease in K in this three-hour period is between 10-100 m, where the temperature profile has developed a strong inversion. Between 4 and 8 hr, fog forms and the temperature actually decreases up through 3 m. The effect of this destabilization on K appears as an increase in K centered near 2 m, which is also the location of the maximum value in K.

No measurements exist on the K behavior in fog at Elmira, but some interpretation is possible from the meager vertical wind data. In the case illustrated in Figures 31 and 32, a change to a vertical wind behavior characteristic of more turbulent conditions occurred when the fog formed and the low-level temperature profile became lapsed. However, comparison of the model results with these observations is of limited value since in Elmira the lapse condition extended through about 100 m and the wind increased when the turbulence increased. The former condition might cause the 17 m level to be influenced by eddies extending through a large depth and the latter condition suggests that the 17 m level might be influenced by increased turbulence associated with stronger wind. In any event, comparison of model results with observations shows that the model's ability to increase K when the temperature structure changes from stable to unstable qualitatively duplicates a characteristic of fog occurrence.

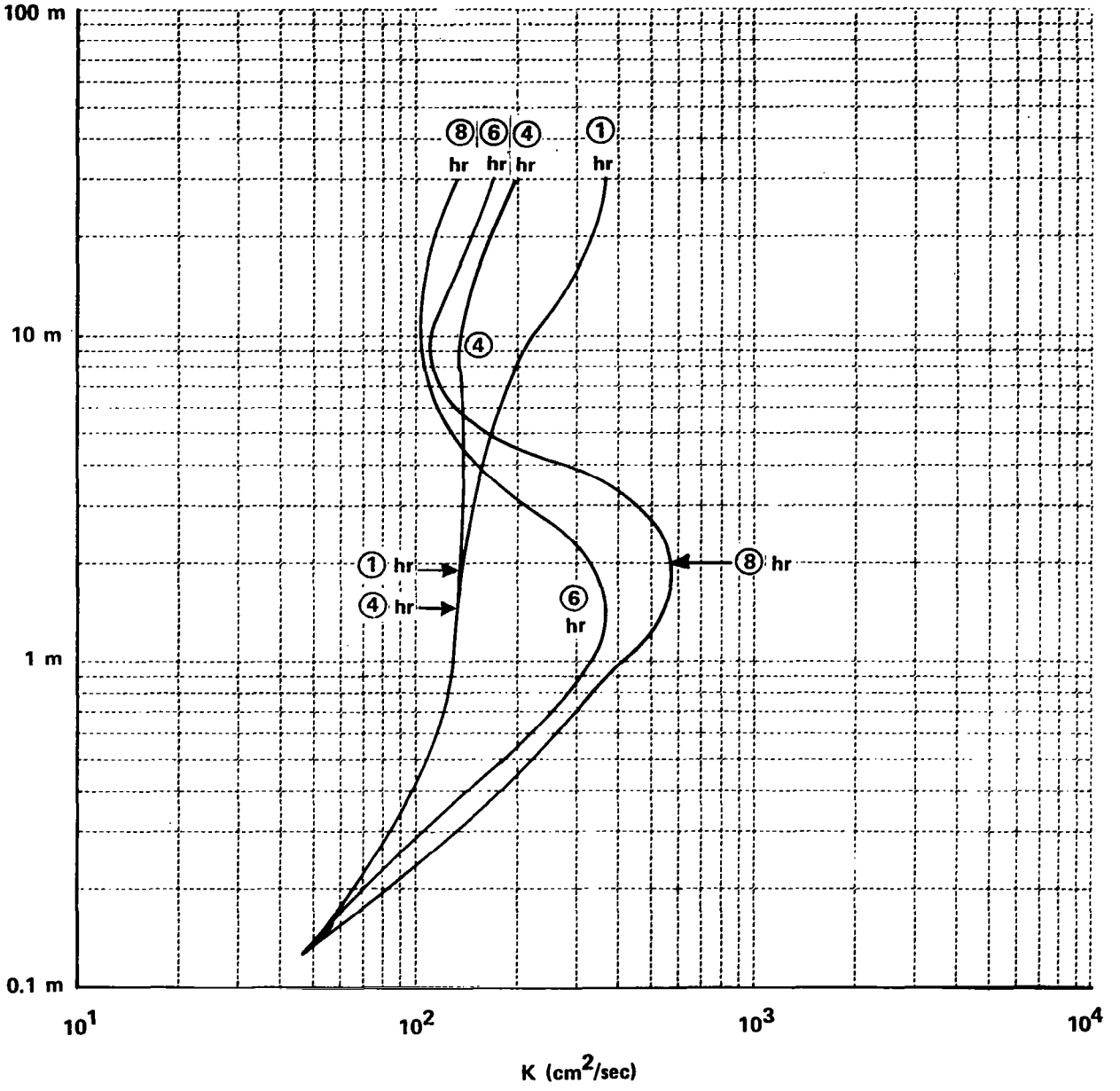

Figure 57 EVOLUTION OF TURBULENT EXCHANGE COEFFICIENT PROFILE FOR MODEL SIMULATION IN WHICH LOW-LEVEL TEMPERATURE PROFILE BECOMES LAPSED

- Model Behavior as a Function of Input Parameters

In the model, the initial temperature profile can be either isothermal or adiabatic, both of which are reasonable. The adiabatic profile is characteristic of late afternoon, while isothermal structure occurs in the early evening (Best et al., 1952). The initial moisture distribution can be specified either as constant mixing ratio or constant dew point depression. The choice of appropriate initial moisture conditions for fog formation is an open question. Funk (1962) points out that "Stewart found a disappointingly irregular behavior of the detailed humidity structure. . . ." Radiosonde observations for Buffalo, New York on the evening prior to a recent fog occurrence indicate that constant mixing ratio is an appropriate initial condition. However, in view of the uncertainties surrounding this question, simulations were run for several combinations of initial profiles of temperature and moisture.

Much of the experimental modeling work was concerned with fog formation as a function of the degree of turbulent diffusion. Analysis showed that after a short initial adjustment period, the K's changed little with time before fog formation. Therefore, K values at t = 4 hr were chosen to label each experiment. A choice of K at the 10 m level, to provide a single K for each experiment, proved fortunate. The result of stratifying the experiments according to this K value is shown in Table VI.

Table VI

Stratification of Numerical Experiments by K-Value at the 10 m Level

	$K_{10} < 10^3 cm^2 sec^{-1}$	$K_{10} > 10^3 cm^2 sec^{-1}$
Fog Cases	12	1
No Fog Cases	1	6

Twelve of thirteen fog cases had a K value of $<10^3$ cm^2 sec^{-1}. The one case with $K > 10^3$ cm^2 sec^{-1} hardly qualifies as a fog as the LWC appears only in the lowest 22 cm and only after 13.5 hours of cooling. Six of seven no fog cases occurred with $K > 10^3$ cm^2 sec^{-1}; the one with $K < 10^3$ cm^2 sec^{-1} had a large dew point depression from which the model could not form fog in a reasonable time (e.g., sunset to sunrise). This result based on K values suggested that fog would form in the model when the K value was small enough so that cooling would be confined to the lower levels. Under these conditions, the cooling at low levels would bring the temperature to the dew point which is also decreasing because of dew formation at the surface.

As a test of this interpretation, the surface temperature change at 2 and 4 hr into the integration was tabulated. Comparison of these temperature changes, between otherwise similar situations, showed that, in general, fog cases possessed larger cooling than no fog cases. Thus, for the present model, a K_{10} value of 10^3 cm^2 sec^{-1} marks the boundary between fog-no fog formation for initial dew point spreads of 5°C or less.

As pointed out earlier, the model is satisfactory in reproducing a temperature structure associated with pre-fog hours. However, attempts to form a fog with the input parameters of this simulation were unsuccessful. In this simulation, $K_{10} = 7 \times 10^3$ cm^2 sec^{-1}, which does not produce fog in a reasonable time.

- Dew Formation

One of the advances of this model over previous ones is reduction of the atmospheric water vapor through dew formation at the ground. However, the formalism for producing dew in the model is highly simplified, and quantitative comparison of model dew formation rates with observed values is of questionable significance. On the other hand, presentation of the overall behavior of the dew formation process in the model is appropriate.

A single dew formation rate was computed for each simulation. For fog cases, the rate was computed for the period starting with initial dew formation and ending when fog formed. For no-fog simulations, the rate

was computed over the period extending from initial dew formation to the end of the simulation, about ten hours. The values range from 5 g m^{-2} hr^{-1} to 35 g m^{-2} hr^{-1}, with the variation related primarily to u^* values.* The higher dew formation rates are of the same magnitude as those measured in Elmira, New York. However, the accompanying u^* values are representative of too large a turbulent transfer compared to the low transfer conditions under which the Elmira observations were made. Whether the source of this discrepancy lies in the modeling of dew formation or in the representativeness of the dew observations (See Chapter II) remains an open question.

- Summary

A one-dimensional numerical model of radiation fog was developed containing the following features:

1. radiational cooling at the earth's surface;
2. continuity of temperature and heat flux across the soil-atmosphere boundary;
3. Turbulent diffusion of heat, water vapor, and liquid water in the atmosphere, and molecular diffusion of heat in the soil;
4. specification of turbulent exchange coefficients in terms of the friction velocity u^*, height, and the predicted local stability;
5. dew formation by water vapor diffusion to the earth's surface, and consequent formation of a dew point inversion;
6. reduction of the net upward infrared radiation at the earth's surface by back radiation from the developed fog;
7. radiative cooling of fog as a result of the radiative flux divergence produced by fog;
8. gravitational sedimentation of fog drops;
9. saturation adjustment - supersaturated water vapor condenses instantaneously until saturation is achieved. Liquid water in an unsaturated region evaporates instantaneously until saturation is achieved or the liquid water is exhausted.

---

*A u^* value of 8 cm sec^{-1} separates the dew rates into two groups with values above and below 20 g m^{-2} hr^{-1}.

Previous numerical models for formation of radiation fog have had little difficulty forming fog because the water vapor content of the atmosphere was held constant. In the present model, in which dew formation takes water vapor out of the atmosphere, correct modeling must be made of the complex process by which the temperature and dew point inversions are brought together. The present model can form fog under these conditions, but all the characteristics of a fog type cannot be duplicated in a single numerical experiment.

Prior to model fog formation, observed temperature profiles and cooling near 100 m were not duplicated. With a proper choice of α^*, it was possible either to duplicate some features of the temperature field or form fog, but it was not possible to accomplish both tasks simultaneously. These results suggest that a considerable improvement in the model might be effected by making the horizontal wind a prognostic variable and including a dependence of the exchange coefficients upon vertical wind shear.

The fogs generated by this model are radiation fogs with tops in the 10-40 m range. The liquid water content for these fogs, however, was generally in the 300-500 mg m^{-3} range, which is larger than the 150 mg m^{-3} frequently observed in natural fogs. An experiment in which the maximum liquid water values generated were 150 mg m^{-3} produced a fog top of only 6 m. The inability of this model to form fogs of 10-40 m depth with reasonably low liquid waters is not completely understood. It appears that the problem lies in the inability of the model to predict deep fogs with realistic initial dew point spreads.

The present model is able to reproduce two characteristic features which occur after thick fog forms. The first involves a rise of surface temperature and conversion of the low-level temperature profile from inversion to unstable. In the model, this temperature behavior occurs when the fog becomes thick enough so that downward radiation emanating from the fog significantly reduces the net radiation leaving the earth's surface. In addition, the model predicts an increase in the low-level turbulent exchange coefficients at this time in agreement with observed increases in vertical wind fluctuations.

The numerical model of radiation fog which has been discussed here constitutes a considerable improvement over previous models in the treatment of dew formation and the turbulent exchange coefficients. The inability of this more complex model to duplicate certain observed fog properties has indicated problem areas that require further research in order to develop a numerical model for the prediction of radiation fog formation and dissipation.

REFERENCES

Battan, L. J., 1959: Radar Meteorology, University of Chicago Press, 161 pp.

Best, A. C., E. Knighting, R. H. Pedlow, and K. Stormouth, 1952: Temperature and Humidity Gradients inthe First 100 m over SE England, Geophys. Mem., 89.

Defant, F., 1951: Local Winds; Compend. of Meteor. (Am. Meteor. Soc.), Boston, 655-672.

Emmons, G. and R. B. Montgomery, 1947: Note on the Physics of Fog Formation, J. Meteor., 4, 205.

Fisher, E. L., and P. Caplan, 1963: An Experiment in Numerical Prediction of Fog and Stratus. J. Atmos. Sci., 20, 425-437.

Fitzgerald, J. W., 1970: Non-Steady-State Supersaturations in Thermal Diffusion Chambers, J. Atmos. Sci., 27, 70-72.

Fleagle, R. G., W. H. Parrott, and M. L. Barad, 1952: Theory and Effects of Vertical Temperature Distribution in Turbid Air, J. Meteor., 9, 53-60.

Fletcher, N. H., 1966: Physics of Rainclouds, Cambridge University Press, 389 pp.

Funk, J. P., 1962: Radiative Flux Divergence in Radiation Fog, Quart. J. Royal Meteor. Soc., 88, 233-249.

Geiger, R., 1965: The Climate Near the Ground, Harvard University Press.

Goody, R. M., 1964: Atmospheric Radiation, Oxford University Press, 436 pp.

Heywood, C. S. P., 1931: Some Observations of Fogs and Accompanying Temperature Gradients, Quart. J. Royal Meteor. Soc., 57, 97-101.

Hosler, C. L., L. G. Davis, D. R. Booker, E. R. Mallory, and J. P. Breon, 1966: Airborne Meteorological System, Final Report NSF GP-2895, Department of Meteorology, The Pennsylvania State University, University Park, Pennsylvania.

Jiusto, J. E., 1964: Investigation of Warm Fog Properties and Fog Modification Concepts, NASA CR-72.

Johnson, J. C., 1954: Physical Meteorology, Massachusetts Institute of Technology, Technology Press, 393 pp.

Kelly, N. D., and J. P. Breon, 1967: Determination of the Aerodynamic Heating of a Reverse Flow Temperature Probe, Report No. 8, NSF GP-4743, Department of Meteorology, The Pennsylvania State University, University Park, Pennsylvania.

Kocmond, W. C. and J. E. Jiusto, 1968: Investigation of Warm Fog Properties and Fog Modification Concepts, NASA CR-1071.

Kondo, J., 1971: Effect of Radiative Heat Transfer on Profiles of Wind, Temperature, and Water Vapor in the Atmospheric Boundary Layer, J. Meteor. Soc. Japan, 2, 75-93.

Korb, G., and W. Zdunkowski, 1970: Distribution of Radiative Energy in Ground Fog, Tellus, 22, 288-320.

Langmuir, I., and K. Blodgett, 1946: A Mathematical Investigation of Water Droplet Trajectories, USAAF Tech. Rept. No. 541B.

Lumley, J. L., and H. A. Panofsky, 1964: The Structure of Atmospheric Turbulence, New York, Interscience Publishers, 239 pp.

Lyons, R., G. Nichols, and J. Cahir, 1962: Physical Processes Important for Short-Range Weather Prediction, Scientific Report No. 1, Contract CwB-10112, Pennsylvania State University, College of Mineral Industries.

McDonald, J. E., 1963: The Saturation Adjustment in Numerical Modeling of Fog, J. Meteor., 20, 476-489.

Plate, E. J., 1971: Aerodynamic Characteristics of Atmospheric Boundary Layers, U. S. Atomic Energy Commission, Critical Review Series, 190 pp.

Richtmeyer, R. D., 1957: Difference Methods for Initial-Value Problems, New York, Interscience Publishers, 238 pp.

Rodhe, B., 1962: The Effect of Turbulence on Fog Formation, Tellus, 14, 49-86.

Saxena, V. K., J. N. Burford, and J. L. Kassner, Jr., 1970: Operation of a Thermal Diffusion Chamber for Measurements on Cloud Condensation Nuclei, J. Atmos. Sci., 27, 73-80.

Schuepp, W., 1945: Untersuchungen über den winterlichen Kaltluftsee in Davos, Verh. Schweiz. Naturf. Ges., 127-128.

Stephens, J. J., 1961: Spectrally Averaged Total Attenuation, Scattering, and Absorption Cross-Sections for Infrared Radiation, J. Meteor., 18, 822-828.

Suomi, V. E., and P. M. Kuhn, 1958: An Economical Net Radiometer, Tellus, 10, 160-163.

Sutton, O. G., 1953: Micrometeorology, New York, McGraw Hill, 333 pp.

Taylor, G. I., 1917: The Formation of Fog and Mist, Quart. J. Royal Meteor. Soc., 43, 241.

Thornthwaite, C. W., 1948-1952: Micrometeorology of the Surface Layer of the Atmosphere, Publ. Climat., 1-5.

Wagner, A., 1931: Klimatologie der freien Atmosphäre, Handbuch der Klimatologie, 1.

_____, 1932: Hangwind-Ausgleichsströmung-Berg und Talwind, Meteor. Z., 49, 209-217.

_____, 1932: Neuere Theorie des Berg and Talwindes, ibid., 49, 329-341.

_____, 1938: Theorie und Beobachtungen der periodischen Gebirgswinde, Beitr. Geophys., 52, 408-449.

Wells, W. C., 1838: An Essay on Dew and Several Appearances Connected with It. Essay appears in book entitled: On the Influence of Physical Agents on Life, by W. F. Edwards, Haswell Barrington and Haswell, Philadelphia, Pennsylvania.

Zdunkowski, W. G., and B. C. Nielsen, 1969: A Preliminary Prediction Analysis of Radiation Fog, Pure and Appl. Geophys., 75, 278-299.